REHABILITATION OF DETERIORATED STEEL BRIDGE GIRDERS IN FLEXURE USING CFRP COMPOSITES

HANY MOHAMED SEIF ELDIN

A Thesis

in

The Department

of

Building, Civil, and Environmental Engineering

Presented in Partial Fulfillment of the Requirements

for the Degree of Master of Applied Science (Civil Engineering) at

Concordia University

Montréal, Québec, Canada

March 2010

Your file Votre référence
ISBN: 978-0-494-67250-1
Our file Notre référence
ISBN: 978-0-494-67250-1

ABSTRACT

REHABILITATION OF DETERIORATED STEEL BRIDGE GIRDERS IN FLEXURE USING CFRP COMPOSITES

HANY MOHAMED SEIF ELDIN

Structural deficiencies in Railway steel bridges are usually the result of deterioration caused by ageing, corrosion, fatigue, and higher load demands. In this context, steel bridge girders are the structural members prone to corrosion which implies a substantially reduction of their flexural capacities. As a result, a large number of steel railway bridges are in need for strengthening or retrofit. In this thesis, experimental and analytical investigations are conducted to predict the reduction in the flexural capacity of existing deteriorated steel girders under static loading and several retrofitting schemes are developed in the light of strengthening the girder cross-section. The experimental study covers the use of two Carbon Fibre-Reinforced Polymer (CFRP) composite types, namely, normal modulus sheets (NM-CFRP) and high modulus strips (HM-CFRP). A total of thirteen medium-scale W-shape steel beams with a span of 1.6m were tested under four-point bending setup. The thirteen beams were divided in four groups such as: i) Group G1 consisted of four beams with different percentages of cross-sectional area reduction without any strengthening; ii) Group G2 consisted of four notched beams strengthened with bonded NM-CFRP sheets. Herein, two out of the four strengthened beams, were bonded using saturant epoxy, while the other two were strengthened using high performance adhesive; iii) Group G3 consisted of two notched beams strengthened with bonded HM-CFRP strip with and without a wrapping system; iv) Group G4

consisted of three notched beams strengthened with unbonding NM-CFRP sheets and a ductile anchoring system. The results of the experimental study underline the effectiveness of the proposed retrofitting schemes in terms of flexural capacity increase and deflection control of the existing corroded steel girders. In addition to the experimental program, an analytical model was developed to set up a numerical method that is capable of predicting the elastic and post-yield behaviour of the unstrengthened and strengthened deteriorated steel girders. This numerical method can be used by designers to calculate the losses in the moment capacity of the deteriorated steel girders to an acceptable level of accuracy. The analytical model was validated using the experimental results that were presented in the experimental program.

To my beloved family

ACKNOWLEDGEMENT

It is with sincere gratitude that I thank my advisors and mentors Dr. Khaled Galal and Dr. Lucia Tirca for tenaciously believing in me throughout this project. Without their financial and academic support, it would be impossible for me to realize this extensive research work.

I would like to kindly acknowledge the financial support of Canadian National Railway Company (CN) and donation of the Carbon fiber materials provided by Fyfe Co. LLC without which this research could not have proceeded. Financial support and encouraging rewards from Concordia University is also greatly appreciated.

I would like to thank Dr. Mohamed Ali who has been a great deal of help throughout my graduate experience. Also, I would like to acknowledge the assistance and technical support during my experimental work of Mr. Jacque Payer, Mr. Joseph Hrib, and Mr. Tiberiu Aldea. Their help, support, and assistance are appreciated.

My dear colleagues Hossam El-Sokkary and Mossab El-Tahan cannot be thanked enough for sincerely supporting me throughout this project. I also would like to extend my sincere gratitude to all my other colleagues namely; M. Sharawy, Ihab, Tamer, Hossein, Nima, Alp, and Riccardo for supporting me and helping me to complete my experimental work.

Finally, I dedicate this thesis to my parents, my brothers, and my sisters for their invaluable supporting during my study. Without their love and their believing in me I could not finish this project. I know they deserve more than what I give and express towards them.

TABLE OF CONTENTS

LIST OF FIGURES XII

LIST OF TABLES XIX

LIST OF SYMBOLS XX

LIST OF ABBREVIATIONS XXII

INTRODUCTION 1

1.1 Background and problem definition 1

1.2 Objectives and scope of work 2

1.3 Thesis layout 4

2 LITERATURE SURVEY 5

2.1 Introduction 5

2.1.1 Traditional strengthening methods for steel members 6

2.1.2 Effect of corrosion on steel bridges 7

2.1.2.1 Galvanic corrosion 8

2.2 Remaining capacity of corroded steel beams 9

2.3 Review on the retrofit of steel structures using FRP 11

2.4 Characterization of the bonding between FRP and steel 12

2.5 Strengthening of steel girders with FRP 16

2.6 Strengthening of steel-concrete composite girders using FRP 19

2.7 Fatigue performance of steel members retrofitted with FRP 23

2.8 Metallic bridges strengthened with FRP 24

2.9 Summary 25

3 EXPERIMENTAL WORK 34

3.1 General 34

3.1.1 Properties of the tested steel beams 35

3.1.2 Materials used 35

3.1.3 Retrofit schemes 36

3.1.4 Specimen labeling convention 38

3.2 Test layout 40

3.2.1 Design of Group 1 beams 41

3.2.2 Design of Group 2 beams 42

3.2.3 Design of Group 3 beams 42

3.2.4 Design of Group 4 beams 43

3.3 Surface preparation 46

3.4 Instrumentation 46

4 TEST RESULTS AND DISCUSSION 71

4.1 General 71

4.2 Results of Group 1 beams 72

4.2.1 Beam BFO 72

4.2.2 Beam BF-H0.33 73

4.2.3 Beam BF-N0.33 73

4.2.4 Beam BF-N0.50 74

4.2.5 The effect of the area loss in tension flange on the behaviour of the deteriorated steel beam 75

4.3 Results of Group 2 beams 75

4.3.1 Beam BF- F1(5)-B1 76
4.3.2 Beam BF-N0.50-F1(5)-B1 77
4.3.3 Beam BF-H0.33-F1(5)-B2 77
4.3.4 Beam BF-N0.50-F1(5)-B2 78
4.3.5 The effect of the adhesive type on the effectiveness of the retrofitting scheme 78
4.4 Results of Group 3 beams 79
4.4.1 Beam BF-H0.33-F2(1)-B2 79
4.4.2 Beam BF-H0.33-F2(1)-B2w 80
4.4.3 The efficiency of the wrapping system 80
4.5 Results of Group 4 beams 81
4.5.1 Beam BF-H0.33-F1(1)-A1D1 82
4.5.2 Beam BF-H0.33-F1 (1)-A2D1 82
4.5.3 Beam BF-H0.33-F1 (5)-A1D2 83
4.5.4 The efficiency of the proposed ductile anchorage system 84
4.6 General discussion 84
5 NUMERICAL MODEL 108
5.1 Introduction 108
5.2 Section analysis in flexure 109
5.3 Validation of the assumptions used in this numerical model 112
5.4 Yielding load for corroded steel girders 114
5.5 Deterioration factor (Ψ_d) 116
6 CONCLUSIONS, RECOMMENDATIONS AND FUTURE WORK 136

6.1 Summary 136
6.2 Conclusions 137
6.3 Recommendations and future work 139
7 REFERENCES 141
A. APPENDIX A 149
8 APPENDIX B 152

LIST OF FIGURES

Figure 2.1 Deficiency ratios of the existing bridges (FHWA 2009) 28

Figure 2.2 Design charts related to deterioration factor (Ψd) (Lindt and Ahlborn 2004) 29

Figure 2.3 Models of corroded sections simulation by reducing the thickness of the element (Rahgozar 2009) 30

Figure 2.4 Bond test methods (Zhao and Zhang 2007) 31

Figure 2.5 Typical strain profile of CFRP bonded to steel plate (Frauenberger et al. 2003) 32

Figure 2.6 Different rehabilitation geometries for steel beams (Mertz and Gillespie 1996) 32

Figure 2.7 Modeling of the bonded reinforcement and required constrains of the steel beam using the commercial code ABAQUS. (Colombi and Carlo 2006-B) 33

Figure 2.8 Typical shear failure of steel girders strengthened with CFRP (Patnaik et al. 2008) 33

Figure 3.1 Measured steel tensile stress-strain relationship 51

Figure 3.2 Steel tension coupon test 51

Figure 3.3 Original and strengthened sections 52

Figure 3.4 Ductile anchorage system 52

Figure 3.5 Test setup 53

Figure 3.6 Typical steel beam cross-sections 54

Figure 3.7 Notches preparation 54

Figure 3.8 Beam 2 BF-H0.33; (a) Elevation of the test setup, (b) Plan view of the bottom flange, and (c) Section at mid-span 55

Figure 3.9 Beam 3 BF-N0.33; (a) Elevation of the test setup, (b) Plan view of the bottom flange, and (c) Section at mid-span 56

Figure 3.10 Beam 4 BF-N0.50; (a) Elevation of the test setup, (b) Plan view of the bottom flange, and (c) Section at mid-span 57

Figure 3.11 Beam 5 BF-H0.33-F1(5)-B1; (a) Elevation of the test setup, (b) Plan view of the bottom flange, and (c) Section at mid-span 58

Figure 3.12 Beam 6 BF-N050-F1(5)-B1; (a) Elevation of the test setup, (b) Plan view of the bottom flange, and (c) Section at mid-span 59

Figure 3.13 Beam 7 BF-H0.33-F1(5)-B2; (a) Elevation of the test setup, (b) Plan view of the bottom flange, (c) Section at mid-span, and (d) Section near to Roller Support 60

Figure 3.14 Beam 8 BF-N050-F1(5)-B2 ; (a) Elevation of the test setup, (b) Plan view of the bottom flange, and (c) Section at the constant moment zone 61

Figure 3.15 Beam 9 BF-H0.33-F2(1)-B2 ; (a) Elevation of the test setup, (b) Plan view of the bottom flange, and (c) Section at mid-span 62

Figure 3.16 Beam10 BF-H0.33-F2(1)-B2w; (a) Elevation of the test setup, (b) Plan view of the bottom flange, and (c) Section near to Roller Support 63

Figure 3.17 Unbonded CFRP sheets ductile anchorage system 64

Figure 3.18 3D-Ductile anchorage system schema 65

Figure 3.19 Ductile anchorage system dimensions; (a) Part 1, (b) Part 3 66

Figure 3.20 Beam 11 BF-H0.33-F1(1)-A1D1; (a) Elevation of the test setup, (b) Section near to the roller support, and (c) Longitudinal profile of the CFRP sheet 67

Figure 3.21 Beam 12 BF-H0.33-F1(1)-A2D1; (a) Elevation of the test setup, (b) Section at mid-span, and (c) Section near the roller support 68

Figure 3.22 Beam 13 BF-H0.33-F1(5)-A2D2; (a) Elevation of the test setup, (b) Section near the pinned support, and (c) Longitudinal profile of the CFRP sheet 69

Figure 3.23 Locations of strain gages and potentiometers; (a) Beam elevation, (b) Typical sections without CFRP, and (c) Typical sections with CFRP 70

Figure 4.1 Definitions of the yield and ultimate loads with their corresponding deflections; (a) Non-strengthened steel beam, and b) Strengthened steel beam..... 88

Figure 4.2 Stress-Strain curves for beam coupons..... 89

Figure 4.3 Stress-Strain curves for the steel coupons, Tyfo® SCH-11UP sheets and Tyfo® UC strips 89

Figure 4.4 Test results of beam BFO; (a) Mode of failure, (b) Load-deflection, (c) Load-strain..... 90

Figure 4.5 Test results of beam BF-H0.33; (a) Mode of failure, (b) Load-deflection, (c) Load-strain 91

Figure 4.6 Test results of beam BF-N0.33; (a) Mode of failure, (b) Load-deflection, (c) Load-strain 92

Figure 4.7 Test results of beam BF-N0.50; (a) Mode of failure, (b) Load-deflection, (c) Load-strain 93

Figure 4.8 Performance of group 1 beams; (a) Load-deflection, (b) Load-strain, (c) Moment-rotation 94

Figure 4.9 Test results of beam BF-H0.33-F1(5)-B1; (a) Mode of failure, (b) Load-deflection, (c) Load-strain..... 95

Figure 4.10 Test results of beam BF-N0.50-F1(5)-B1; (a) Mode of failure, (b) Load-deflection, (c) Load-strain..... 96

Figure 4.11 Test results of beam BF-H0.33-F1(5)-B2; (a) Mode of failure, (b) Load-deflection, (c) Load-strain 97
Figure 4.12 Test results of beam BF-N0.50-F1(5)-B2; (a) Mode of failure, (b) Load-deflection, (c) Load-strain 98
Figure 4.13 Performance of group two beams; (a) Load-deflection, (b) Load-strain, (d) Moment-rotation 99
Figure 4.14 Test results of beam BF-H0.33-F2(1)-B2; (a) Mode of failure, (b) Load-deflection, (c) Load-strain 100
Figure 4.15 Test results of beam BF-H0.33-F2(1)-B2w; (a) Mode of failure, (b) Load-deflection, (c) Load-strain 101
Figure 4.16 Performance of group 3 beams; (a) Load-deflection, (b) Load-strain, (d) Moment-rotation 102
Figure 4.17 Test results of beam BF-H0.33-F1(1)-A1D1; (a) Mode of failure, (b) Load-deflection, (c) Load-strain 103
Figure 4.18 Test results of beam BF-H0.33-F1(1)-A2D1; (a) Mode of failure, (b) Load-deflection, (c) Load-strain 104
Figure 4.19 Test results of beam BF-H0.33-F1(5)-A2D2; (a) Mode of failure, (b) Load-deflection, (c) Load-strain 105
Figure 4.20 performance of group four beams; (a) Load-deflection, (b) Load-strain, (d) Moment-rotation 106
Figure 4.21 Load-deflection relative performance of beams: BF-N0.50, BF-N0.50-F1(5)-B1 and BF-N0.50-F1(5)-B2 107

Figure 4.22 Load-deflection relative performance of beams: BF-H0.33, BF-H0.33-F1(5)-B1, BF-H0.33-F1(5)-B2, BF-N0.50, BF-N0.50-F1(5)-B1 and BF-N0.50-F1(5)-B2 107

Figure 5.1 Design Stress-Strain curve for steel section 122

Figure 5.2 Development length per layer for Tyfo SCH-11UP and Tyfo UC 122

Figure 5.3 Assumed linear strain profile and corresponding stress profile applicable for elastic and post-yield range 123

Figure 5.4 Analytical and experimental Moment-Curvature for sections: (a) S1; (b) $S1_{33\%;}$ (c) $S1_{50\%}$ 124

Figure 5.5 Analytical and experimental Moment-Curvature for sections: (a) S1F1B1; (b) $S1_{33\%}$F1B1; (c) $S1_{50\%}$ 125

Figure 5.6 Analytical and experimental Moment-Curvature for sections: (a) S1F1B2; (b) $S1_{33\%}$F1B2; (c) $S1_{50\%}$F1B2 126

Figure 5.7 Analytical and experimental Moment-Curvature for sections: (a) S1F2B2; (b) $S1_{33\%}$F2B2; (c) $S1_{50\%}$F2B2 127

Figure 5.8 Analytical Moment-Curvature for sections S1, $S1_{33\%,}$ and $S1_{50\%}$ 128

Figure 5.9 Analytical Moment-Curvature for sections S1 with CFRP (F1B1) 5 layers of Tyfo SCH-11UP with Tyfo S, (F1B2) 5 layers of Tyfo SCH-11UP with MB-3, (F2B2) 1 strip of Tyfo UC with MB-3 128

Figure 5.10 Analytical Moment-Curvature for sections $S1_{33\%}$ with CFRP (F1B1) 5 layers of Tyfo SCH-11UP with Tyfo S, (F1B2) 5 layers of Tyfo SCH-11UP with MB-3, (F2B2) 1 strip of Tyfo UC with MB-3 129

Figure 5.11 Analytical Moment-Curvature for sections $S1_{50\%}$ with CFRP 129

Figure 5.12 Stress-Strain curve for ductile material 130
Figure 5.13 Determination of yield stress by using the offset method 130
Figure 5.14 Numerical Load-Deflection for corroded steel girder 131
Figure 5.15 Experimental, proof yield, and proportional Limit of the tested beams..... 131
Figure 5.16 Deterioration factor vs. corroded length ratio for unstrengthened deteriorated beam 132
Figure 5.17 Deterioration factor vs. corroded length ratio for two unstrengthened deteriorated beams with different inertia losses..... 133
Figure 5.18 Deterioration factor vs. corroded length ratio for two unstrengthened deteriorated beams with the same inertia losses 134
Figure 5.19 Deterioration factor vs. corroded length ratio for strengthened deteriorated beam using 5 layers of Tyfo SCH-11UP with Tyfo S (F1B1), 5 layers of Tyfo SCH-11UP with MB-3 (F1B2), 1 strip of Tyfo UC with MB-3 (F2B2) 135
Figure B.1 Test results of beam BFO (a) Moment-Rotation; (b) Deformed shape 152
Figure B.2 Test results of beam BF-H0.33 (a) Moment-Rotation; (b) Deformed shape 153
Figure B.3 Test results of beam BF-N0.33 (a) Moment-Rotation; (b) Deformed shape 154
Figure B.4 Test results of beam BF-N0.50 (a) Moment-Rotation; (b) Deformed shape 155
Figure B.5 Test results of beam BF-H0.33-F1(5)-B1 (a) Moment-Rotation; (b) Deformed shape 156
Figure B.6 Test results of beam BF-N0.50-F1(5)-B1 (a) Moment-Rotation; (b) Deformed shape 157
Figure B.7 Test results of beam BF-H0.33-F1(5)-B2 (a) Moment-Rotation; (b) Deformed shape 158

Figure B.8 Test results of beam BF-N0.50-F1(5)-B2 (a) Moment-Rotation; (b) Deformed shape 159

Figure B.9 Test results of beam BF-H0.33-F2(1)-B2 (a) Moment-Rotation; (b) Deformed shape 160

Figure B.10 Test results of beam BF-H0.33-F2(1)-B2w (a) Moment-Rotation; (b) Deformed shape 161

Figure B.11 Test results of beam BF-H0.33-F1(1)-A1D1 (a) Moment-Rotation; (b) Deformed shape 162

Figure B.12 Test results of beam BF-H0.33-F1(1)-A2D1 (a) Moment-Rotation; (b) Deformed shape 163

Figure B.13 Test results of beam BF-H0.33-F1(5)-A2D2 (a) Moment-Rotation; (b) Deformed shape 164

LIST OF TABLES

Table 2.1 Summary of structural strengthening of metallic bridges (NCR 2007) 27

Table 3.1 Material properties (abstract from the Manufacture's Data sheet) 48

Table 3.2 Adhesives properties (abstract from the Manufacture's Data sheet) 48

Table 3.3 Test matrix 49

Table 3.4 Section properties of original and deteriorated steel cross sections 50

Table 4.1 Summary of the test results 86

Table 4.2 Summary of the comparison results 87

Table 5.1 Numerical Yielding and Ultimate Moment for different sections 120

Table 5.2 Experimental, Proportional, and Proof yielding moment for tested beams 121

LIST OF SYMBOLS

a	parameter determined from deterioration analysis
A_{cfrp}	area of CFRP, mm^2
A_{cor}	reduction area of the tension flange, mm^2
A_g	gross area of the cross-section, mm^2
b	parameter determined from deterioration analysis, width of the cross-section, mm
c	average corrosion penetration, microns
C_E	environnemental degradation factor
d	depth of cross-section, mm
E_{cfrp}	Young's modulus of CFRP, GPa
E_{frp}	Young's modulus of FRP, GPa
E_s	Young's modulus of steel, GPa
f'_{frpu}	mean strength of the FRP reported by the manufacturer, MPa
f_{cfrp}	stress in the CFRP, MPa
f_{frp}	stress in the FRP, MPa
f_{frpu}	ultimate tensile strength of the CFRP, MPa
f_y	yield stress of the steel, MPa
I_g	moment of inertia of the gross section, mm^4
L_b	total bond length, mm
$L_{b/layer}$	bond length per layer, mm
L_d	effective development length, mm
m	number of shear planes

M_r	moment resistance of steel beam cross-section, kN.m
M_y	yielding moment of the steel beam, kN.m
n	number of years or number of layers
ø	curvature, 1/mm
P	load applied by the hydraulic actuator, N
S	section modulus of the actual net area, mm^3
T_{cfrp}	axial force in CFRP, kN
t_{frp}	FRP thickness, mm
T_L	loss of the load carrying capacity, kN
Vr	factored shear resistance, kN
Y`	neutral axis depth, mm
α	factor of safety
Δ_x	distance between two strain gages
$\Delta\varepsilon$	strain difference
ε_c	compression strain of the steel cross-section
ε_{cfrp}	tensile strain of the CFRP
ε_{frpu}	ultimate tensile strain of the GFRP
ε_x	strain at any level of the cross-section
ε_y	yielding strain of steel beam cross-section
μ	average bond stress, MPa
μ_{max}	debonding stress, MPa
φ_b	resistance factor
Ψ_d	deterioration facto

LIST OF ABBREVIATIONS

AISC	American Institute of Steel Construction
ASTM	American Society for Testing and Materials
CFRP	Carbon Fibre-Reinforced Polymer
CISC	Canadian Institute of Steel Construction
FHWA	Federal Highway Administration
FRP	Fibre-Reinforced Polymer
GFRP	Glass Fibre-Reinforced Polymer
HM-CFRP	High Modulus Carbon Fibre-Reinforced Polymer
HSS	Hollow Steel Sections
LRFD	Load and Resistance Factor Design
NM-CFRP	Normal Modulus Carbon Fibre-Reinforced Polymer

CHAPTER 1

INTRODUCTION

1.1 BACKGROUND AND PROBLEM DEFINITION

Due to increasing traffic loads and deterioration of steel bridges, a large number of existing steel bridges require strengthening or even replacement. If strengthening appears to be an attractive option, the replacement alternative may involve costs and closure of traffic for long periods or, at least, substantial interference with the normal traffic flows. A traditional retrofit method for repairing structurally deficient steel members consists of attaching cover plates to these members through bolts or welding such that their flexural capacity to be increased. There are many disadvantages associated with these methods, such as: (1) the procedure is labour intensive and time consuming; (2) it requires drilling and extensive lap splice detailing; (3) traffic may have to be interrupted for a period of time; (4) a potential development for weld fatigue cracking at the cover plate ends and a region of high stress concentrations near the bolts; and (5) increase in the weight of the members. Consequently, in the last few years, extensive research was focused on strengthening steel bridges with fibre reinforced polymer (FRP) composite materials. The advantages of using this composite material are mainly due to their high strength to weight ratio, high fatigue resistance, and easiness and speed in the strengthening work intervention. While most of the previous research was focused on applications of adhesive-bonded FRP sheets or strips, it was found that there are many variables controlling the bond performance between FRP and steel, such as: bond length, adhesive type, adhesive thickness, surface preparation, and FRP type. Also, due to its

recent development, the long-term performance of the epoxy-bonded FRP strengthening method is not fully comprehended.

1.2 OBJECTIVES AND SCOPE OF WORK

The main objectives of this research are: to investigate the behaviour of steel bridge girders with locally and uniformly distributed corrosion over the tensile flange area and to analyze the influence of the location and area of corrosion; to explore different techniques which are able to increase the flexural capacity of deteriorated girders in elastic and post-yield ranges versus their original capacity by using bonded and unbonded Carbon Fibre Reinforcement Polymer composites material CFRP; and to evaluate the efficiency of the proposed retrofitted techniques. In order to achieve these main objectives, experimental and analytical studies are conducted. The scope of the research program is as follows:

EXPERIMENTAL PROGRAM

Through the experimental phase, a series of thirteen medium-scale deteriorated steel beams were tested to examine the behaviour of the unstrengthened and strengthened corroded steel girders. The tested beams were divided into four groups such as:

1. First group, G1 consisted of four beams with different percentages of simulated corrosion in order to investigate the influence of the area and location of corrosion on the flexural capacity of the deteriorated beam.
2. Second group, G2 consisted of four retrofitted beams strengthened with CFRP sheets bonded to the tension flange. The purpose of this studied group is to

emphasize the bond behaviour between the CFRP and steel including the effect of the CFRP and adhesive type.

3. Third group, G3 consisted of two strengthened beams with high-modulus CFRP laminate strips externally bonded to the bottom flange of the tested beam with the aim to characterize the influence of wrapping on the behaviour of retrofitted steel girders. The wrapping system was applied at one beam only.
4. Fourth group, G4 consisted of three simulated corroded beams strengthened with unbonded CFRP sheets by using ductile anchorage system. The main objective of this proposed scheme is two-fold: to reach the full capacity of the CFRP sheets and to increase the ductility of the strengthened steel bridge girders.

ANALYTICAL PROGRAM

In addition to the experimental work, an analytical procedure was developed and a numerical method was set up with the aim of predicting the elastic and post-yield behaviour of the unstrengthened and strengthened deteriorated steel girders. This numerical method can be used by designers to calculate the losses in the moment capacity of the deteriorated steel girders for an acceptable level of accuracy. As a result, the required amount of CFRP can be calculated based on the demanded level of safety. The carried out analysis is based on a moment-curvature method which satisfies equilibrium and compatibility. The analytical model was validated using the experimental results that were presented in the experimental work.

1.3 THESIS LAYOUT

The research work in this project is reported in six chapters. In chapter 1, background information related to strengthening of steel bridge girders using FRP composites is discussed in addition to the objectives and scope of the research program. Chapter 2 provides a literature review of the previous research topics which focused on the behaviour of corroded steel girders, traditional rehabilitation or/and strengthen techniques for existing corroded steel girders, and different techniques for the rehabilitation or/and strengthening of corroded steel girders by using FRP in different schemes. Chapter 3 discusses details related to the experimental program and includes: design, construction, test setup, and instrumentation of the tested beams. In Chapter 4, the results of each group of the experimental program are presented and discussed separately. Additionally, comparison between the different proposed strengthening schemes, as used in chapter 3, are conducted in this chapter. Chapter 5 contains the analytical model that was developed to predict the flexural behaviour of the strengthened and unstrengthened deteriorated steel bridge girders. This model is validated using the results of the experimental program which are presented in chapter 4. Chapter 6 contains the conclusions drawn from both experimental and analytical studies of this research program, as well as proposed recommendation for further research work. In addition, Appendix A presents a design example of the ductile anchorage system while, Appendix B provides additional results from the experimental program.

CHAPTER 2

LITERATURE SURVEY

2.1 INTRODUCTION

Large number of existing highway bridges in North America was designed and built in mid- 1900s for a design life of 75 years. As a result, in the coming decades, a high percentage of the existing bridge infrastructure will be in need to either strengthen their structurally deficient members or to upgrade their structural system. The Federal Highway Administration of the United States of America (FHWA), a part of the U.S. Department of Transportation, has developed a program to rate the deteriorated bridges through biannual inspection. According to the report which was carried out, the FHWA has a total of 603,168 bridges as of August 2009. 11.8% of these bridges were classified as structurally deficient while 13.0% were classified as functionally obsolete. More than 40% of the bridges that were classified as being deficient are steel structures. Similar bridge inventory data could not be found in Canada. However, the state of the bridges in Canada is expected to be more severe due to the harsh weather conditions. Based on the data from the FHWA, Figure 2.1 indicates the ratio of bridges with deficiencies among the highway bridges network in USA.

2.1.1 TRADITIONAL STRENGTHENING METHODS FOR STEEL MEMBERS

Many steel bridges in use today are in need of rehabilitation due to the loss of material in order to carry larger loads as demanded by an increased traffic. One of the most common strengthening methods in order to increase the load carrying capacity of deteriorated steel girders is to attach steel cover plates by welding, bolting, or adhering with or without additional use of bolts.

The addition of steel plates increases the section modulus and hence the flexural and the shear capacities of the deteriorated girder. Welding steel plates does not result in loss in the cross-section and is more economical compared to bolting or adhering steel plates. However, this method also holds some disadvantages, such as; high tensile residual stresses in the location of the weld which will reduce the fatigue life of the member. Several requirements are needed to be followed in order to ensure the quality of weld, such as: filler material, the surface of the base material, the treatment way, and the welder. However, using bolted steel plates does not have the same problems as was found in the welding processes, even if bolting steel plates reduces the cross-section area of the member and in consequence its capacity. The surface condition at the interface of the connected members is a very important parameter and any interfered materials will prevent the required friction to have good connection between these members. Albrecht and Sahli (1988) have concluded that the use of adhesively bonded steel plates with bolts increases the fatigue life by 20% over that of using conventionally welded plates.

All of the traditional retrofit methods applied to steel members add a significant weight to the structure, and it reduces their strengthening effectiveness. The added steel plates are also susceptible to corrosion, which leads to an increase in the future

maintenance costs. Also, these methods are labor and cost-intensive coupled with the need for on-site welding or drilling operations. The need for adopting durable material and cost-effective retrofit techniques is evident. In this case, one of the possible solutions is to use high performance, nonmetallic materials such as CFRP. The durability issues as well as the higher strength and stiffness required for the retrofit of the steel members make the using of the CFRP quite promising for rehabilitation and strengthening of the steel bridge structures.

2.1.2 EFFECT OF CORROSION ON STEEL BRIDGES

One significant cause of deterioration in steel bridges is the corrosion due to extensive use of deicing salts during the winter weather. Corrosion is one of the main contributors to the deficiency of steel bridge structures. The first step in the evaluation process is to identify the mechanism of the corrosion. Knowledge of the corrosion type can provide an indication of the degree and propagation of damage. Pitting and uniform corrosion are the most common shapes of corrosion observed in the steel bridges. Pitting corrosion occurs due to chemical or physical changes in the metal and it creates localized damage. Localized corrosion often occurs along the bottom flange of stringers and girders or in web of bridge columns. Uniform corrosion causes a relatively equally distributed reduction of the metal and it is usually found on flat surface such as girder webs, gusset plates, and flanges. The progression rate of the corrosion depends on the type of steel, the member consider and its location, the surface protection, and the presence of the pollutants as described by Albrecht (1984). The rate of corrosion is hard to be predicted and any change in the aforementioned factors could affect the level of

corrosion and its rate. The most common effect of corrosion is loss of material from the surface which leads to thinner sections, loss of material strength and rust on the surface. As a result, the section properties of the member would be reduced, therefore causing a reduction in their carrying capacity. Also, the class of the section may be changed due to the loss of compression flange and web thickness due to corrosion.

Kayser and Nowak (1989) developed a corrosion damage model for a simple-span steel girder bridges. The corrosion loss follows a power function

$$C = a \times n^b \tag{2.1}$$

where C is the average corrosion penetration in microns, n is the number of years and a and b are the parameters determined from deterioration analysis of the experimental data.

2.1.2.1 GALVANIC CORROSION

Galvanic corrosion results when two metals with different electrochemical potential are in contact with an electrolyte (e.g. water). Electrons exchanged occur due to the difference in the conductivity. The larger the potential difference is, the greater the probability of galvanic corrosion occurs. The metal with lower electrode potential becomes the anodic corrosion site while the higher electrode potential becomes the cathode. As a result of a high difference of conductivities between steel and carbon (the standard electrode potential of mild steel is -0.44 and for carbon +0.34) and due to the low electrode potential of steel, the steel surface becomes the anodic corrosion site, it oxidizes and corrosion occurs at a higher rate.

In order to prevent the galvanic corrosion, therefore to isolate the CFRP from the steel, precautions can be taken by using a non-conductive layer, such as an epoxy film or GFRP sheet. West (2001) concluded that isolating the CFRP from the steel surface by using an adhesive layer is sufficient to prevent the galvanic corrosion. On the other hand, Dawood (2006) found that mixing a small amount of glass beads into 1 mm adhesive thickness between the steel and the CFRP it slowed significantly the galvanic corrosion.

2.2 REMAINING CAPACITY OF CORRODED STEEL BEAMS

Kulicki et al. (1990) outlined a report about the guidelines for field inspection - of existing bridges. In this report is given the evaluation process of the load carrying capacity of bridges and methods for evaluating corroded members capacities. The guidelines includes: e: selection of the evaluation methods, evaluating the strength of the bridge members, defining the type of loads to be used loads calculation, and the required safety levels. The corrosion effect consists of thinning web or/and flange sections and as a results decreasing the load carrying capacity in shear, bearing, and bending.

Lindt et al. (2005) presented the results of experimental and analytical study of deteriorated steel beams with simulated percentages of material damage at the level of member cross-sections. In this respect, damaged area of various sizes and shapes was simulated. They developed a model that can provide a simplified approach for computing the reduced capacity of typical bridge girders. Four W18×106 beams, 36" in length with a bearing length of 5" and different damage depths and heights were tested at Michigan Technological University. A 0.25 inch steel plate was welded to the top flange of the girder in order to represent the deck effect and to simulate the rotational restraint of the

upper flange. Out of the four specimens they tested, two specimens experienced damage at the level of the web only, while the others two specimens experienced damage at the level of the web and flange with fillet included. In addition, for determining the remaining beam capacity, a numerical analysis was performed and a finite element method was used. . Based on the experimental and analytical results, design charts were developed for practical applications in order to allow designers to directly read the deterioration factor Ψ_d, and the ratio of the reduced beam capacity for given damage areas Two ensembles of design charts were developed:, one for asymmetric damage (one-side damage) and the other - for symmetric damage (two-side damage) as shown in Figure 2.2

Rahgozar (2009) carried out an analysis of two deteriorated I-beam samples with the purpose to obtain minimum curves for reliable estimation of the remaining shear, moment, and bearing capacity. Corrosion was simulated by a reduction in the thickness of the web and the flange as shown in Figure 2.3. Alongside the analytical work, four existing corroded beam, designed and erected 30 years ago were tested to evaluate their remained capacity. The results showed that a uniform thickness losses equal to 50% implies a 30% reduction of the remaining ultimate load capacity. Besides the effect of corrosion on the carrying capacity of the studied member, the class of the element section can also be changed (e.g. class two to class three). In consequence, the failure mechanism which depends on the relative thickness loss at various locations can be modified.

2.3 REVIEW ON THE RETROFIT OF STEEL STRUCTURES USING FRP

While extensive studies have been conducted on the use of externally bonded FRP for increasing the bending and shear capacity of concrete structures (where it has proved to be a suitable), little research has been completed on the feasibility and efficiency of using FRP to retrofit steel and composite structures.

Hollaway and Cadei (2002) published a review on upgrading metallic structures using advanced polymer composites. As mentioned in their review, the Civil Engineering Research Federation (2001) issued a report addressing the durability of FRP Composites in civil infrastructure. Their report identified seven areas into the long-term durability are needed for more research: alkaline environment, thermal effects, ultraviolet effects, creep and relaxation effects environment, fatigue performance, and fire performance. These areas were addressed in detail in their state-of-the-art as well as prestressing FRP plates before bonding and field application.

Shaat et al. (2004) presented a review on the use of FRP material in retrofitting steel structures. They addressed several issues including retrofit of steel girders, improving the fatigue life of steel girders using FRP, surface preparation, durability of steel members retrofitted with FRP and other factors to avoid debonding between the steel surface and FRP. As mentioned in their review, FRP sheets or strips can be used for strengthening steel structures to resist higher loads as well as a rehabilitated material for restoring the lost capacity of deteriorated sections. On the other hand, previous researches showed that bonding the FRP reinforcement to the compression side is not effective as bonding it to the tension side due to its low resistance of buckling.

Zhao and Zhang (2007) carried out an excellent review on strengthening steel structures using FRP. Four different bond testing methods were reported; applying direct load to FRP plate, applying direct load to steel element without or with a gap, and applying indirect load to the FRP and steel plate in a beam (see Figure 2.4). Strengthening of steel hollow section members, fatigue crack propagation in FRP-steel system, and bond between FRP and steel were discussed briefly in their report.

2.4 CHARACTERIZATION OF THE BONDING BETWEEN FRP AND STEEL

Bond between FRP and steel members has been considered as one of the main variables able to control the behaviour of FRP-strengthened steel members. There are many factors that characterizing the bond performance between the FRP and the steel such as; adhesive type, adhesive thickness, surface preparation, bond length, and the FRP type.

Miller (2000) carried out an experimental study to calculate the force transfer of reinforced tensile steel members using adhesively bonded CFRP strips. Six 914 mm long steel plates were strengthened using double side CFRP strips. All the specimens were loaded in tension until failure. Out of the six specimens, three specimens were bonded with Ciba-Geigy AV8113/HV8113 epoxy, while the other three were bonded using ITW Plexus MA555 structural adhesive. A glass fabric layer was placed between the steel plate and the CFRP laminates to prevent any galvanic corrosion. In terms of peel stresses, the ends of the CFRP strips were beveled to a 45% angle to reduce adhesive shear and peel stresses. An analytical model of the bonded joint was also conducted to investigate the adhesive shear stress and the CFRP strain distribution.

Frauenberger et al. (2003) published a detailed report on the bond behaviour of steel structures strengthened using FRP laminates. Seven different series of specimens were tested under static load. Six series consisted of discontinuous and one series of continuous specimens. All the specimens were designed such that the failure mode was controlled only by rupture or debonding of the FRP laminates. Their report addressed in detail the effects of the many factors that characterize the bond performance such as: specimen type, bonded length, horizontal wrapping of the specimens with CFRP sheets, FRP laminate type, adhesive type and thickness, surface preparation and curing time. An experimental work was done at University of Missouri-Rolla in United States, where a total of 56 specimens were tested to investigate the effect of the previous variables. Although the mode of failure of all specimens was observed to be debonding, two different strain distributions were observed. The first one was characterized as a brittle failure because the strain values dropped significantly while the second one was considered as ductile failure as it led to a load transfer over the bond length (see Figure 2.5)

The average bond stress between two locations was defined as:

$$\mu = t_{frp} E_{frp} \frac{\Delta_{\varepsilon}}{\Delta_x} \tag{2.2}$$

where μ is the average bond stress, t_{frp} is the FRP thickness, E_{frp} is the E-Modulus of the FRP, Δ_ε is the strain difference between two points, and Δ_x is the distance between two strain gages.

The effective bond length of the FRP to steel member can be defined as the shortest bond length engaging the largest possible strength of the FRP (Nozaka. 2001).A simplified equation for the development length was suggested by Frauenberger:

$$L_d = \frac{f_{frp}\, t_{frp}}{\alpha\, \mu_{max}} \tag{2.3}$$

where L_d is the effective development length, f_{frp} is the limit stress of the FRP, t_{frp} is the FRP thickness, μ_{max} is the debonding stress, and α is a factor of safety.

Based on the experimental results, they concluded that wrapping the specimens with CFRP-sheets did not impact the failure load and the peak strain significantly. The FRP laminate and adhesive properties had minor effect on the failure load and the peak strains.

El Damatty and Abushagur (2003) discussed the results of an experimental and analytical program which has been conducted to evaluate the shear and peel behaviour of strengthened steel connections using bonded FRP. A total of twenty hollow steel sections (HSS) bonded with GFRP plates were tested using MTS machine. The load was applied to the specimen through a thick plate attached to the top of the GFRP strips. Three types of failure modes were characterized in their experimental program; cohesive failure between the adhesive and the GFRP plates, cohesive failure between the adhesive and the steel section, and combination of the failure mode one and two. The in-plane and out-of-plane behaviour of the tested CFRP plates were described by a closed-form analytical solution.

Colombi and Poggi (2006) conducted an experimental program at the University of Milan to study the performance of strengthened tensile steel members using bonded CFRP pultruded plates. A total of eight specimens were tested under axial tensile static load, displacement control with a constant rate equal to 0.008 mm/s. In the first group, CFRP strips were used as double side strengthened for continuous steel plates to investigate the mode of failure of the adhesive joint and the load transfer mechanism. Double lap joints were tested in the second group. While in the last group, the bolted joints were reinforced with CFRP to study the local stress near the edge of the CFRP plates or near the discontinuities. In addition to the experimental program, an analytical model was carried out using the commercial finite element code ABAQUS to evaluate the static performance of the strengthened steel plates in the linear elastic zone.

Several other researchers conducted an experimental and/or analytical study that focused on the bond behaviour between the FRP and Steel plates or beams. Buyukoztrurk et al. (2004) reported a review of the progress achieved in the area of strengthening reinforced concrete and steel members using FRP composites. Stratford and Cadei (2005) described a method for designing the adhesive joint between a strengthening FRP plate and a beam. On another application of FRP in strengthening steel, Fawzia et al. (2006) carried out an experimental study to identify the behaviour of strengthened steel plates using CFRP plates under axial load. In addition to the experimental program, a nonlinear finite element analysis was conducted to predict the modes of failure and the load capacity. Al-Emrani and Kliger (2006) summarized the results of an analytical study conducted to study the interfacial shear stress in beams strengthened with bonded prestressed laminates.

2.5 STRENGTHENING OF STEEL GIRDERS WITH FRP

Gillespie et al. (1996) conducted an experimental study at the University of Delaware. Four deteriorated girders were taken from a 55 years old highway bridge. The bridge was constructed in 1940 in Vally View, Pennsylvania in western Schuylkill County. The girders had varied corrosion losses and it was noticed that the corrosion was mostly concentrated on the tension flange. To measure the loss in the elastic stiffness, the four girders were tested under three-point loading test at Lehigh University (1995). After that, they were delivered to the University of Delaware. Two of the deteriorated four girders were rehabilitated using FRP and tested until failure occurred. Although one of the girders had 32% stiffness loss while the other girder had 20%, the same percentage of the composite material was used to retrofit the both girders. Each girder was elastically cycled up to 222 kN and back. After two cycles, the girders were loaded until failure. Based on the test results, an average of 25% increase in stiffness and 100% increase in the ultimate load-carrying capacity were achieved. In addition to the full scale steel girders, a total of eight 1.50 m long W 8×10 steel beams using five different retrofitting schemes were tested until failure such as; composite plated, sandwich-reinforced, composite-wrapped, channel pultrusion-reinforced, and strip pultrusion-reinforced (see Figure 2.6). The specimens were tested under (1) service load, (2) and up to failure. The test results showed that increasing in the strength from 37% to 71% was achieved. The most effective retrofitted system under the service load and up to the ultimate strength was observed to be the sandwich-reinforced system.

Liu et al. (2001) investigated the behaviour of steel bridge members reinforced with FRP composite materials. Four W12×14 girders with clear span of 96 inch were tested under three point bending configuration. The first beam was tested as a control beam while the second beam had a 4" wide notch in the mid-span tension flange to simulate the severe loss of section due to corrosion. The third and fourth beams were strengthened with 3.94" wide CFRP laminates that covered the full length of the beam and one quarter of the beam length, respectively. Based on the experimental and the analytical results, increasing in stiffness and load capacity of deteriorated steel girders can be achieved by using bonded CFRP laminates.

Colombi and Carlo (2006-B) discussed the results of an experimental and analytical program which have been conducted to identify the static behaviour of reinforced steel beams using CFRP strips. Four steel beams were tested under three-point bending test. The clear span of these beams was 2.50 m. Out of the four beams; one beam was tested without strengthening as a reference case while the others were strengthened with bonded CFRP strips. Different analytical and numerical analysis were conducted in their paper to validate the experimental results. A finite element model was developed using the commercial code ABAQUS to evaluate the stresses in the reinforced beams and in the adhesive (see Figure 2.7).

An experimental and analytical study was conducted by Lenwari et al. (2006) to investigate the bonding strength of steel beams strengthened with CFRP strips. A total of seven W100×17.2 steel beams were tested using four-point bending test after reinforced with CFRP plates. Three different lengths of CFRP plates were used in this investigation. A unidirectional CFRP plate, Sika CarboDure H514, with a two-part epoxy adhesive,

Sikadur 30, was used to strengthen the tested beams. A steel plate was welded to the compression flange to prevent any compression failure. Increasing in the ultimate flexural capacity was achieved for all tested beams with different ratio of CFRP.

Patnaik et al. (2008) conducted an experimental study in order to describe the behaviour of steel beams strengthened with CFRP. To investigate the increasing in the flexural capacity, three beams were strengthened using boded CFRP to the tension flange. While to enhance the shear capacity, three others beams were retrofitted using bonded CFRP to the web. A unidirectional laminate strip was used in this investigation (Tyfo UC Composite Laminate Strip system) with a manufacturer tensile modulus of 155Gpa and a tensile strength of 2790MPa. Built up steel section was used for all beams. The first type of beams was strengthened to fail in flexural with a flange width and thickness of 152.5 mm and 9.5 mm, respectively and web height and thickness of 305 mm and 9.5 mm, respectively. The second type was designed to fail in shear with a flange width and thickness of 254 mm and 12.7 mm, respectively and web height and thickness of 330 mm and 3.2 mm, respectively. Four point bend tests were performed with a clear span of 3.15 m and 610 mm constant moment zone. Based on the experimental results, the CFRP laminates could significantly improve the ultimate flexural and shear capacity to 30% and 26%, respectively. A typical shear failure mode is shown in Figure 2.8.

Deng et al. (2004) presented an analytical model to calculate the stresses in reinforced beam under thermal and mechanical loads. Hollaway et al. (2006) discussed the advantages and limitations of bonding FRP composites to steel structural members. An ultra high and high stiffness CFRP were used in this study and two test techniques namely, double shear and flexural test. The composite material was used for reinforced

the artificially degraded structural member. A similar experimental study was conducted by Photiou et al. (2006) who strengthened an artificially degraded rectangular cross-section and testing them under four-point loading. Ezzeldin (2006) developed a numerical investigation to investigate the effect of bonding CFRP strips to the webs of I-Section steel beams in order to increase the flexural capacity.

2.6 STRENGTHENING OF STEEL-CONCRETE COMPOSITE GIRDERS USING FRP

Sen and Liby (1994) conducted the first study to investigate the applications of using CFRP to steel-concrete composite girders. An experimental and analytical study was carried out on wide flange steel beams reinforced with CFRP. A total of six 20' long beams consisted of composite W24×24 steel section assembly with a 28"wide and 4.5" thick reinforced concrete slab were tested in this investigation. CFRP laminates 6" wide, 12' long and two different thicknesses of 0.08" and 0.22" were bonded to the tension flange using the FR-1272 two-part epoxy adhesive. Based on the test results, the authors concluded that the high percentage of the load transferred to the CFRP laminate occurred after the tension flange had been yielded. This study indicated that the CFRP laminates can increase the ultimate flexural capacity from 11 to 15%, depending on the tensile strength of the steel member and the CFRP laminate.

Miller et al (2001) investigated the flexural behaviour of reinforced steel composite girders using CFRP laminates through experimental and numerical studies to evaluate the potential benefit of using the CFRP laminates. A brief review of several laboratory studies carried out at the University of Delaware were presented in their paper which confirmed that CFRP plates has significant impact in increasing the flexural

capacity of steel bridge girders. Four full scale strengthened bridge girders were tested to evaluate the performance of the retrofitted system in terms of stiffness and strength. The four girders were 21-ft American standard steel beams S24×80 taken from an existing bridge. The corrosion was observed to be uniform along the length of the tested girders. First, the deteriorated girders were tested under static three-point bending test without rehabilitation. Afterward, the four girders were strengthened with a single layer of full-length bonded CFRP plates. The experimental results showed that the CFRP composite material increased the elastic stiffness from 10% to 37%, while the ultimate capacity increased from 17% to 25%.

Tavakkolizadeh and Saadatmanesh (2003) investigated the effect of CFRP sheets on the behaviour of deteriorated composite steel-concrete beams under static loading. Three large-scale composite girders were tested in this study. The steel girders were W355×13.6 A36 structural steel. A composite concrete slab 910 mm wide by 75 mm thick was used in all girders. In order to evaluate this technique, three different damage levels of 25, 50, and 100% loss of the bottom flange were considered. Different number of CFRP sheet layers of 1, 3, and 5 were used to retrofit the different levels of damage. Four point bending tests were performed with a clear span of 4.78 m to test the girders until failure occurs. Based on the analytical and experimental results, the retrofitted system showed an increasing in the ultimate load-carrying capacities of the girders significantly increased by 44, 51, and 76% for 25, 50, and 100% damaged, respectively. In addition, the yield load of the girders increased as a result of retrofitting. The authors reported that the efficiency of members strengthened with the CFRP sheet was decreased as the number of the CFRP layers was increased.

El-Saidy et al (2004) carried out an experimental and analytical study in order to describe the behaviour of steel concrete composite beams strengthened using bonded CFRP plates. Removing part of the tension flange was used to simulate the damage of the beam, which was varied between no damage and loss of 75% of the bottom flange. A total of six 3.05 m long beams comprised of W8×15, grade A572 structural steel, attached to 812 mm wide by 76 mm thick concrete slabs, with an average compressive strength 33 MPa, were tested. The experimental study consisted of two controls undamaged beams, and four damaged beams which strengthened using bonded CFRP strips to reach to their original strength. All beams were tested in four-point bending static loading to failure to observe their behaviour in the elastic, inelastic, and ultimate states. The analytical study developed in their paper was based on some assumptions such as; small deformations, plane sections before bending remain plane after bending, tensile strength of concrete is neglected and full bond between the CFRP and steel was considered. Based on the analytical and experimental results, the elastic flexural stiffness of deteriorated beams can be increased by 50%, while the strength of the damaged beams can reach to its original strength.

The behaviour of steel-concrete composite girders reinforced using High Modulus (HM) CFRP was investigated by Dawood et al. (2006). Two types of CFRP laminates were used in this program, DC-1 with a tensile strength and a tensile modulus equal to 1224 MPa and 229 GPa, respectively, and THM-450 with a tensile strength and a tensile modulus equal to 1224 MPa and 229 GPa, respectively. Two-part epoxy adhesive, Spabond 345, was used to bond the CFRP plates to the tension flange of the steel girder. A total of nine steel girders were tested in this investigation. The beams were

strengthened with different levels of CFRP plates and tested in a four point bending test. The first phase simulate the behaviour of the strengthened girder under static load while in the second phase, the behaviour of the beams under overloading conditions was investigated. The fatigue behaviour of the strengthened girder was considered in the third phase. Three beams were tested in each phase. Based on the experimental results and the analytical model of the tested girders, the following equation was proposed by the authors for design the strengthened girder:

$$f_{FRP,u} = C_E\,(f`_{FRP,u} - 3\sigma) \tag{2.4}$$

Where $f_{FRP,u}$ is the design strength of the FRP materials, C_E is the environmental degradation factor (typically taken as 0.85 for CFRP), $f`_{FRP,u}$ is the mean strength of the FRP reported by the manufacturer and σ is the reported standard deviation of the FRP strength.

Another study was conducted by AL-Saidy et al. (2007). The paper presented an analytical parametric study on the behaviour of steel-concrete composite beam that has been strengthened with CFRP Strips. The parametric study had in-depth coverage on the effect of the concrete compressive strength, the yield strength of the steel, the stiffness of the CFRP strip, the thickness of the CFRP strip and the ultimate strain of the CFRP strip. The composite section which is used in this investigation consisted of a W18×46 steel section with a 190 mm thick reinforced concrete slab and an effective slab width of a 1900 mm. The yield strength of the steel beam was 250 MPa and the compressive strength of the slab concrete was 21MPa. The authors reported that when the damage in the bottom flange was 75% the reduction in the ultimate moment capacity reached 32%. Based on the analytical results, using a thin strip CFRP with high stiffness has impact

efficient than using a thick strip with low stiffness. In addition to, the concrete compressive strength has a slight effect on the ultimate moment capacity of the strengthened or unstrengthened composite sections. Also it was mentioned that reinforced steel member by using CFRP reduces the ductility of the girder element. Moreover, using CFRP to strengthen steel section with low yield stress is more efficient than using it to retrofit steel members with high yield stress steel.

2.7 FATIGUE PERFORMANCE OF STEEL MEMBERS RETROFITTED WITH FRP

Recently, few researchers have conducted experimental and analytical studies to investigate the fatigue performance of steel plates or beams strengthened with a bonded FRP. Farahani et al. (2007) developed an energy-based fatigue damage parameter to assess the fatigue damage of unidirectional GRP and CFRP composites while Nozaka et al. (2005) reported a fundamental study on the use of CFRP strips for repairing fatigue damaged tension flanges of steel girders. Deng et al (2005) carried out a fatigue test program of a series of small scale beams strengthened using CFRP plate to evaluate the change in the stiffness of the retrofitted beams with crack development and to develop curves to estimate the design fatigue lives.

To prevent fatigue cracking or to extend fatigue life, Jones and Civjan (2003) summarized the results of an experimental and analytical study to investigate the efficiency of strengthening steel fatigue tension coupons using bonded CFRP. Cold rolled A36 steel bars with a measured yield and ultimate stresses of 345 MPa and 490 MPa, respectively, were tested in this investigation under axial tension. Out of 29 specimens

that were tested, eight specimens had a center hole while the others were notched at the ends. The finite element model program ANSYS 5.7 was used in this study to develop Static linearly elastic models to determine the stress concentration based on geometry of the specimens. Based on the experimental and analytical results, an increase in the fatigue life for all specimens tested was achieved.

An experimental program was conducted by Tavakkolizadeh and Saadatmanesh (2003) to investigate the impact of bonded CFRP strip to steel beams in order to extend the fatigue life. A total of fifteen unretrofitted beams and six retrofitted beams were tested under different stress range cycles. All specimens were S127×4.5 A36 with clear span of 1.22 m. the experimental results showed that retrofitted beams experienced longer fatigue lives in range of 2.6 to 3.4 times the unretrofitted beams for stress ranges of 345, 207 MPa, respectively. In addition, the retrofitted beams were able to carry a few extra cycles even after the tension flange had completely cracked. The average total number of cycles until failure occurred for retrofitted beams was 3.5 times the one for unretrofitted beams.

2.8 METALLIC BRIDGES STRENGTHENED WITH FRP

The National Research Council Canada (NRC) published a technical document (2007) that mentioned several examples of strengthened bridges with FRP and other metallic structures throughout Europe as well as in the USA. Summary of the structural strengthening of metallic bridges is shown in Table 2.1. The Hythe Bridge, built in 1874 over the river Thames, is a two spans bridge with a clear span of 7.8 m. The main girders were prestressed by CFRP laminates and sheets (Luke 2001). The Tickford Bridge made

up of six girders with a span equal to 18.29m and was built in 1810 near Newport Pagnell (UK). To increase the traffic volume (Lane and Waed 2000), a total of 14 layers of FRP were laminated on the substrate to strengthen the bridge. A single span bridge, Slattocks Canal Bridge that was built in 1936 over the Rochdale canal (UK), was strengthened with two CFRP laminates. The CFRP laminates were applied to the existing girders (Luke 2001). A timber deck with steel girders bridge, Acton Bridge, was strengthened by applying Pultruded CFRP laminates to the tension flange of the girders in order to increase the fatigue resistance (Moy et al. 2000). The King Street Bridge is a railway bridge built in England in 1870. It has six metallic girders that maintain masonry arches. Two CFRP laminates were applied longitudinally to tension flange of the girder while other GFRP laminates were applies transversally to prevent galvanic corrosion.

The Corona Bridge was built in 1850 and is characterized by three cast iron arches. In 2002, the arches and their decorative openings were strengthened with aramid tri-axial sheets and mono-directional strips to increase the resistance due to any impact load and to stop any further damages. Christina Creek, Ashland, and 7838.5S092 bridges in USA were strengthened using bonded CFRP laminates to increase the fatigue lifetime.

2.9 SUMMARY

A review of previous research on FRP strengthened steel structures was presented in this chapter. Based on the findings of several experimental investigations, it is shown that externally bonded CFRP can be used to effectively strengthen and repair steel bridge members, especially cast ironing section. As mentioned earlier, there is not much experimental work associated to the remaining capacity of corroded Beams. Also, more

research is still needed to investigate the behaviour of strengthened deteriorated steel beams using CFRP sheets as most of the previous research have focused on CFRP laminates. Also, it was shown that there are many factors that characterize the bond performance between the FRP and the steel. However, extensive research is needed in the field of strengthening deteriorated steel beams using new methods, e.g. mechanically anchored CFRP sheets.

Table 2.1 Summary of structural strengthening of metallic bridges (NCR 2007)

Strengthening Context	Type	Material	Strengthening Method	Final Result	Date
Tickford Bridge, England. Vehicle Bridge	Concrete arches and Structure	Cast Iron	Bonding of pre-impregnated CFRP laminates with polyester Underlay	Reduction of stresses on the original material	1999
Hyhte Bridge, England. Vehicle Bridge	Reserved T girders and masonry arches	Cast Iron	pre-stressing of CFRP laminates	Elimination of tensile stress on girders due to variation of loading conditions	2000
Slattocks Canal Bridge, England. Vehicle Bridge	T girder and concrete deck	Steel Early	Bonding of CFRP laminates	Increase of the load bearing capacity	2000
King Street. Bridge, England. Vehicle Bridge	T girder and masonry arches	Cast Iron	Bonding of pre-impregnated CFRP and GFRP laminates	Increase of the load bearing capacity	2000
Acton Bridge, England. Railway Bridge	T girder and timber deck	Steel Early	Bonding of CFRP laminates	Reduction of strain on the original material, increase in service life and fatigue resistance	2000
Corona Bridge, Italy. Pedestrian Bridge	Cast iron arches	Cast Iron	Bonding of aramid tri-axial laminates and mono-directional strips	Reduction of vulnerability to thermal shocks and impacts loading	2002
Christina Creek Bridge, USA. Vehicle Bridge	Composite steel-concrete girders and deck	Steel	Bonding of CFRP laminates	Pilot project to analyze the fatigue resistance as well as sensitivity to environmental agents	2000
Ashland Bridge, USA. Vehicle Bridge	Composite steel-concrete girders and deck	Steel	Bonding of CFRP laminates	Stress reduction on the original material to increase the fatigue lifetime	2002
7838.5s092 Bridge, USA. Vehicle Bridge	Composite steel-concrete girders and deck	Steel	Bonding of CFRP laminates	Stress reduction on the original material to increase the fatigue lifetime	2003

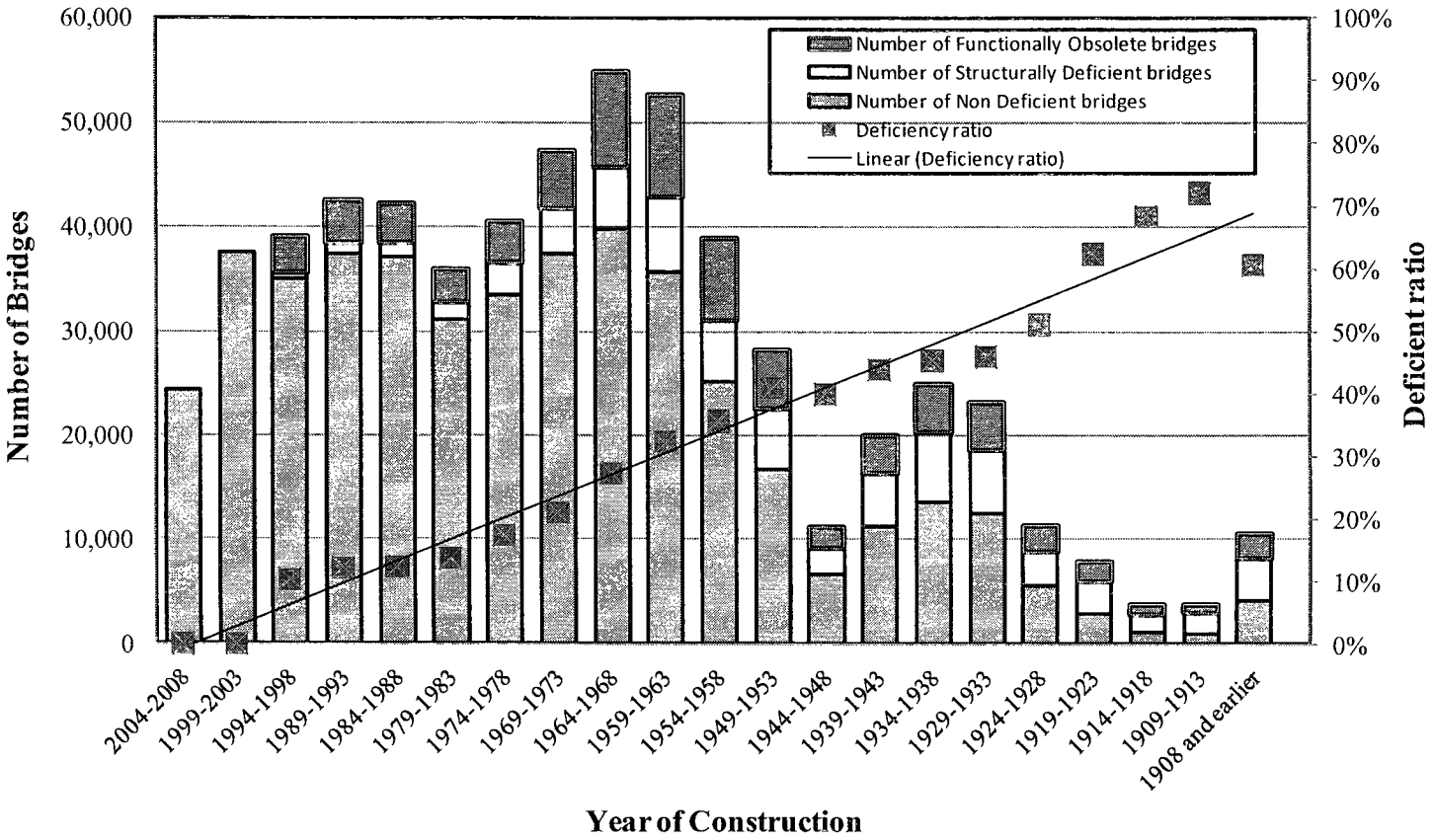

Figure 2.1 Deficiency ratios of the existing bridges (FHWA 2009)

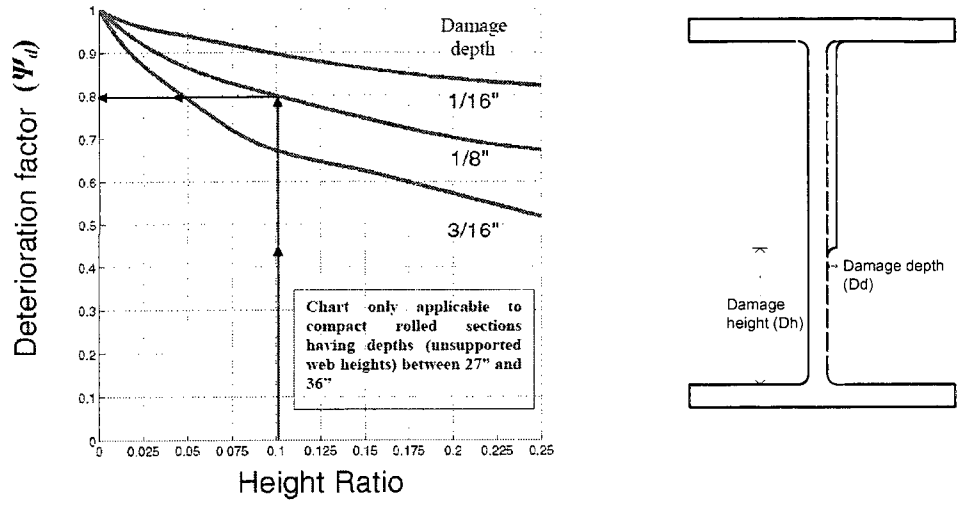

(a) Design chart for damage on one side of the web

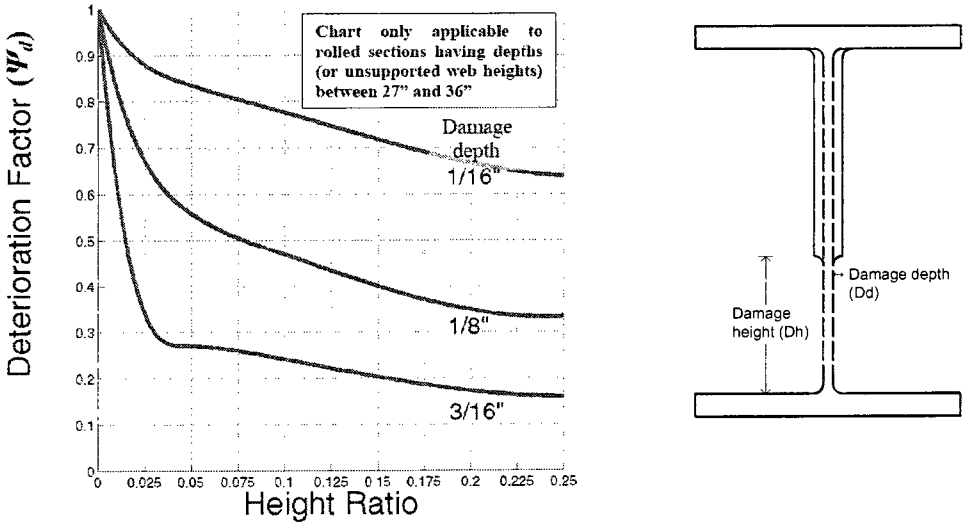

(b) Design chart for damage on both sides of the web

Figure 2.2 Design charts related to deterioration factor (Ψd) (Lindt and Ahlborn 2004)

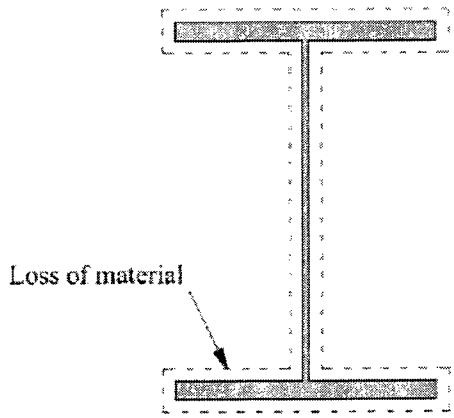

Loss of Material

Flanges	ξT_N
Web	ξt_N

where T_N and t_N are the thicknesses of the flanges and web of as-new section,
$\xi = \%LFT/100 = \%LWT/100$,
$\%LFT$ = Percentage loss of flange thickness
$\%LWT$ = Percentage loss of web thickness

(a) Uniform thickness loss (Model 1)

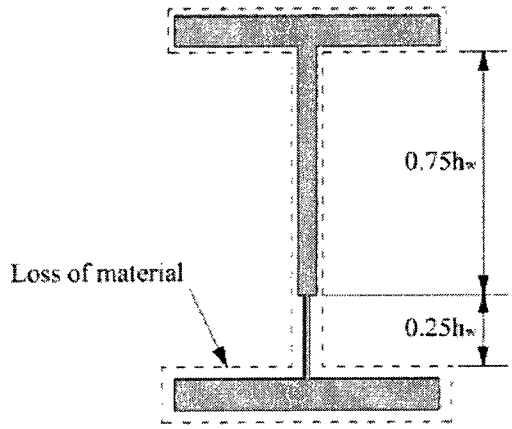

Loss of Material

Top Flange	$0.75\xi T_N$
Upper part of the web $(0.75h_w)$	$0.25\xi t_N$
Lower part of the web $(0.25h_w)$	$1.25\xi t_N$
Bottom flange	$1.3\xi T_N$

where $\xi = \%LFT/100$

(b) Varying thickness loss (Model 2)

Figure 2.3 Models of corroded sections simulation by reducing the thickness of the element (Rahgozar 2009)

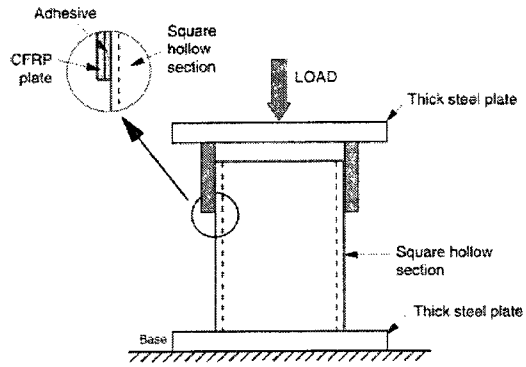

(a) Applying direct load to FRP plate

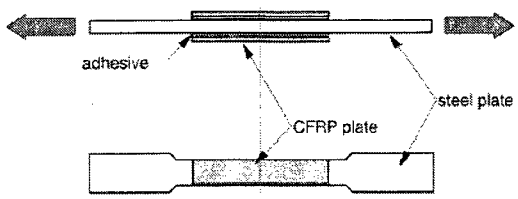

(b) Applying direct load to steel element without any gap

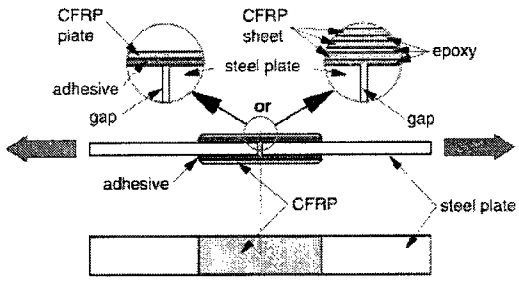

(c) Applying direct load to steel element with a gap

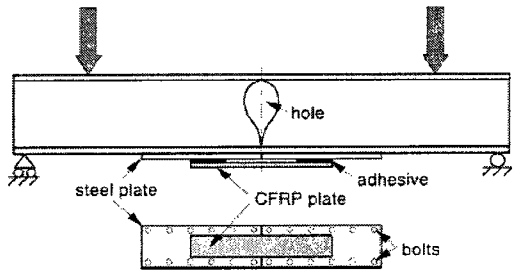

(d) Applying indirect load to the FRP and steel plate in a beam

Figure 2.4 Bond test methods (Zhao and Zhang 2007)

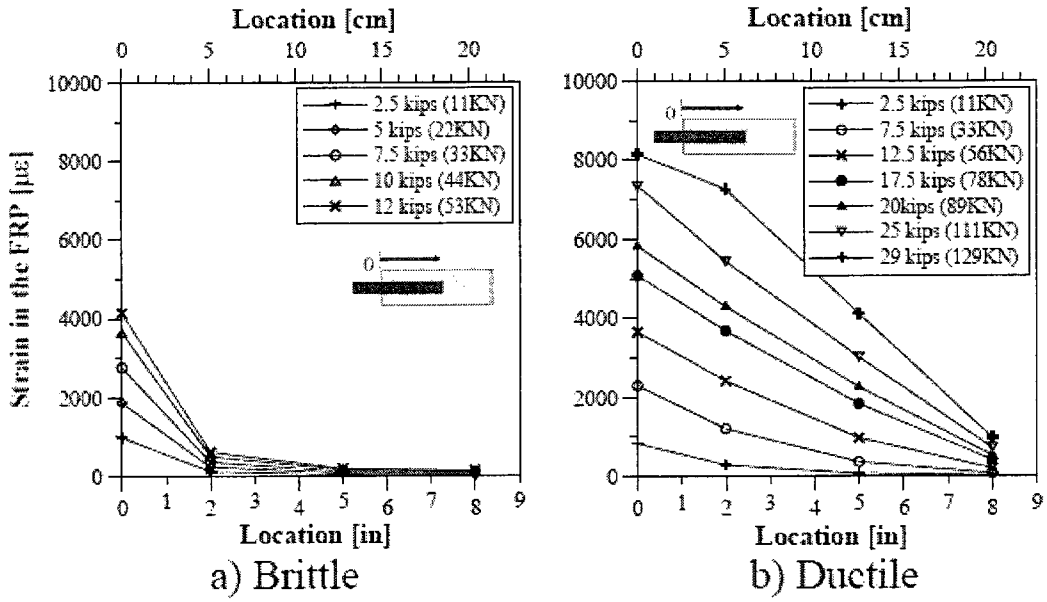

Figure 2.5 Typical strain profile of CFRP bonded to steel plate (Frauenberger et al. 2003)

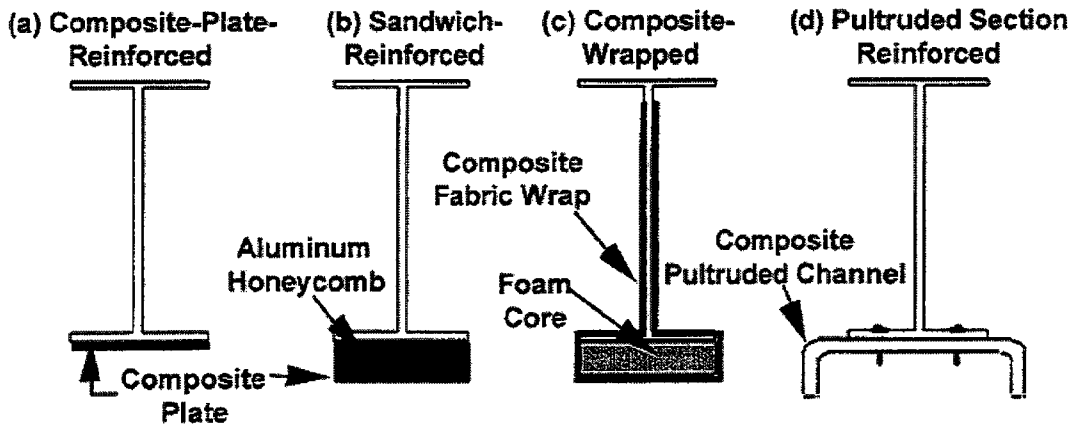

Figure 2.6 Different rehabilitation geometries for steel beams (Mertz and Gillespie 1996)

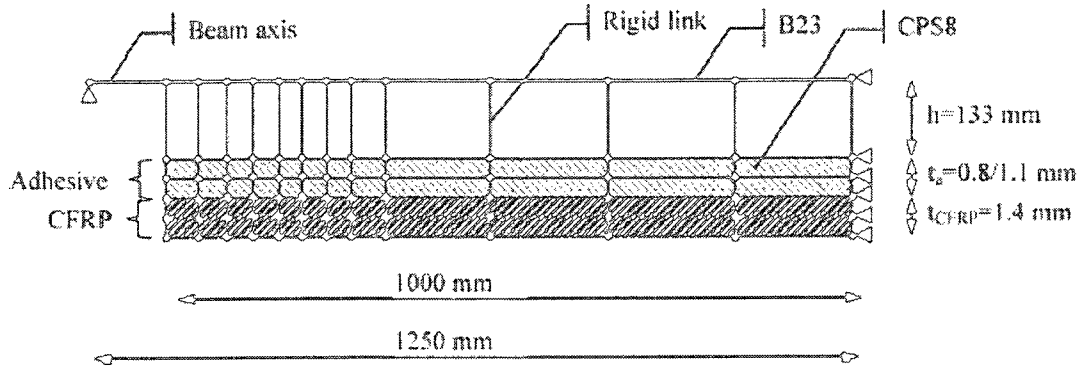

Figure 2.7 Modeling of the bonded reinforcement and required constrains of the steel beam using the commercial code ABAQUS. (Colombi and Carlo 2006-B)

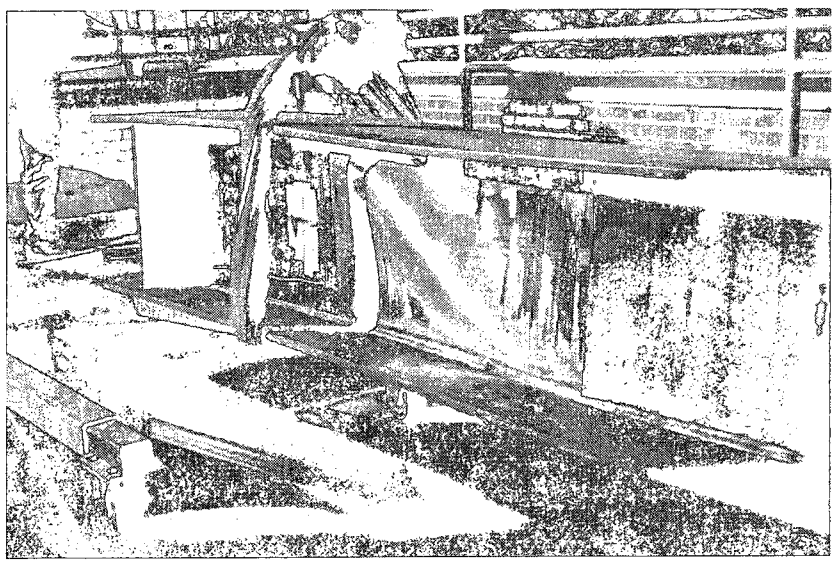

Figure 2.8 Typical shear failure of steel girders strengthened with CFRP (Patnaik et al. 2008)

CHAPTER 3

EXPERIMENTAL WORK

3.1 GENERAL

The main objectives of this research work were to predict the reduction in the flexural capacity of existing deteriorated steel beams under static loading and to develop retrofitting schemes capable of increasing their flexural capacity to the original design level. In order to achieve these objectives, an experimental research program was carried out at the Engineering Structural Research Laboratory of Concordia University. A total of thirteen W 150×30 steel beams with a clear span of 1.6 m and different level of deterioration due to corrosion were tested under four-point bending test. Out of the thirteen beams, four beams were prepared to emphasize different level of corrosion and were tested without retrofitting to investigate their behaviour and the other nine beams were strengthened using CFRP sheets and strips to evaluate the effectiveness of the proposed retrofitting schemes in term of stiffness and strength. All the tested beams were designed by controlling the failure mechanism such that the out-of-plane buckling to be avoided. In this respect, the unstrengthened beams were controlled only by in-plane buckling mechanism, while the strengthened beams by rupture or debonding of the CFRP materials. This chapter describes in details the experimental protocol including: specimen designation, construction of the specimens, material properties, instrumentation, experimental setup and experimental procedure.

3.1.1 PROPERTIES OF THE TESTED STEEL BEAMS

A uniaxial tension test was performed on three dog-bone specimens according to ASTM E 8M-1 (2007). Out of the three specimens, one specimen was cut from the web, while the others were cut from the top and bottom flange, respectively. All the specimens had a gauge length of 50 mm, a gauge width of 12.7 mm, and a thickness of 9.3 mm and 6.6 mm from the flange and the web, respectively. Average yield strength (F_y) of 310 MPa and modulus of elasticity (E) of 198.7 GPa were obtained from the specimens. A typical stress-strain relationship for the three dog-bone specimens is shown in Figure 3.1. The test setup and the typical failure mode for the tested specimens are shown in Figure 3.2.

3.1.2 MATERIALS USED

The steel plates used in this investigation are characterized by 6.35 mm and 12.7 mm thickness, a modulus of elasticity of 200 GPa and yielding strength of 300 MPa. Two types of CFRP composite material were used in this study, Tyfo SCH-11UP and Tyfo UC. Tyfo SCH-11UP is a unidirectional carbon fibre sheet with a tensile modulus of 102 GPa and a thickness of 0.27 mm, while Tyfo UC composite is a unidirectional carbon fibre laminate strip system with a high tensile modulus of 155 GPa and a thickness of 1.4 mm. To prevent any galvanic reaction between the steel surface and the carbon fibre, as discussed before in Chapter 2, one layer of Tyfo EP-DB was used between the carbon fibre reinforced polymers and the bottom flange of the tested steel beams. Tyfo EB-DB system is an open weave glass fibre was used as a dielectric barrier between the CFRP composite material and steel. In addition to Tyfo EP-DB was used to prevent any

galvanic reaction, it also allows adhesive to pass through the opens weave and fully develop the required bond strength. The mechanical properties of the steel plates and the CFRP composite materials are shown in Table 3.1.

Two types of adhesive were used in this experimental program: Tyfo S and Tyfo MB-3. Tyfo S is a two-component saturant epoxy which is combined with Tyfo SCH-11UP sheets to provide a wet-layup composite system. Tyfo MB-3 is a two-component viscous epoxy adhesive which is specially designed to bond the CFRP laminates to the steel surface. Tyfo MB-3 provides excellent peel and impact strength for bonding fibre reinforced polymers to steel surface. Table 3.2 shows the mechanical properties of the adhesive material which were used in this investigation.

3.1.3 RETROFIT SCHEMES

Figure 3.3 indicates the strengthened cross-section and the designation of the variables used. In this context, A_o, A_{cor} and A_{CFRP} are the original cross section area, the lost area of the tension flange which simulated the corrosion and the area of the CFRP used in the strengthening process. The design approach was based on balancing the loss of the load carrying capacity (Eq. 3.1) by an increased load due to the retrofit scheme (Eq. 3.2).

$$T_L = A_{cor} F_y \tag{3.1}$$

where T_L, A_{cor} and Fy are the loss of the load carrying capacity, the reduction area of the tension flange and the yield strength of the tested steel beam, respectively.

$$T_{CFRP} = A_{CFRP} F_{rup} \tag{3.2}$$

where, T_{CFRP}, A_{CFRP} and F_{rup} are the increasing of the load due to the retrofit scheme, the area of the CFRP used in the retrofitting and the ultimate tensile strength in the primary fibre direction, respectively.

According to the loss in the load carrying capacity balance, the following equation can be used to determine the required CFRP cross sectional area:

$$A_{CFRP} = \frac{A_{cor} F_y}{F_{rup}} \tag{3.3}$$

Where,

$A_{cor\ (max)}$ = 50% from the tension flange area = 711.45 mm^2

F_y = 310 MPa

F_{rup} = 1062 MPa Tyfo SCH-11UP

= 2790 MPa Tyfo UC

As a result,

For all strengthened beams using Tyfo SCH-11UP

$$A_{CFRP} = \frac{711.45 \times 310}{1062} = 207.7\ mm^2$$

$\cong$ **5 layers (150 × 0.27) mm^2** = 202.5 mm^2

For all strengthened beams using Tyfo UC

$$A_{CFRP} = \frac{711.45 \times 310}{2790} = 76.5\ mm^2$$

$\cong$ **1 strip (50.8 × 1.4) mm^2** = 71.1 mm^2

For ductile anchorage system, this system was divided into three parts as shown in Figure 3.4. The material properties of the steel plates which were used for the ductile anchorage system are shown in Table 3.1.

As shown in Figure 3.4, part 1 was designed to transfer the load from the CFRP to two ductile coupons (part 2). These two ductile coupons were used to control the ductility of the anchorage system as will be shown after and to transfer the load to part 3. Part 3 was designed to transfer the load to the tension flange near to the supports, as minimum stress in the tension flange, using four high tensile bolts. The force in the ductile coupons was controlled to be axial tension force by allowing parts 1 and 2 to rotate around axis AA` of part 3 as shown before in Figure 3.4. Appendix A presents a design example of the ductile anchorage system.

3.1.4 SPECIMEN LABELING CONVENTION

To facilitate the reference of each beam tested under different conditions the specimen labeling convention is as follows:

$$(BF)-\begin{pmatrix}0\\H0.33\\N0.33\\N0.50\end{pmatrix}-\begin{pmatrix}F1(1)\\F1(5)\\F2(1)\end{pmatrix}-\begin{pmatrix}B1\\B2\\B2w\\A1D1\\A2D1\\A2D2\end{pmatrix}$$

Where:

- The first variable in the beam notation refers to the flexural capacity of the beam.
- The second variable in the beam notation describes the shape and the area of the reduction in the beam cross-section. The designations H and N refer to locally and

uniformly deterioration, respectively, while 0.33 and 0.50 are used to refer to the percentage of the area reduction of the tension flange.

- The third variable refers to the CFRP material type used to increase the flexural capacity and the number of layers. The designation F1 and F2 are stand for Tyfo® SCH-11UP and Tyfo® UC, respectively.
- The fourth variable depicts the techniques used to attach the CFRP composite material to the bottom flange of the tested beam. The designations B1, B2, B2w, A1,A2,D1 and D2 are used to refer to;
    a. (B1) Bonded by using saturant epoxy Tyfo® S.
    b. (B2) Bonded by using high performance adhesive Tyfo® MB-3.
    c. (B2w) Bonded by using high performance adhesive Tyfo® MB-3 with Tyfo® CH-11UP wraps.
    d. (A1) anchored by using Coupon1.
    e. (A2) anchored by using Coupon2.
    f. (D1) anchored by using detail 1.
    g. (D2) anchored by using detail 2.

The following example illustrates the used beam notation. When a beam is referred to as:

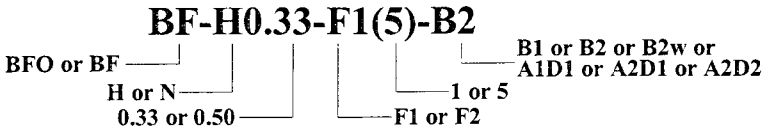

This means that:

We are investigating the flexural capacity of a deteriorated steel beam with 8-6.35 mm holes in the bottom flange at the mid-span cross section strengthened with 5 layers of Tyfo® SCH-11UP bonded to the bottom flange using Tyfo® MB-3.

3.2 TEST LAYOUT

In this experimental program, a series of thirteen small-scale deteriorated steel beams were tested to examine the behaviour of the unstrengthened and strengthened deteriorated steel girders. Each specimen was cut to a length of 2.0 m and was tested with a clear span of 1.6 m. The clear span selected to have a (h/L) ratio equal to 0.1, where (h/L) is the ratio of the total depth to the clear span of the tested beam. The tested beams were divided into four group: group one (G1) consisted of four beams with different percentage of deterioration to investigate the behaviour of the deteriorated beam and to determine the remaining capacity, while the other three groups were designed to evaluate the effectiveness of the proposed retrofit schemes. Four beams were strengthened with CFRP sheets bonded to the tension flange and were tested in group two (G2) to characterize the static behaviour of steel beams strengthened with CFRP sheets. Group three (G3) consisted of two beams strengthened with high-modulus CFRP laminate strips, which were externally bonded to the bottom flange of the tested beam. Unbonded CFRP sheets were used to strengthen three deteriorated steel beams in group four (G4) by using ductile anchorage system.

Based on the previous discussion in Chapter 2 (Literature review), the corrosion was mostly concentrated on the bottom flange. As a result, the corrosion in all tested beams was simulated by a reduction area in the tension flange. Two different damage levels of 33% and 50% area reduction of the tension flange were considered in this study. 100 mm depth transverse stiffeners were provide on either side of the web of the all tested beams at the location of the applied loads and supports to prevent local web

yielding and web crippling as specified by the CAN/CSA S16-09 Limit States Design of Steel Structures (2009). The test setup is shown schematically in Figure 3.5.

3.2.1 DESIGN OF GROUP 1 BEAMS

Three beams out of four in this group (group 1) were designed to investigate the behaviour of locally and uniformly deteriorated steel beams. The relation between the deterioration ratio and the remaining moment capacity was one of the major objectives in this group. Out of the four beams, one beam, BFO, was designed to demonstrate the behaviour of a non-deteriorated steel beam. The flexural capacity of this beam was used as a control beam or to define the capacity of the initial beam. Figure 3.6 presents a typical cross-section of non-deteriorated beam. In order to observe the effectiveness of the locally and uniformly deterioration on the remaining capacity, three steel beams were designed with two different level of deterioration. Beams BF-H0.33 and BF-N0.33 had a 33% area reduction of the tension flange, while beam BF-N0.50 had a 50% area reduction. This area reduction was constructed by using mailing machine as shown in Figure 3.7. Figures 3.8, 3.9, and 3.10 show test setup, plan view of the bottom flange, and section at the mid-span for beams BF-H0.33, BF-N0.33, and BF-N0.50, respectively. As shown in these Figures, the area reduction in beams BF-N0.33 and BF-N0.50 was notches with a length of 450 mm in the mid-span to simulate the uniformly deterioration, while in beam BF-H0.33, it was a concentrated reduction in the mid-span to simulate the locally deterioration. The cross-section area properties of the different sections are shown in table 3.4

3.2.2 DESIGN OF GROUP 2 BEAMS

The proposed retrofitting scheme for the corroded beams in this group was bonding CFRP sheets to the bottom flange of the deteriorated beams. In order to observe the effectiveness of this scheme, four deteriorated beams strengthened with 5 layers of Tyfo SCH-11UP were tested. Two out of the four beams, have simulated local deterioration as beam BF-H0.33, while the other two beams have simulated uniform deterioration as beam BF-N0.50. To investigate the influence of the epoxy type on the bonding behaviour and in consequence the increased flexural capacity of the retrofitted beam, two types of epoxy were used in this group A two-component saturated epoxy Tyfo S was used for bonding the CFRP sheets to the BF-H0.33-F1(5)-B1 and BF-N0.50-F1(5)-B1 beams as shown in Figures 3.11 and 3.12. On the other hand, a two-component viscous epoxy was used to bond Tyfo SCH-11UP sheets to the tension flange of beams BF-H0.33-F1(5)-B2 and BF-N0.50-F1(5)-B2. It is very important to mention that, for the four beams, Tyfo S was combined with Tyfo SCH-11UP sheets to provide a wet-layup composite system before bonding it to the tested beams. Figures 3.13 and 3.14 show the test setup, the plane of the tension flange of the beam and a cross-section at its mid-span.

3.2.3 DESIGN OF GROUP 3 BEAMS

In order to investigate the influence of the CFRP type on the strengthening scheme, two strengthened deteriorated beams were tested in this group. Beams BF-H0.33-F2(1)-B2 and BF-H0.33-F2(1)-B2 with local deterioration effect simulated by 8 holes of 6.35 mm diameter and located in the tension flanges at the beam mid-span (similar to BF-H0.33) were strengthened by epoxy bonding of one layer of Tyfo UC to

their tension flange. Tyfo MB-3 was used to bond the CFRP laminate strip to the tested beams, while one layer of Tyfo EB-DB system was used as a dielectric barrier between the Tyfo UC and the tension flange to prevent any galvanic reaction. Test setup, the plan of the bottom flange of the beam, and cross-section of the beam at its mid-span can be seen in Figure 3.15. To characterize the influence of wrapping on the behaviour of strengthening steel beam, one layer of Tyfo SCH-11UP with a width of 200 mm was used to wrap the CFRP laminate strip at the both ends of the beam BF-H0.33-F2(1)-B2w as shown in Figure 3.16.

3.2.4 DESIGN OF GROUP 4 BEAMS

Based on the previous discussion of the characterization of the bonding between FRP and steel (Chapter 2), there are several parameters which affect the bonding behaviour such as: the adhesive type, adhesive thickness, surface preparation, and the bond length. Debonding of the CFRP materials is a one of the most common failure modes. Therefore, the stress in the CFRP composite material will not reach their tensile strength. The proposed retrofitting scheme, used in this group, is an unbonded CFRP sheets added through a ductile anchorage system as can be seen in Figure 3.17. The main objective of this proposed scheme is to reach the full capacity of the CFRP sheets using a ductile anchorage system instead of letting the CFRP material to have a brittle behaviour The failure mode for t all beams in this group was controlled by CFRP sheets rupture. The proposed scheme is composed of an unbonded CFRP sheet(s) which were wrapped around two steel plates at its ends (Part 1). In order to do not have stress concentration and rupture of the FRP sheets, part 1 had rounded corners. Duct tape was used to cover

the contact area between part 1 and the CFRP sheets to do not have any bond stress between them as shown in Figure 3.18. Part 1 was then linked to steel plate (part 3) which is anchored to the tension flange of the tested beam using four high tensile steel bolts, through two steel link members part 3. The steel link members were designed as a conventional tensile test dog-bone specimen. Based on this setup, the forces in the steel link member will be always tensile axial force with any moment in them. More details about the dimensions of the ductile anchorage system were discussed before in part 3.1.1. Figure 3.19 shows the full dimensions of Parts 1 and 3. Three beams were tested in group 4; BF-H0.33-F1(1)-A1D1, BF-H0.33-F1(1)-A2D1, and BF-H0.33-F1(1)-A2D2. All the tested deteriorated beams were prepared with a local deterioration identical to beam BF-H0.33.

3.2.4.1 BEAM BF-H0.33-F2(1)-A1D1

One layer of Tyfo SCH-11UP was used to strengthen the deteriorated steel beam BF-H0.33-F2(1)-A1D1 by wrapping it around the anchorage system (part one) with an overlap of 350 mm (end detail 1) as can be seen in Figure3.20. This overlap was used to avoid debonding between the CFRP sheets. The steel link member (A1) was designed to have rupture in the CFRP sheet before yielding occurred as shown below.

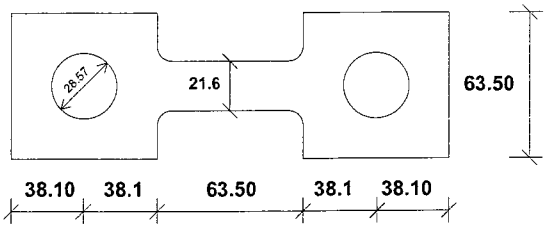

3.2.4.2 BEAM BF-H0.33-F2(1)-A2D1

Similar to the strengthening process of the beam BF-H0.33-F(1)-A1D1, one layer of unbonded anchorage Tyfo SCH-11UP was used to strengthen the beam BF-H0.33-F(1)-A2D1 with the same end detail. The steel link member which was used in this beam was design to have a yield stress lesser than the ultimate strength of the CFRP sheet as can be seen below.

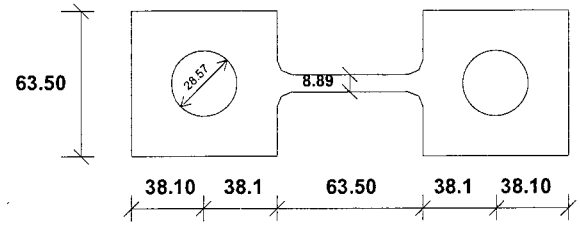

3.2.4.3 BEAM BF-H0.33-F2(5)-A2D2

Five layers of Tyfo SCH-11UP were used to strengthen the deteriorated steel beam BF-H0.33-F(5)-A2D2 by wrapping it around the anchorage system (part one). Three rounds of CFRP sheets were used in the end detail, first two rounds were wet while the last one was dry, (end detail 1) as shown in Figure 3.22. The steel link member (A1) was designed to yield before having rupture in the CFRP sheets.

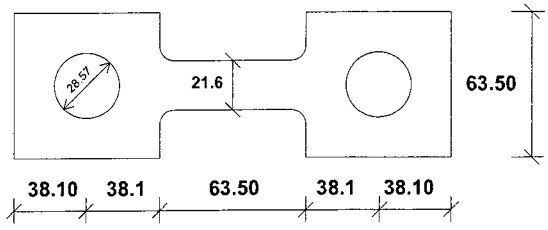

3.3 SURFACE PREPARATION

To achieve a maximum bonding effectiveness, all the tension/bottom flange of the beams which were strengthened using bonded CFRP sheets or laminate strip were grinded using sandpaper in order to remove rust and mill scale. Grinding of the surface was accomplished until a near white rough surface of the steel flange was observed. After grinding, the surface was wiped with solvent (acetone) for removing any oil residue on the surface. This clean surface was maintained until CFRP composite materials were placed in a dry and clean environment.

Several steps were taken to prepare the retrofit materials. The CFRP sheets and laminate were cut to the proper length using a band saw. Then, the adhesive was applied to the underside of the tension flange along the required length. One layer of GFRP was applied before the CFRP sheets or laminates were carefully adhered along the length of the beam. Then, a wooden clamping system was used to clamp the CFRP sheets or laminates to the beam for 24 hours and to ensure that the adhesive had set sufficiently prior to removal the clamps. The adhesive was allowed to cure at ambient room temperature for one week before testing.

3.4 INSTRUMENTATION

All beams were monotonically loaded using a 3000 kN hydraulic actuator with maximum stroke 152.4 mm, reacting against a rigid loading frame. The beams were loaded beyond the elastic strength and failure occurred where the load – carrying capacity of the member was largely decreased. The strains were measured with strain gages incorporated into quarter Wheatstone bridge configuration with the data acquisition

system with gage length 5 mm. Strains were measured at various location along the length of the beam to determine the maximum strain. The strain gages were installed at five separate locations along the beam such as (1) at mid-span, (2) under the two points load, and (3) at 27.5 cm from each support. At each of these locations, strain gages were installed in different places. The vertical deflections of the beam were measured using eight potentiometers that were located at different points in order to obtain the longitudinal profile of the beam at various load levels. A load cell with maximum capacity of 200 ton was used to measure the applied load from the actuator. Figure 3.23 shows the locations of strain gages and potentiometers for typical sections without and with CFRP Composite materials.

Table 3.1 Material properties (abstract from the Manufacture's Data sheet)

	Steel	Tyfo® SCH-11UP	Tyfo® UC
Tensile Strength	Fy=310 MPa, Fu=450MPa*	1062 MPa	2790 MPa
Tensile modulus	200 GPa	102 GPa	155 GPa
Ultimate Elongation	4.44%	1.05%	1.8%
Thickness/layer		0.27mm	1.4mm
Width/layer		150 mm	50.8 mm

*) strength was calculated based on coupon test

Table 3.2 Adhesives properties (abstract from the Manufacture's Data sheet)

	Tyfo S	Tyfo MB-3
Tensile Strength	72.4 MPa	16.7 MPa
Tensile modulus	3.18 GPa	_
Ultimate Elongation	5.0%	2.7%
Compressive Strength	_	28.2 MPa
Bond strength to Metal	good	Excellent
Thickness/layer	_	0.25 mm

Table 3.3 Test matrix

	Beam	ID	Area Losses mm^2	Retrofit material CFRP	Epoxy Material	Retrofit Method
Group 1	B1	BFO	None	____	____	____
	B2	BF-H0.33	8- 6.35 mm dia. holes	____	____	____
	B3	BF-N0.33	2-(25.4×450)mm^2 Notch	____	____	____
	B4	BF-N0.50	2-(38.1×450)mm^2 Notch	____	____	____
Group 2	B5	BF-H0.33-F1(5)-B1	8- 6.35 mm dia. holes	SCH-11UP (5 layers)	Tyfo S	Fully Bonded
	B6	BF-N0.50-F1(5)-B1	2-(38.1×450) mm^2 Notch	SCH-11UP (5 layers)	Tyfo S	Fully Bonded
	B7	BF-H0.33-F1(5)-B2	8- 6.35 mm dia. holes	SCH-11UP (5 layers)	MB-3	Fully Bonded
	B8	BF-N0.50-F1(5)-B2	2-(38.1×450) mm^2 Notch	SCH-11UP (5 layers)	MB-3	Fully Bonded
Group 3	B9	BF-H0.33-F2(1)-B2	8- 6.35 mm dia. holes	UC strip (1strip1.4mm)	MB-3	Fully Bonded
	B10	BF-H0.33-F2(1)-B2w	8- 6.35 mm dia. holes	UC strip (1strip1.4mm)	MB-3	Fully Bonded
Group 4	B11	BF-H0.33-F1(1)-A1D1	8- 6.35 mm dia. holes	SCH-11UP (1 layers)	____	Ductile anchorage system
	B12	BF-H0.33-F1(1)-A2D1	8- 6.35 mm dia. holes	SCH-11UP (1 layers)	____	Ductile anchorage system
	B13	BF-H0.33-F1(5)-A1D2	8- 6.35 mm dia. holes	SCH-11UP (5 layers)	____	Ductile anchorage system

Table 3.4 Section properties of original and deteriorated steel cross sections

		Original Cross-Section	33% area reduction	50% area reduction
Elastic Neutral-axis	mm	78.5	67.885	61.34
Cross-section Area (A)	mm^2	3759.24	3289.7	3047.8
Moment of Inertia about x axis (Ix)	mm^4	16999044	14048678	12231200
Moment of Inertia about y axis (Iy)	mm^4	5554760	3606322	3130101
Section Modulus about x axis (Sx)	mm^3	216584	157646	127867
Plastic Modulus about x axis (Zx)	mm^3	241767	198423	170410
Area reduction of the bottom flange		0%	33%	50%
Reduction in the (Ix)		0%	17.4%	28%
Reduction in the (Sx)		0%	27.2%	40.1%
Reduction in the (Zx)		0%	17.9%	29.5%

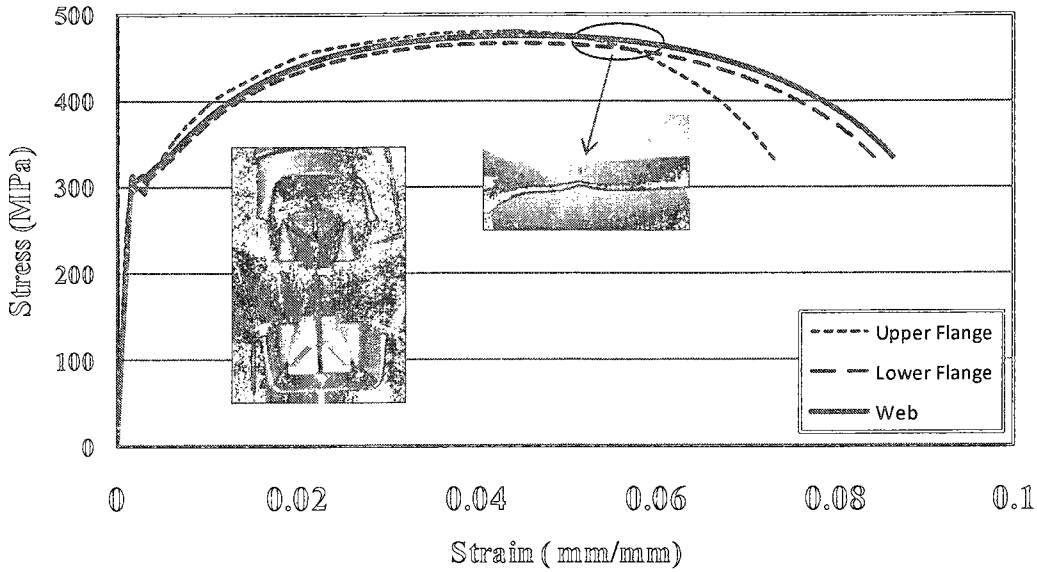

Figure 3.1 Measured steel tensile stress-strain relationship

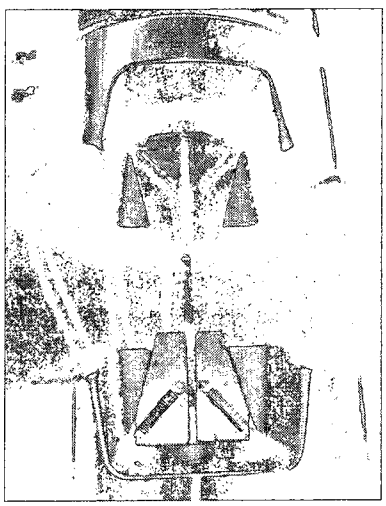

(a) Steel tension Coupon test setup

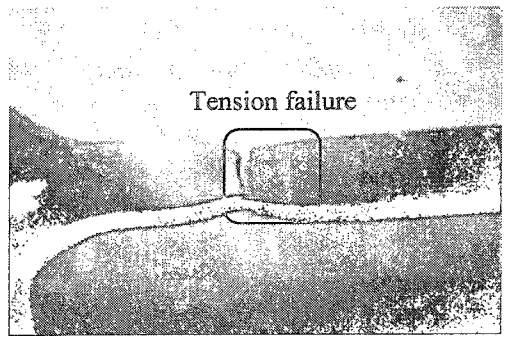

(b) Steel tension Coupon typical failure

Figure 3.2 Steel tension coupon test

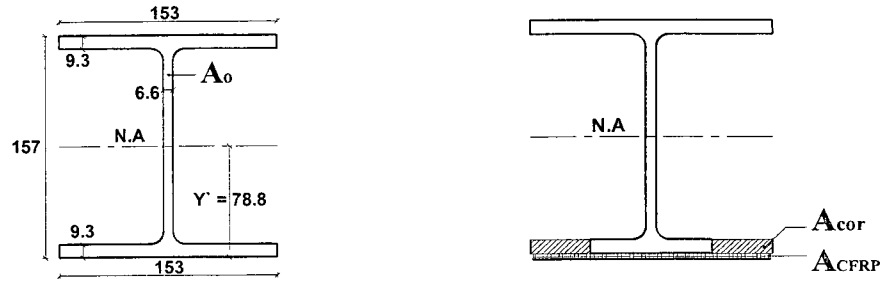

(a) Original section (b) Strengthened section

Figure 3.3 Original and strengthened sections

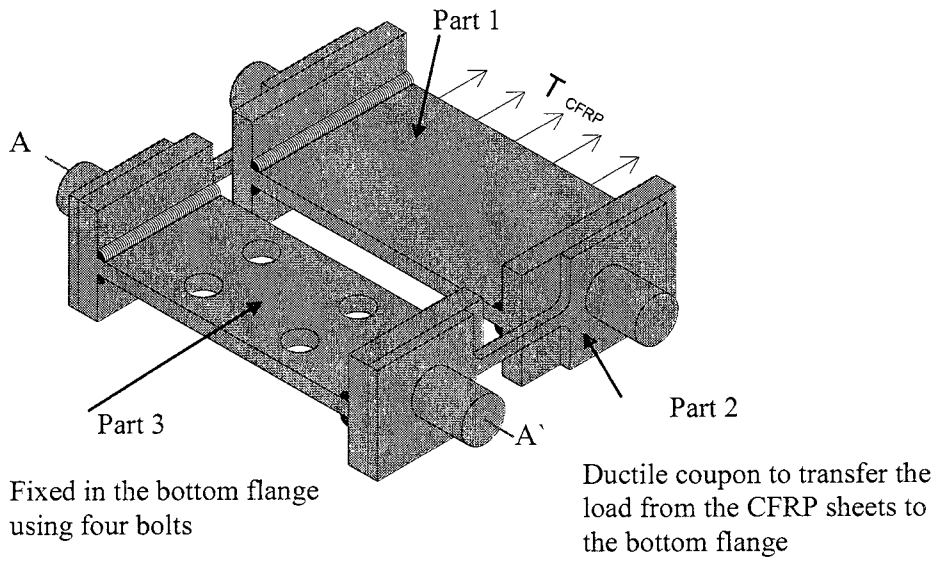

Figure 3.4 Ductile anchorage system

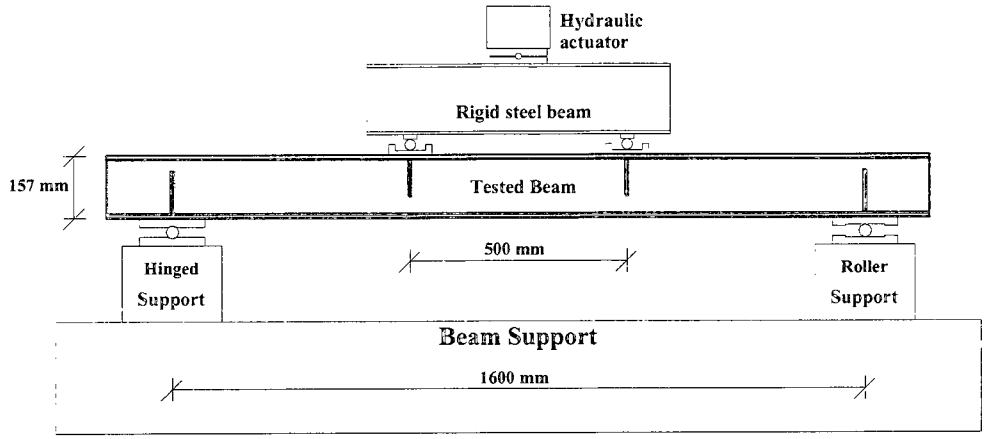

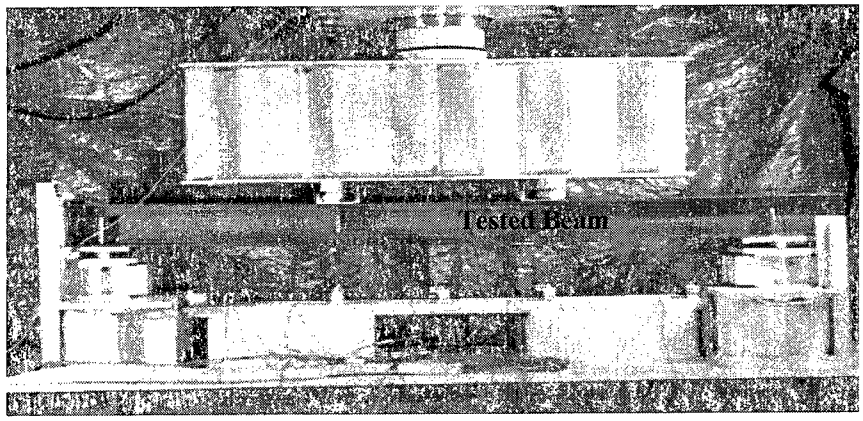

Figure 3.5 Test setup

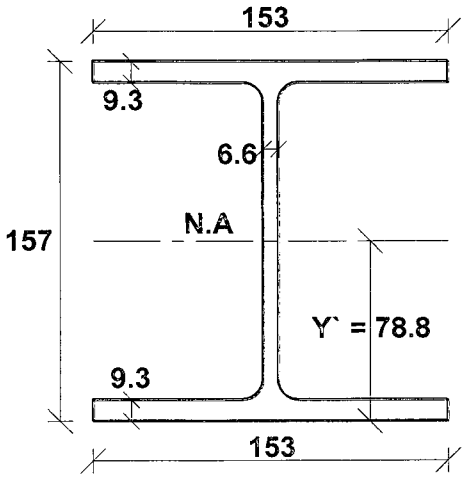

Figure 3.6 Typical steel beam cross-sections

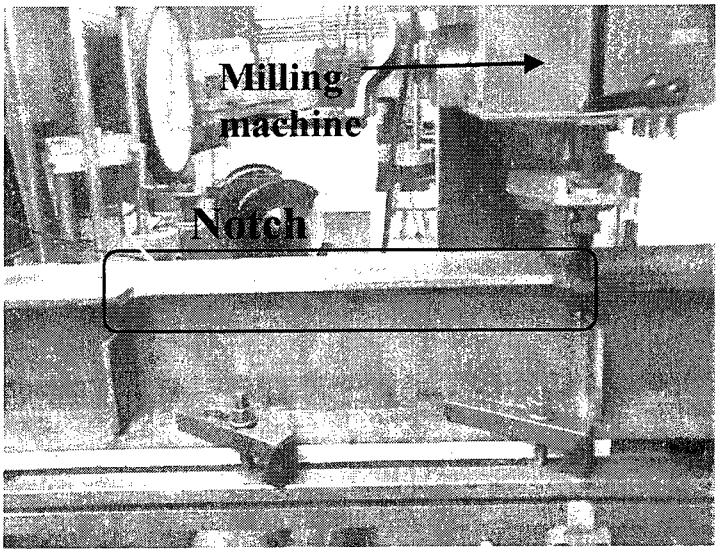

Figure 3.7 Notches preparation

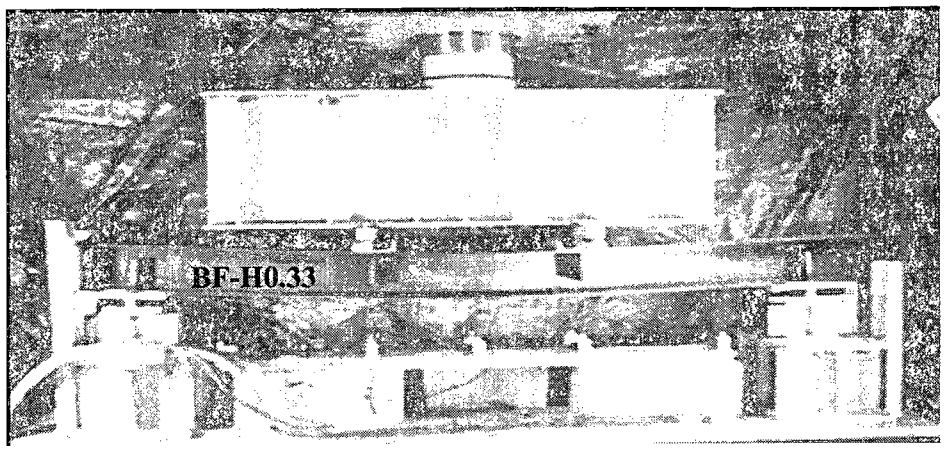

(a) Elevation of the test setup

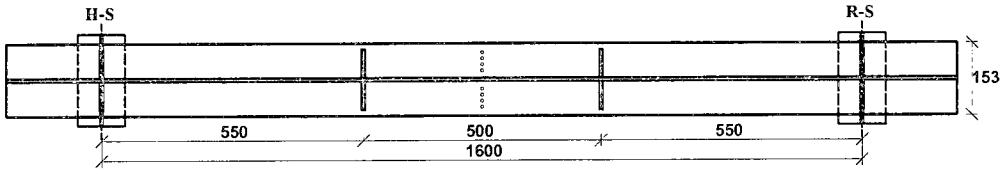

(b) Plan view of the bottom flange

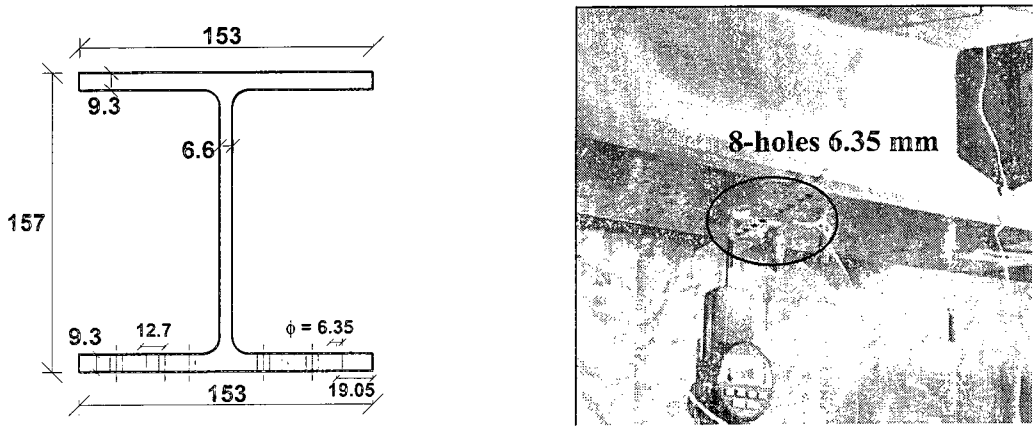

(c) Section at mid-span

Figure 3.8 Beam 2 BF-H0.33; (a) Elevation of the test setup, (b) Plan view of the bottom flange, and (c) Section at mid-span

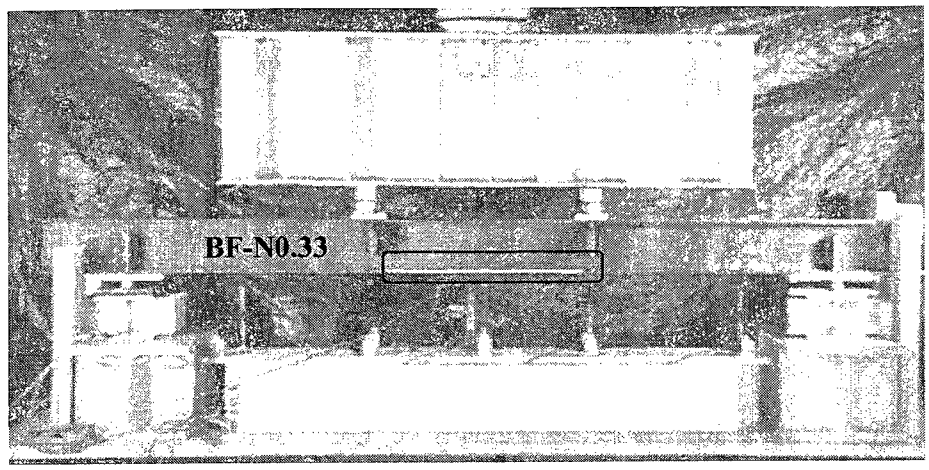

(a) Elevation of the test setup

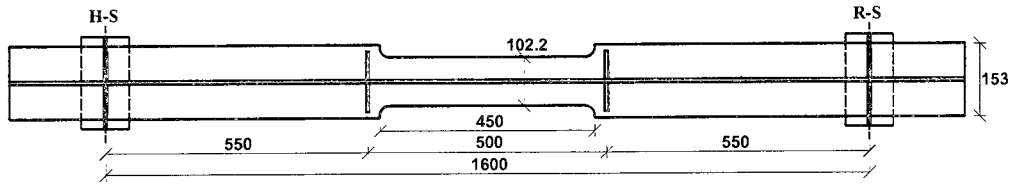

(b) Plan view of the bottom flange

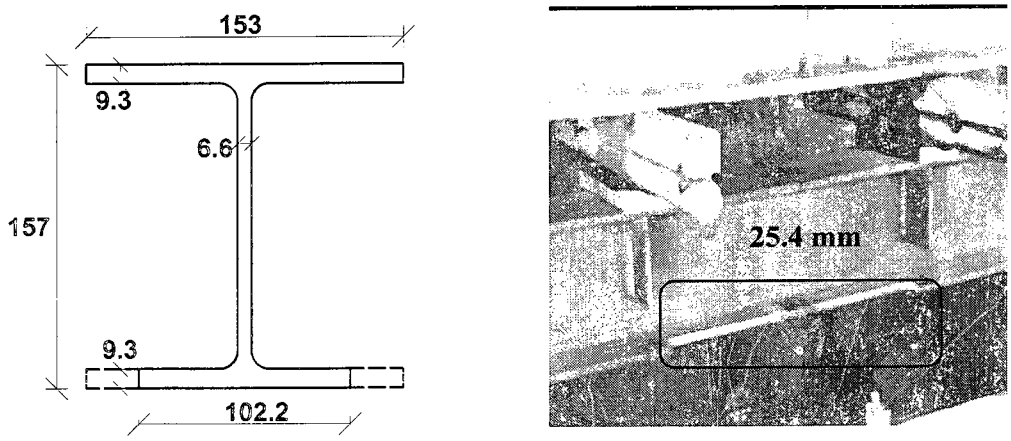

(c) Section at mid span

Figure 3.9 Beam 3 BF-N0.33; (a) Elevation of the test setup, (b) Plan view of the bottom flange, and (c) Section at mid-span

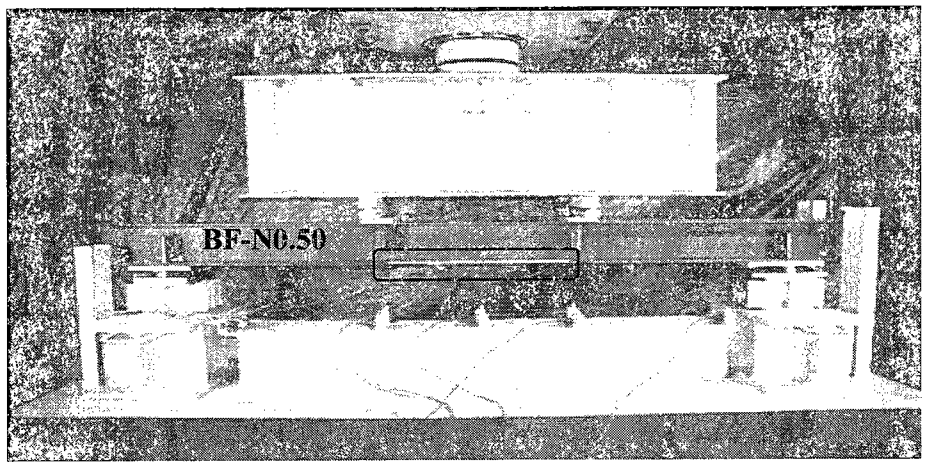

(a) Elevation of the test setup

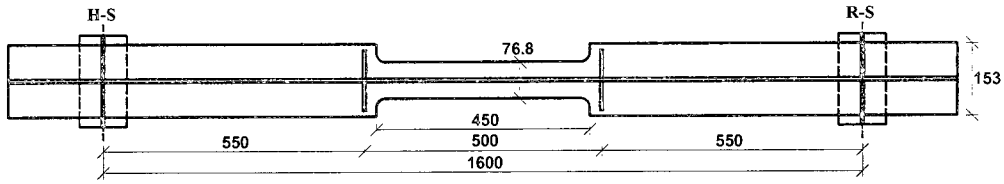

(b) Plan view of the bottom flange

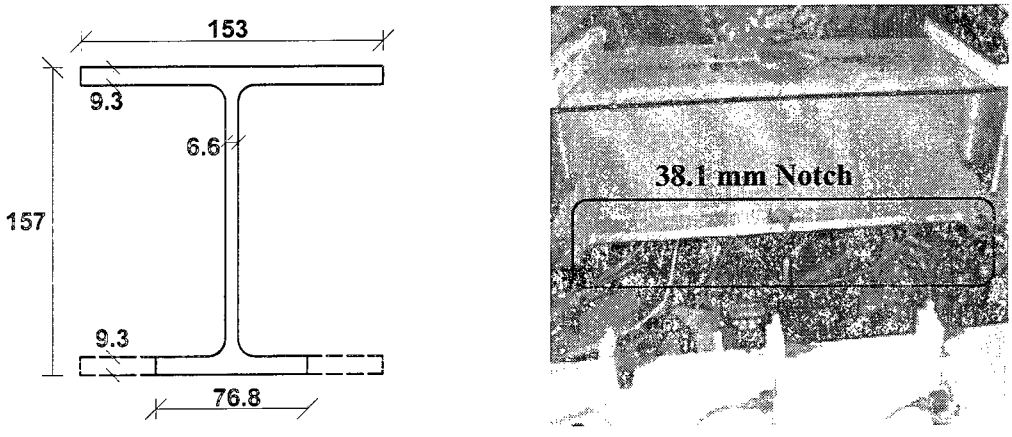

(c) Section at mid span

Figure 3.10 Beam 4 BF-N0.50; (a) Elevation of the test setup, (b) Plan view of the bottom flange, and (c) Section at mid-span

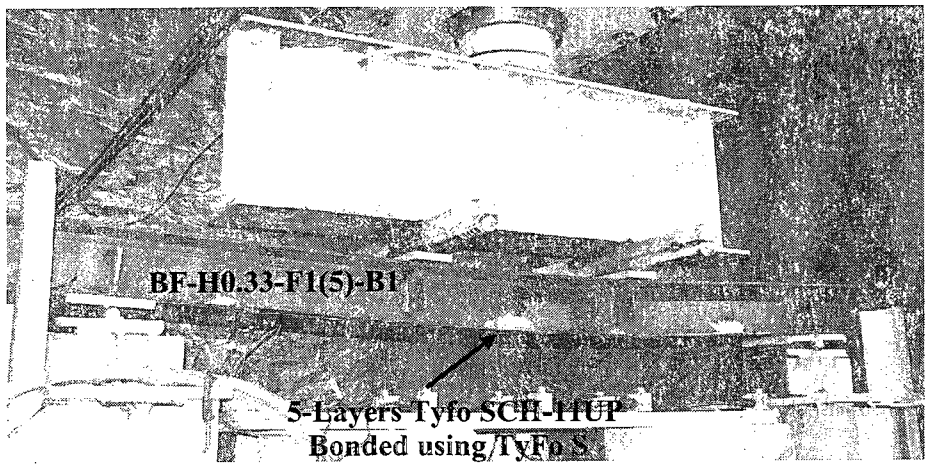

(a) Elevation of the test setup

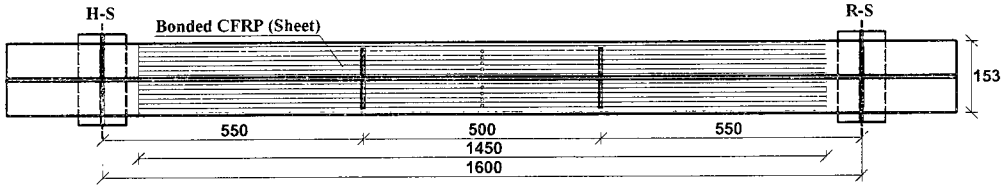

(b) Plan view of the bottom flange

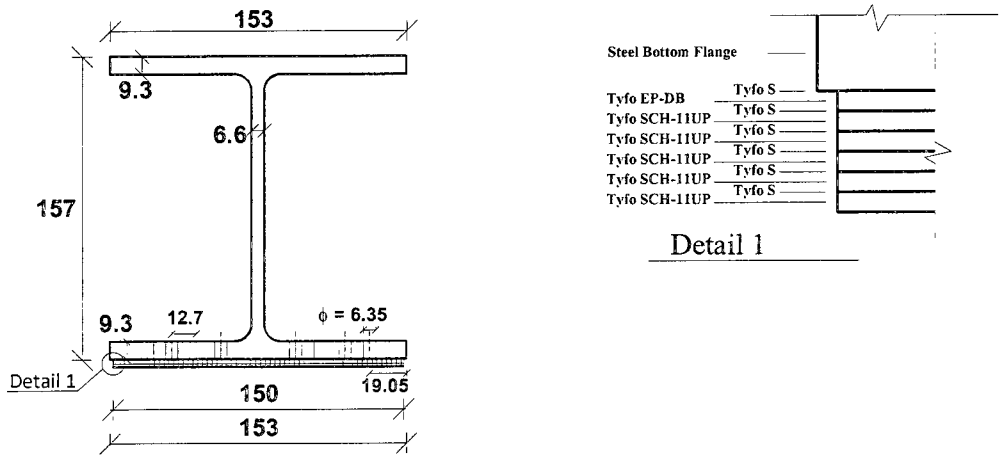

(c) Section at mid span

Figure 3.11 Beam 5 BF-H0.33-F1(5)-B1; (a) Elevation of the test setup, (b) Plan view of the bottom flange, and (c) Section at mid-span

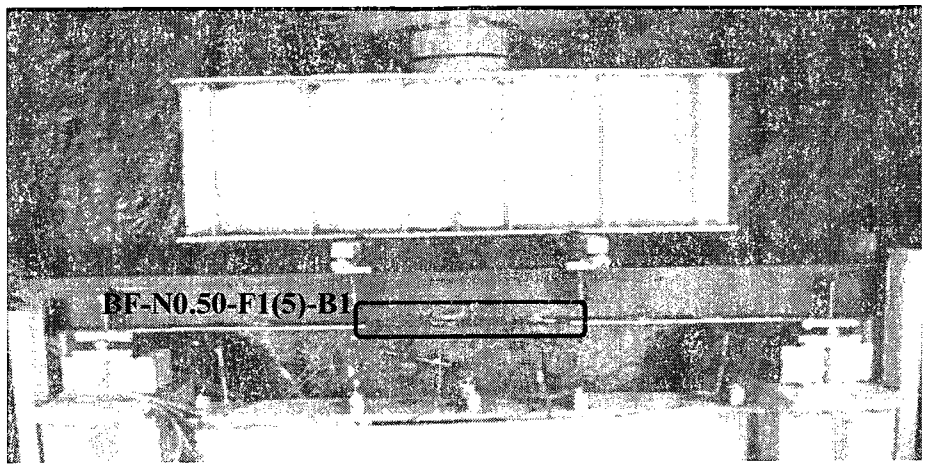

(a) Elevation of the test setup

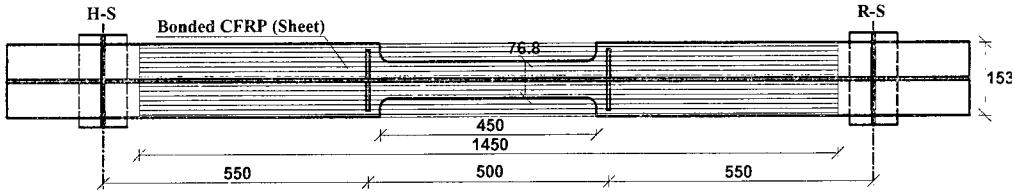

(b) Plan view of the bottom flange

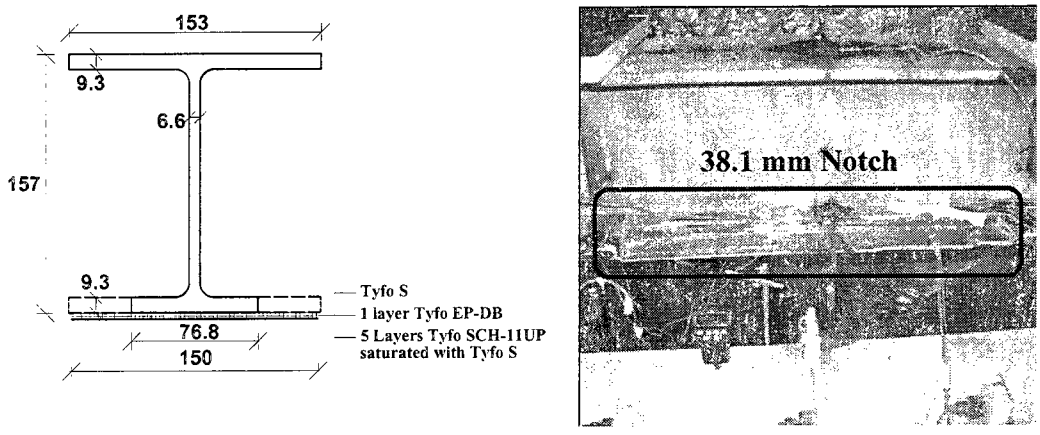

(c) Section at mid span

Figure 3.12 Beam 6 BF-N050-F1(5)-B1; (a) Elevation of the test setup, (b) Plan view of the bottom flange, and (c) Section at mid-span

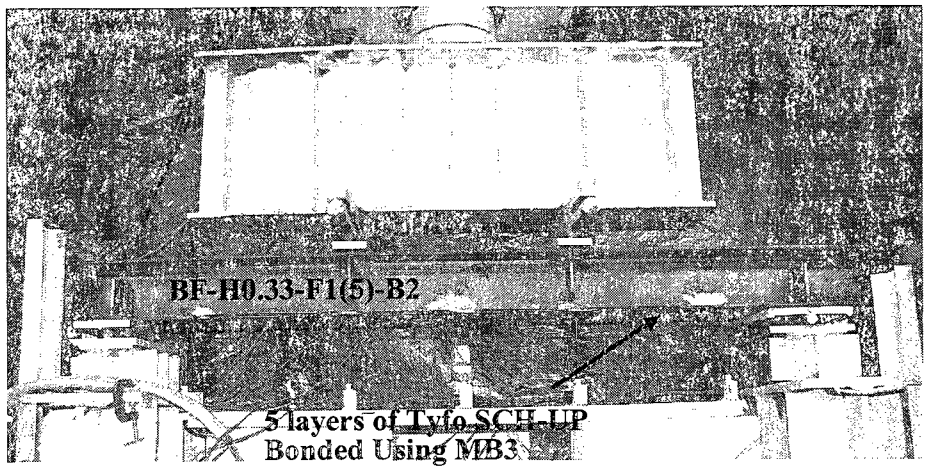

(a) Elevation of the test setup

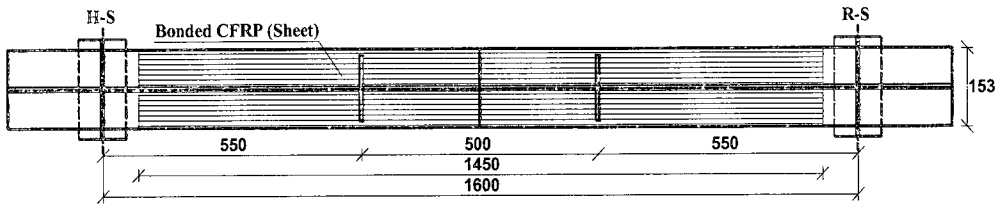

(b) Plan view of the bottom flange

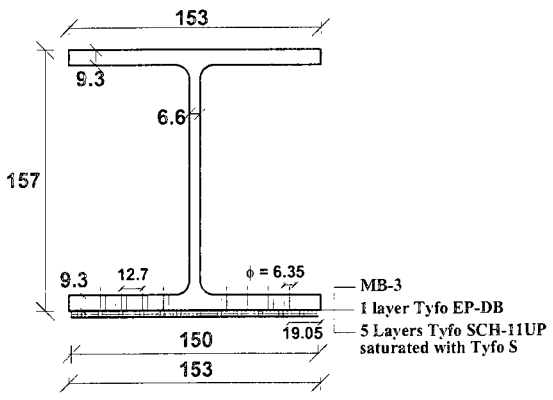

(c) Section at mid span

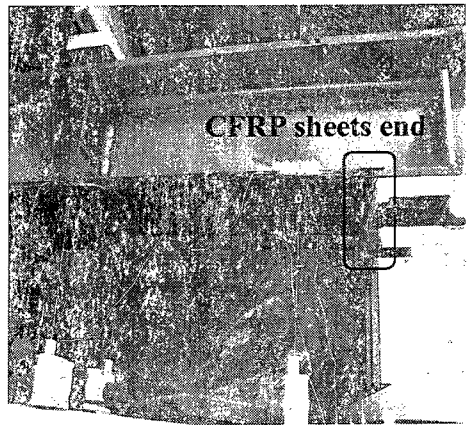

d) Section near to the roller support

Figure 3.13 Beam 7 BF-H0.33-F1(5)-B2; (a) Elevation of the test setup, (b) Plan view of the bottom flange, (c) Section at mid-span, and (d) Section near to Roller Support

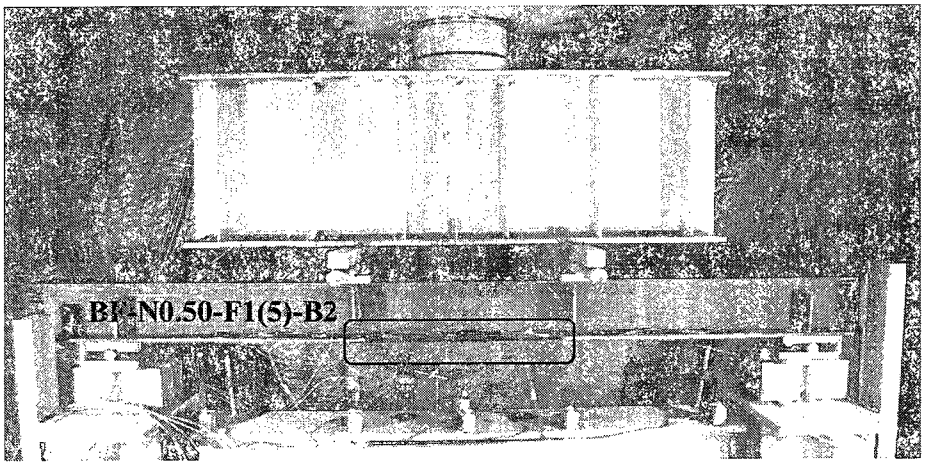

(a) Elevation of the test setup

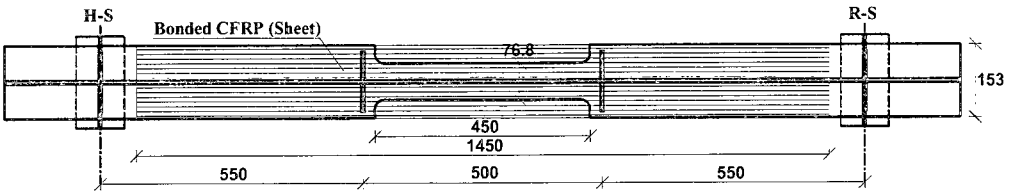

(b) Plan view of the bottom flange

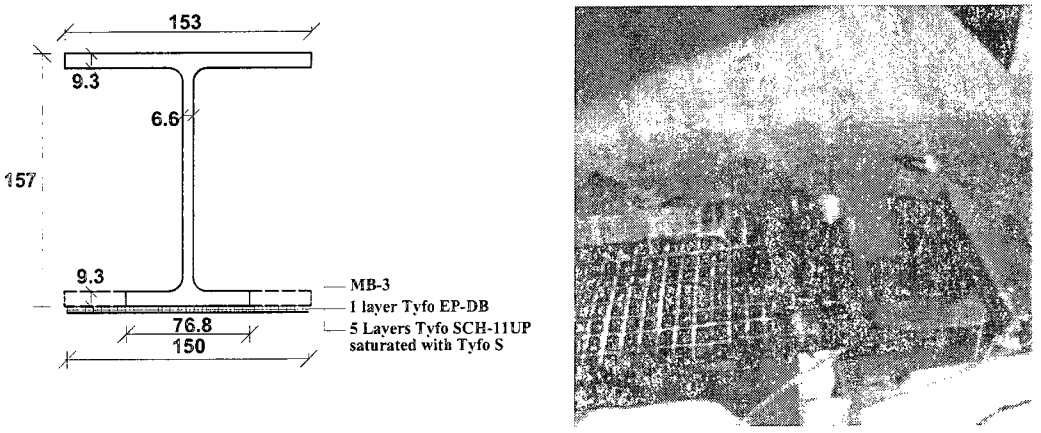

(c) Section at the constant moment zone

Figure 3.14 Beam 8 BF-N050-F1(5)-B2 ; (a) Elevation of the test setup, (b) Plan view of the bottom flange, and (c) Section at the constant moment zone

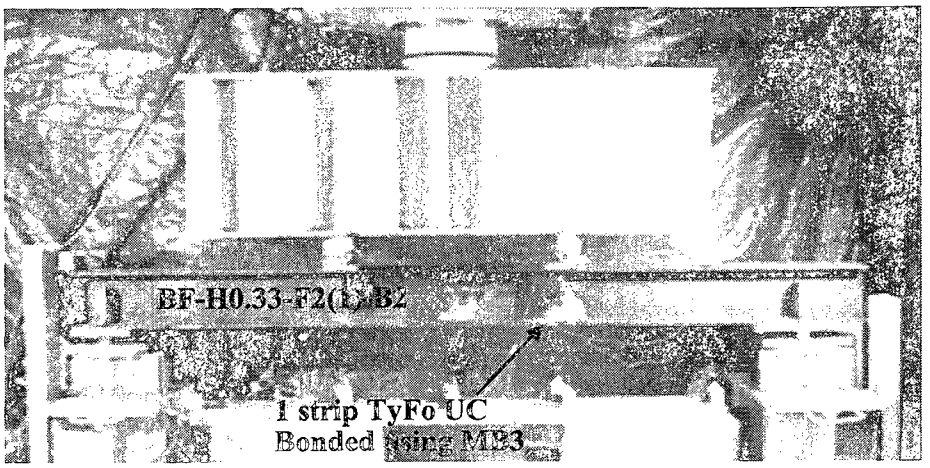

(a) Elevation of the test setup

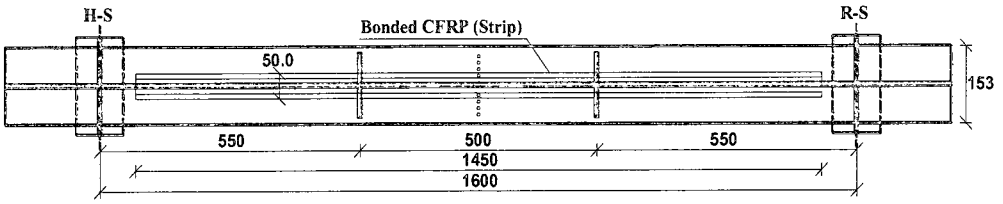

(b) Plan view of the bottom flange

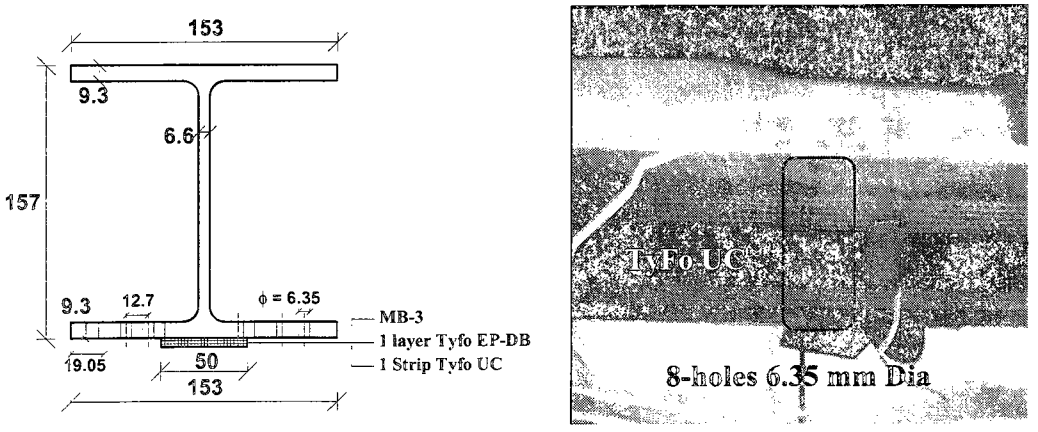

(c) Section at mid span

Figure 3.15 Beam 9 BF-H0.33-F2(1)-B2 ; (a) Elevation of the test setup, (b) Plan view of the bottom flange, and (c) Section at mid-span

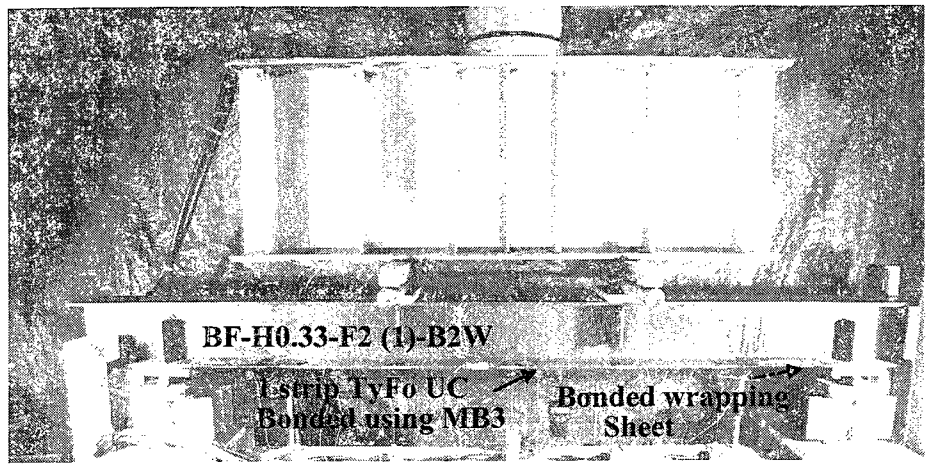

(a) Elevation of the test setup

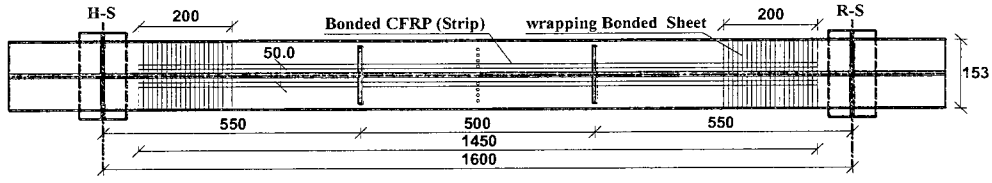

(b) Plan view of the bottom flange

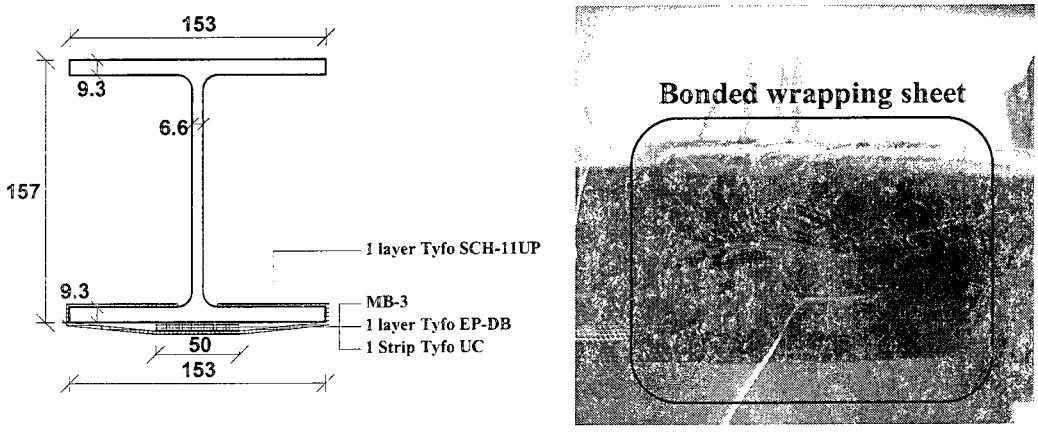

(c) Section near to the roller support

Figure 3.16 Beam10 BF-H0.33-F2(1)-B2w; (a) Elevation of the test setup, (b) Plan view of the bottom flange, and (c) Section near to Roller Support

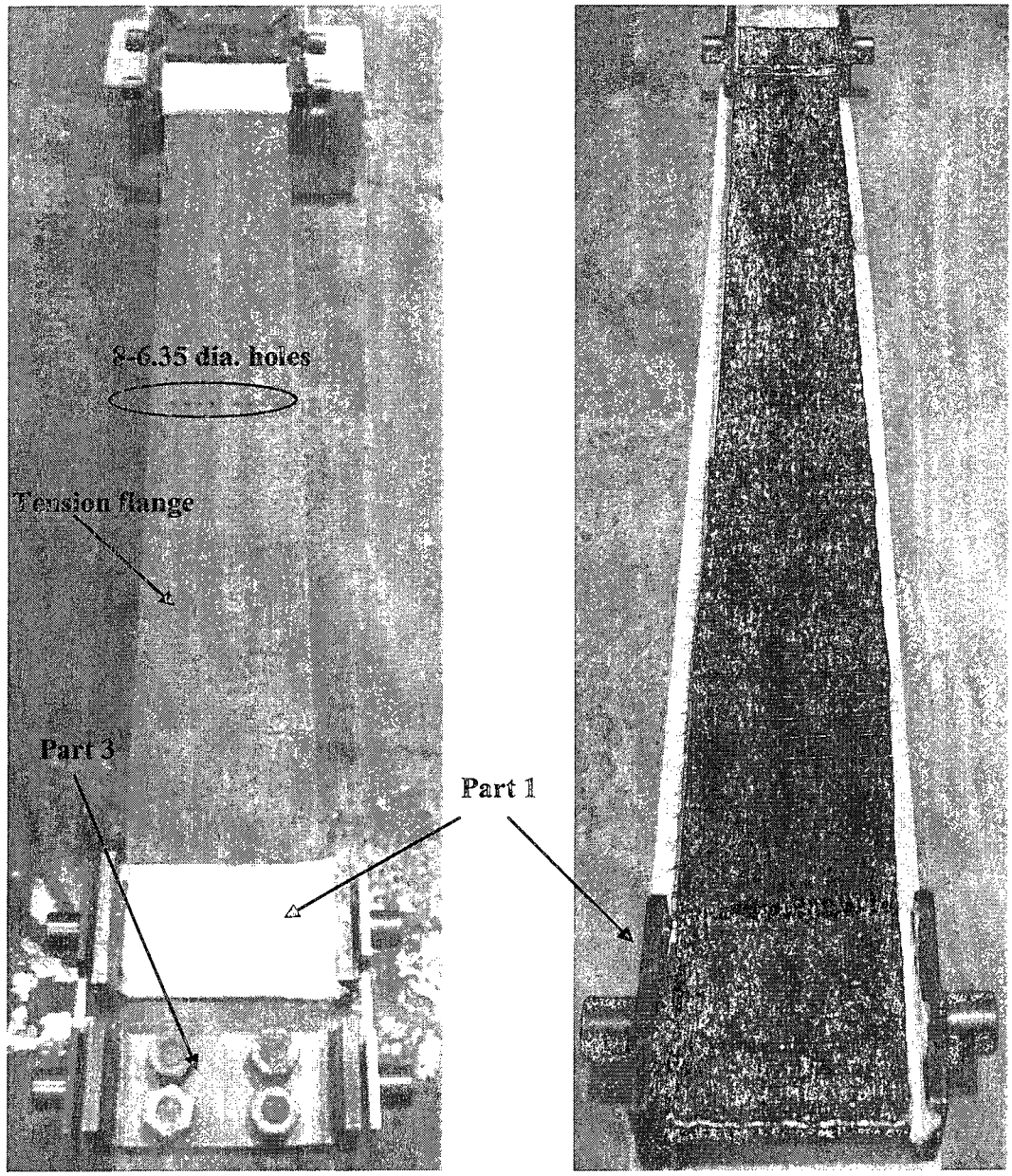

(a) Before installing the CFRP sheets (b) After installing the CFRP sheets

Figure 3.17 Unbonded CFRP sheets ductile anchorage system

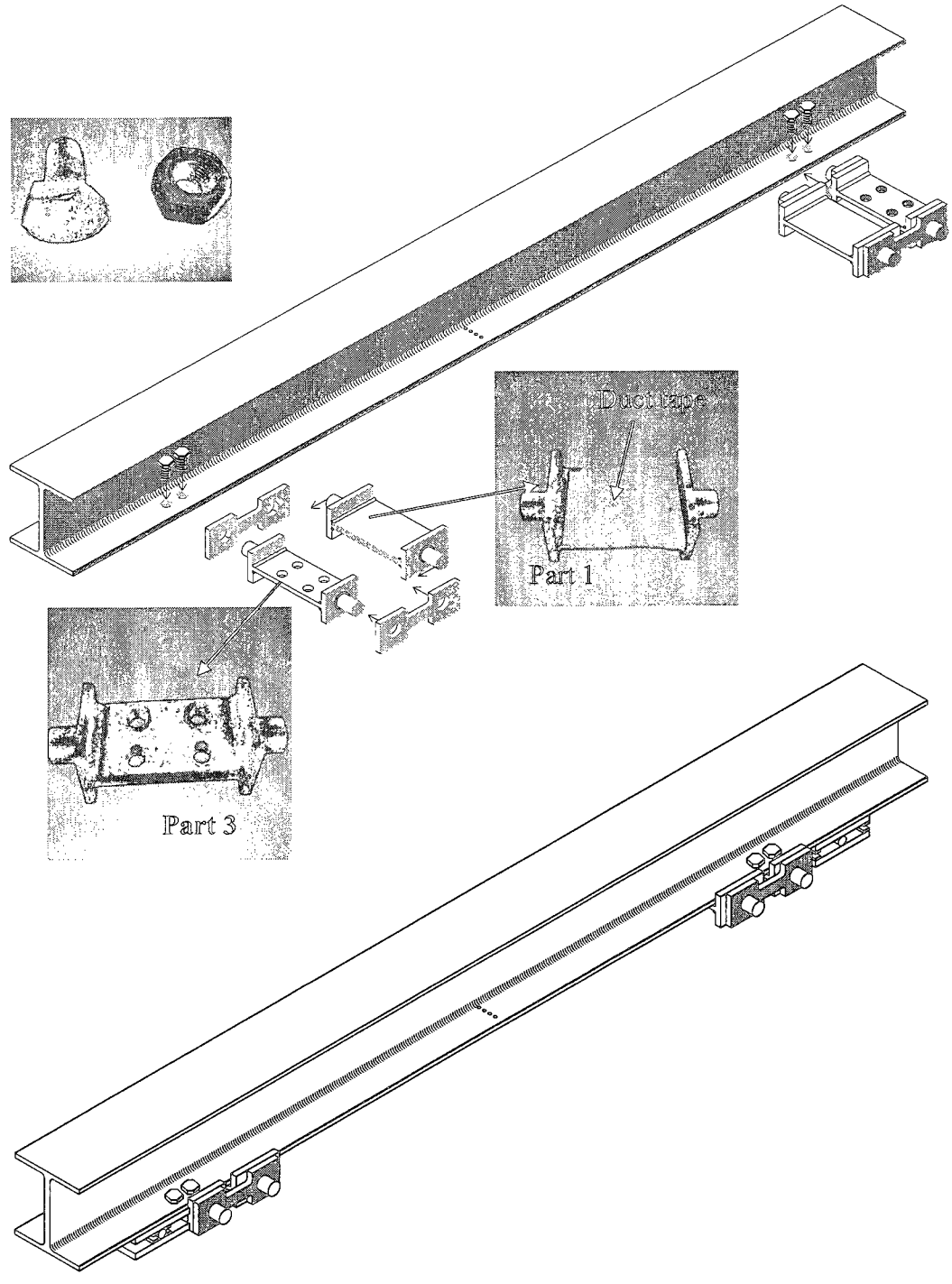

Figure 3.18 3D-Ductile anchorage system schema

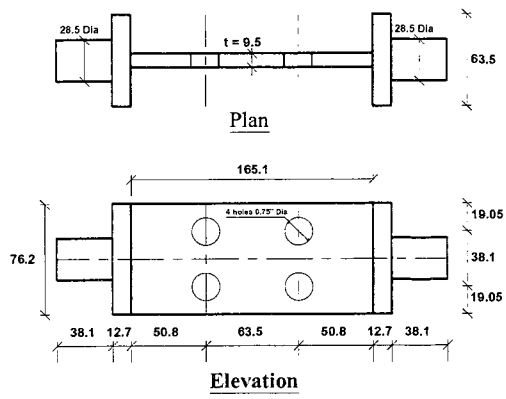

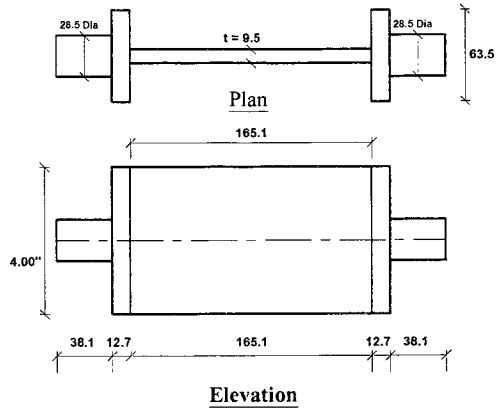

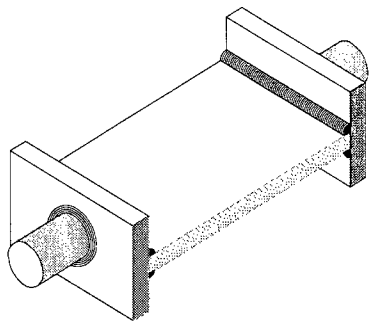

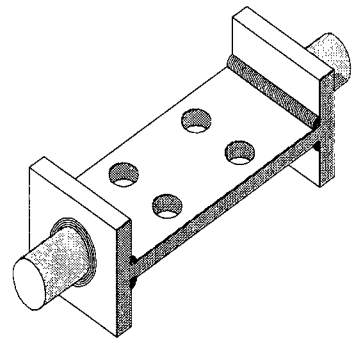

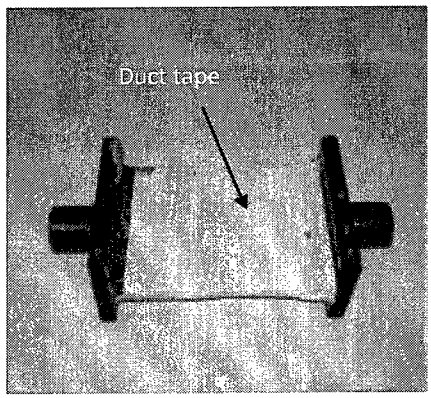

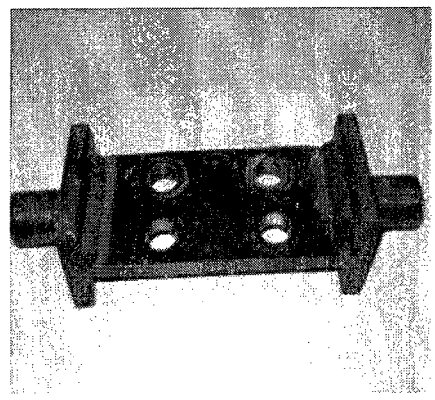

(a) Part 1

(b) Part 3

Figure 3.19 Ductile anchorage system dimensions; (a) Part 1, (b) Part 3

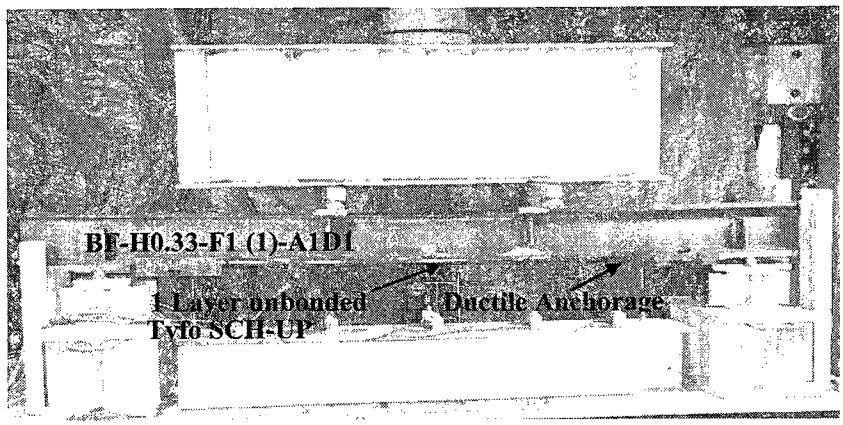

(a) Elevation of the test setup

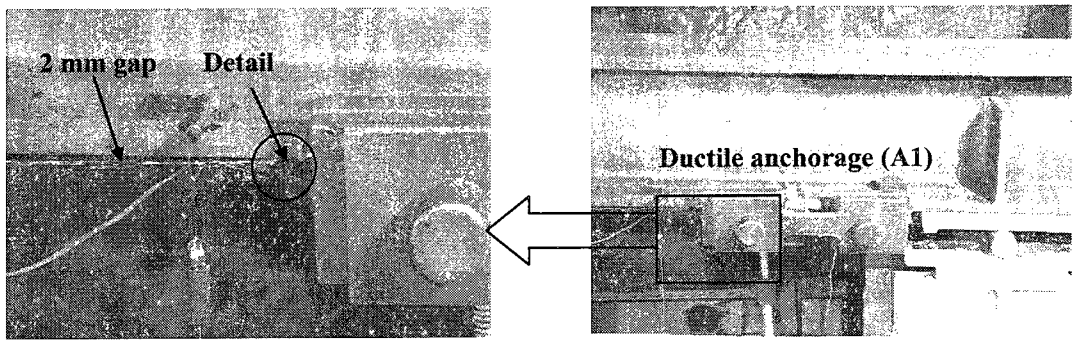

(b) Section near to Roller Support

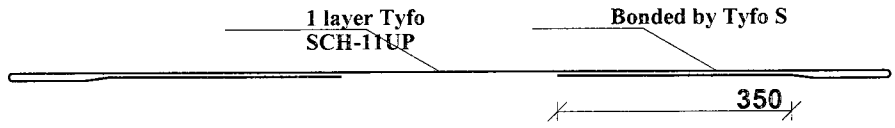

(c) Longitudinal profile of the CFRP sheet (for Detail 1)

Figure 3.20 Beam 11 BF-H0.33-F1(1)-A1D1; (a) Elevation of the test setup, (b) Section near to the roller support, and (c) Longitudinal profile of the CFRP sheet

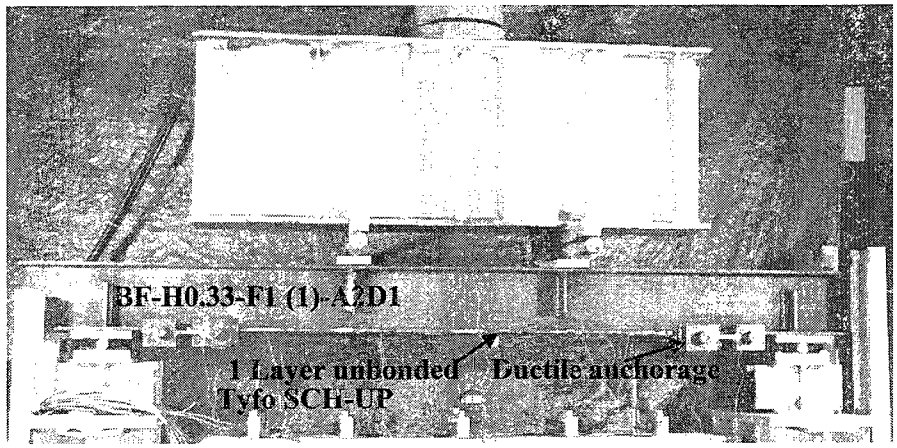

(a) Elevation of the test setup

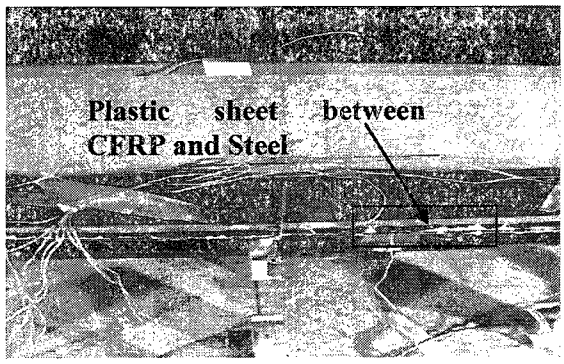

(b) Section at mid span

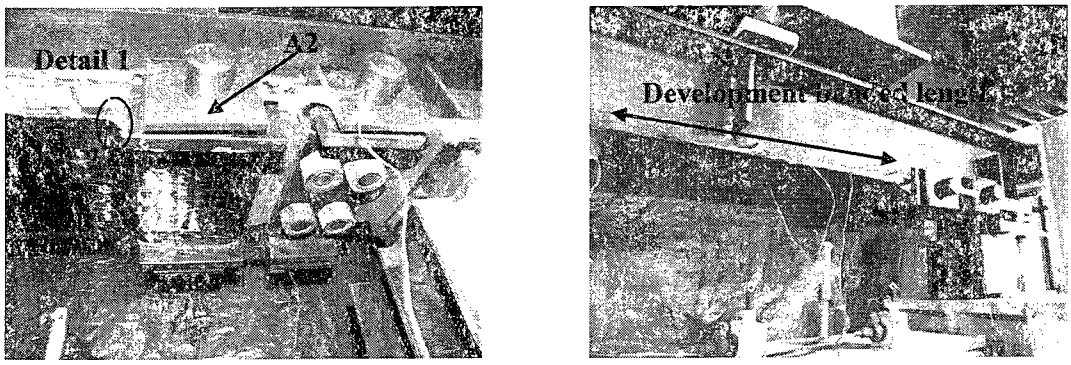

(c) Section near to Roller Support

Figure 3.21 Beam 12 BF-H0.33-F1(1)-A2D1; (a) Elevation of the test setup, (b) Section at mid-span, and (c) Section near the roller support

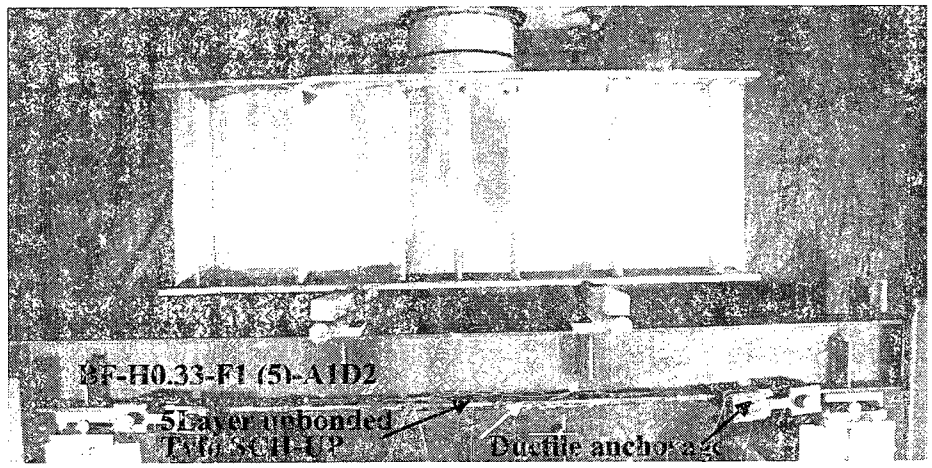

(a) Elevation of the test setup

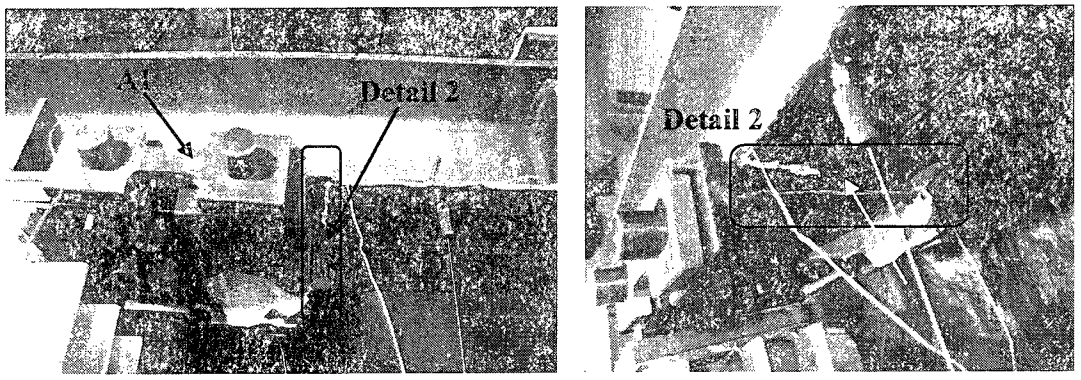

(b) Section near to Hinged Support

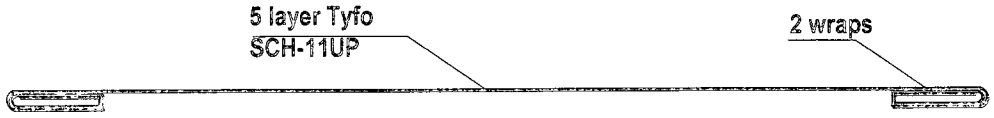

(c) Longitudinal profile of the CFRP sheet (for Detail 2)

Figure 3.22 Beam 13 BF-H0.33-F1(5)-A2D2; (a) Elevation of the test setup, (b) Section near the pinned support, and (c) Longitudinal profile of the CFRP sheet

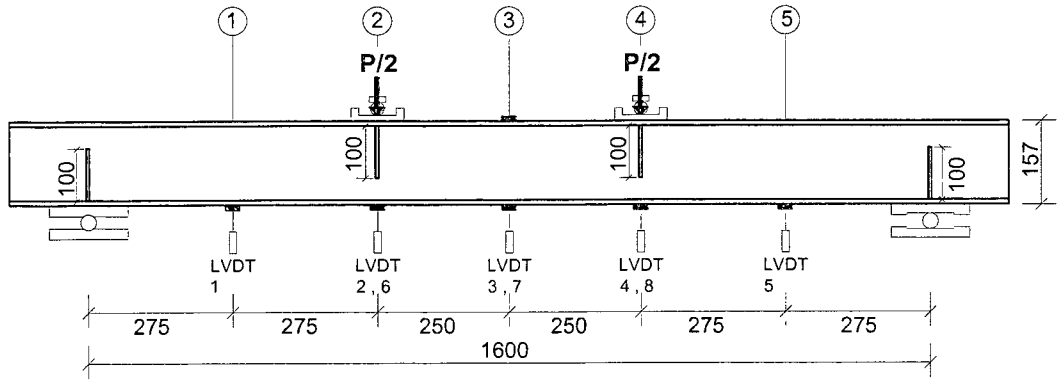

a) Beam Elevation

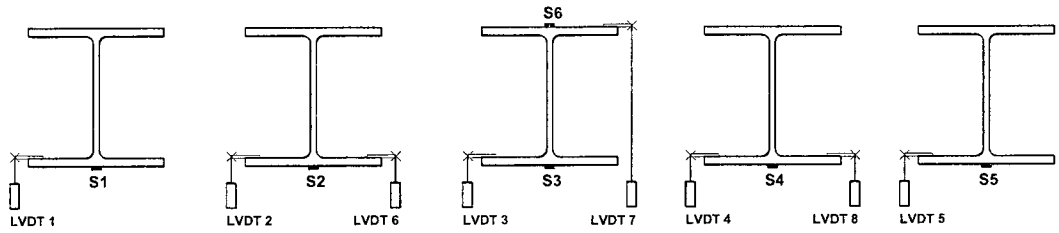

Section 1 Section 2 Section 3 Section 4 Section 5

b) Typical Sections without CFRP

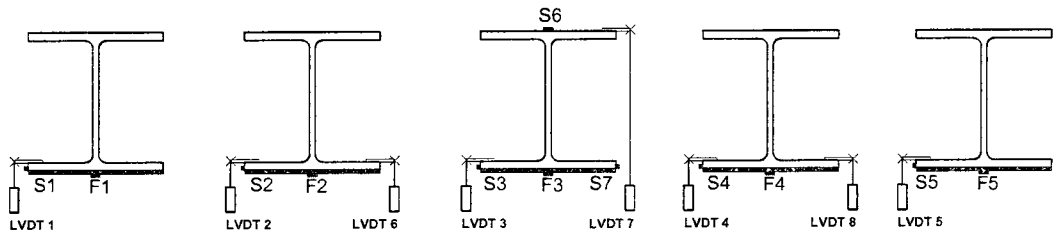

Section 1 Section 2 Section 3 Section 4 Section 5

c) Typical Sections with CFRP

Figure 3.23 Locations of strain gages and potentiometers; (a) Beam elevation, (b) Typical sections without CFRP, and (c) Typical sections with CFRP

CHAPTER 4

TEST RESULTS AND DISCUSSION

4.1 GENERAL

In this chapter, the experimental results for all beam tested are presented. The tested beams are divided into four groups as discussed in Chapter 3. First Group consisted of four beams with different levels of area reduction without strengthening. The Second tested Group consisted of four notched beams strengthened with bonded CFRP sheets. Out of the four strengthened beams, two beams were bonded using saturated epoxy (Tyfo S), while the other two were strengthened using high performance adhesive (Tyfo MB-3). Two notched beams were tested in the Third Group. These beams were strengthened using bonded CFRP strip, one without and one with wrapping system. The fourth Group consisted of three notched beams that were strengthened using ductile anchoring CFRP sheets. A summary of the test results including the yielding, ultimate strength with their associated deflections, and the failure modes are shown in Table 4.1. The table also includes the maximum strain at yield. The results and observations of each group are described individually including the load-deflection, load-strain, and the mode of failure. Table 4.2 presents a summary of the comparison results between all the tested beams. Figure 4.1 (a and b) shows yielding P_y and ultimate load P_u with their corresponding deflections for the unstrengthened and strengthened beams. The stress-strain curve for the beams coupons and the CFRP composite materials, used in the experimental program are shown in Figures 4.2 and 4.3. For each of the studied beams,

Figure (a) was allocated to the mode of failure and Figures (b) and (c) were allocated to the Load-deflections and Load-strains curves of the tested beam at different locations.

4.2 RESULTS OF GROUP 1 BEAMS

Four beams in group 1 were prepared to investigate the behaviour of steel beams with locally and uniformly corroded tensile flange area. Out of the four beams, the BFO beam was designed to perform as a non-deteriorated beam, labelled the control beam, whereas the other three steel beams were designed with two different levels of deterioration. Beams BF-H0.33 and BF-N0.33 has a 33% tension flange area reduction, while beam BF-N0.50 has a 50%. The tension flange area reduction of the beam BF-N0.33 was in form of notches with a length of 450 mm located in the mid-span for simulating the effect of uniformly distributed corrosion. Meanwhile, the tension flange area reduction of beam BF-H0.33 was concentrated in the mid-span to simulate the behaviour of the beam with a local deteriorated cross-sectional area.

4.2.1 BEAM BFO

The control beam BFO started to yield at a load of 245 kN and the corresponding maximum deflection and strain of the tension flange for this yield load were equal to 7.70 mm and 1568 με, respectively. The failure mode was in-plane plastic buckling of the compression flange as shown in Figure 4.4 (a). The beam reached the 331 kN ultimate load (failure load) which was 1.35 times the yielding load. At failure, the mid-span deflection of the top and bottom flanges was found to be 81.75 mm and 73.60 mm, respectively. It is worth mentioning that the plastic buckling of the compression flange

started approximately at a load of 315 kN. The corresponding load-deflections and load-strains curves at different locations are shown in Figures 4.4 (b and c).

4.2.2 BEAM BF-H0.33

The BF-H0.33 beam was designed to simulate the behaviour of a deteriorated steel girder due to the local corrosion effect. It was observed that the mid-span cross-section started to yield at a load of 180 kN, while the overall behaviour of the beam was still in the elastic stage. Under this load, the strain and the deflection at the mid-span were measured to be 1530 με and 5.8 mm, respectively. Beam BF-H0.33 started yielding at almost the same yielding load as beam BFO (242 kN) with a mid-span deflection of the bottom flange equal to 8.00 mm and a maximum strain of 7000 με at the deteriorated section. As can be seen in Figure 4.5 (a), the failure mode was observed to be in-plane plastic buckling. The ultimate load capacity of 330 kN represents 1.36 times the applied load at yield. The mid-span deflections of the top and bottom flanges were recorded as being 69.80 mm and 76.93 mm, respectively. The applied load versus the deformations and the strains at different locations are illustrated in Figures 4.5 (b and c). Similar to beam BFO, the plastic buckling of the compression flange started approximately at a load of 312 kN.

4.2.3 BEAM BF-N0.33

This beam, prepared to simulate the uniformly distributed corrosion in the constant moment zone started to yield at a load of 175kN, while the deflection and the maximum strain of the tension flange were equal to 5.90 mm and 1550 με, respectively.

From the load-deflection relationship, beam BF-N0.33 started yielding at load 190 kN. At this load, the mid-span-deflection and the maximum strain of the tension flange were measured to be 6.40 mm and 1640 με, respectively. Figure 4.6 (a) shows the beam failure mode which was observed to be in-plane plastic buckling of the compression flange. The plastic buckling started at an approximate load of 285 kN. The beam reached an ultimate load of 311 kN which is 1.64 times the load at yield. The mid-span deflections of the top and bottom flanges were measured as 74.30 mm and 81.00 mm, respectively. The Load-deflections and Load-strains curves of the beam at different locations are shown in Figures 4.6 (b and c).

4.2.4 BEAM BF-N0.50

In a similar manner with the BF-N0.33 beam, the BF-N0.50 beam was propose to simulate the behaviour of a uniformly corroded tension flange area of steel bridge girder with a different percentage of cross-sectional area loss. As the other deteriorated beams, the mid-span section started yielding at a load equal to 140 kN, while the corresponding maximum deflection and the strain were 5.50 mm and 1540 με, respectively. At a load of 155 kN, the beam started to yield with a corresponding maximum deflection and strain of the tension flange equal to 5.80 mm and 1660 με, respectively, as shown in Figures 4.7 (b and c). After the plastic buckling started developing at an approximate load of 270 kN, failure in the compression flange occurred, as shown in Figure 4.7 (a). The maximum recorded load of 290 kN was 1.87 times the applied load at yield. The mid-span deflection of the top and bottom flanges was measured as 95.40 mm and 103.50 mm, respectively.

4.2.5 THE EFFECT OF THE AREA LOSS IN TENSION FLANGE ON THE BEHAVIOUR OF THE DETERIORATED STEEL BEAM

As shown in the Table 4.2, the remaining yielding load capacity can be reduced to 63% of the original capacity for a member with a 50% reduction at the bottom flange as simulated to emphasise the uniform corrosion effect. The ratio of the ultimate load to the yielding load (P_u/P_y) was increased with the increasing of the corrosion ratio (from 1.35 for beam BFO to 1.87 for beam BF-N0.50). The same observation can be seen from the displacement ductility (Δ_u / Δ_y) which increased from 9.56 for beam BFO to 16.53 for beam BF-N0.50.

By analysing the behaviour of beam BF-H0.33, another interesting observation is shown. As can be seen in Figure 4.8 (a), there is a slight difference in the load-deformation behaviour of the locally deteriorated beam and the control beam. For the two beams, almost the same yield and ultimate load has been recorded in the test results at the same corresponding deflections. The main difference in their behaviour is the strain at the mid-span (the deteriorated section) as shown in Figure 4.8 (b). This implies that the local corrosion effect materialised in one section only have a local influence on the strains of the corroded section only and a negligible effect on the load-deformation behaviour of the whole beam. Figure 4.8 (c) shows the moment rotation curve for Group 1 beams.

4.3 RESULTS OF GROUP 2 BEAMS

The proposed retrofitting scheme in this group of beams was through bonding CFRP sheets to the bottom flange of the deteriorated beams. In order to observe the effectiveness of this scheme, four deteriorated beams were tested after strengthening with

5 layers of Tyfo SCH-11UP. Two out of the four beams had local deterioration similar to beam BF-H0.33, while the other two beams had uniform deterioration as per beam BF-N0.50. Two types of epoxy were used for this group of beams in order to investigate the influence of the epoxy type on the bonding behaviour with the aim to increase its flexural capacity. Tyfo S was used for bonding the CFRP sheets to beams BF-H0.33-F1(5)-B1 and BF-N0.50-F1(5)-B1, while Tyfo MB-3 was used for beams BF-H0.33-F1(5)-B2 and BF-N0.50-F1(5)-B2. It is important to mention that, for the four beams, Tyfo S was combined with Tyfo SCH-11UP sheets to provide a wet-layup composite system before bonding it to the tested beams.

4.3.1 BEAM BF- F1(5)-B1

The strengthened beam BF-F1(5)-B1 started to yield at a load of 245 kN and the corresponding maximum deflection of the tension flange was equal to 7.90 mm. Figure 4.9 (a) illustrates the failure mode which was observed as sudden failure by peeling off of the CFRP sheets. The failure load was reported as 307 KN with a maximum strain in the CFRP sheets of 4882 με. The maximum deflection of 18.10 mm at failure was 2.30 times the equivalent deflection at yield. The load-deflection and load-strains performances of the beam at different locations can be seen in Figures 4.9 (b and c). It is important to mention that by continuing the process of loading after debonding occurred the behaviour of the studied beam was similar to that of the control beam BFO.

4.3.2 BEAM BF-N0.50-F1(5)-B1

This beam was used to simulate the behaviour of a CFRP strengthened steel bridge girder that has uniform deterioration in its middle third span. Beam BF-N0.50-F1(5)-B1 started to yield at a load of 181 kN. The corresponding maximum deflection and strain of the bottom flange at yield was 5.70 mm and 1548 με, respectively. At the ultimate load of 262 kN and its corresponding deflection at the mid-span of the tension flange equal to 12.10 mm, the failure mode was characterized by the peeling off of the CFRP sheets as shown in Figure 4.10 (a). The maximum strain of the CFRP was reported as 4363 με. The corresponding Load-deflections and Load-strains diagrams at different locations are shown in Figure 4.10 (b and c).

4.3.3 BEAM BF-H0.33-F1(5)-B2

The behaviour of a CFRP strengthened steel girder with an initial locally corroded effect at beam mid-span was analyzed by using MB-3, adhesive material, on the beam BF-H0.33-F1(5)-B2. Similarly to beam BF-H0.33, the mid-span section started to yield at a load of 200 kN, while the behaviour of the beam was still in the elastic zone. When the maximum deflection of the bottom flange at yield was 8.20 mm, beam BF-H0.33-F1(5)-B2 started to yield under a load of 253 kN. As can be seen in Figure 4.11 (a), the failure mode was observed to be rupture in the CFRP sheets. The failure load was recorded as 375 kN with a maximum strain in the CFRP sheets of 10032 με. At failure, the maximum deflection of 51.00 mm was 6.25 times the equivalent deflection at yield (as shown in Figures 4.11 (b and c).

4.3.4 BEAM BF-N0.50-F1(5)-B2

Similar to beam BF-N0.50-F1(5)-B1, beam BF-N0.50-F1(5)-B2 simulated the behaviour of a strengthened uniform deteriorated steel girder. This beam started to yield at a load of 195 kN and the corresponding maximum deflection and strain of the tension flange was equal to 6.5 mm and 1630 με, respectively. The failure mode was observed to be rupture in the CFRP sheets as shown in Figure 4.12(a). The failure load was measured as 307 kN with a maximum strain in the CFRP equal to 10518 με. The corresponding deflection at failure was 24.00 mm which represents 3.70 times the deflection at yield. The applied load versus the deformations and strains at different locations are shown in Figure 4.12 (b and c).

4.3.5 THE EFFECT OF THE ADHESIVE TYPE ON THE EFFECTIVENESS OF THE RETROFITTING SCHEME

Figure 4.13(a) presents the load-deflection performance of Group 2 beams at their mid-span. From the chart, it can be seen that the load–deflection behaviour of all beams was linear until yielding of the steel occurred. After yielding, the behaviour of the beam was observed to be non-linear until the CFRP sheets failed by rupture or debonding. As expected, after the CFRP failure, the behaviour of the beam followed a similar behaviour to that of an unstrengthened beam. As can be seen in Figure 4.13(a), the type of the adhesive has no influence on the elastic or the inelastic stiffness, while it has a major effect on the mode of failure, as well as in the ultimate flexural capacity. The corresponding load-strain performance of Group 2 beams at the member mid-span is shown in Figure 4.13(b). Figure 4.13(c) shows that beams BF-H0.33-F1(5)-B2 and BF-

N0.50-F1(5)-B2 exhibited significantly larger rotation in comparison to beams BF-H0.33-F1(5)-B1 and BF-N0.50-F1(5)-B2, respectively.

4.4 RESULTS OF GROUP 3 BEAMS

Two locally deteriorated beams such as: Beams BF-H0.33-F2(1)-B2 and BF-H0.33-F2(1)-B2 were strengthened by using epoxy bonding of one layer of Tyfo UC to their tension flanges. Tyfo MB-3 was used to bond the CFRP laminate strip to the tested beams, while one layer of Tyfo EB-DB system was used as a dielectric barrier between the Tyfo UC and the tension flange to prevent any galvanic corrosion reaction. To characterize the influence of wrapping on the behaviour of strengthening steel beam, one layer of Tyfo SCH-11UP with a width of 200 mm was used to wrap the CFRP laminate strip at the both ends of the BF-H0.33-F2(1)-B2w beam.

4.4.1 BEAM BF-H0.33-F2(1)-B2

Beam BF-H0.33-F2(1)-B2 is similar to beam BF-H0.33-F1(5)-B2 except that it has 1 longitudinal CFEP strip instead of 5 CFRP sheets. This beam started to yield at a load of 250 kN with a maximum deflection of the tension flange equal to 8.40mm. As shown in Figure 4.14(a), the failure mode was observed as sudden failure by the peeling off of the CFRP strip. The maximum applied load of 344 kN at failure was found to be 1.38 times the applied load at yield. The maximum deflection of 46.10 mm at failure is 5.50 times the equivalent deflection at yield (see Figure 4.14(b)). The maximum strain in the CFRP strip was recorded as 10032 με. The corresponding Load-strains diagram at

different locations is shown in Figure 4.14 (c). It is important to mention that at a deflection of 6.20 mm and a load of 190 KN, the mid-span cross-section started to yield.

4.4.2 BEAM BF-H0.33-F2(1)-B2W

Beam BF-H0.33-F2(1)-B2w was strengthened with 1 CFRP strip, transversally wrapped at its ends by 1 layer of CFRP sheets in an attempt to eliminate the peel-off failure of the previous studied BF-H0.33-F2(1)-B beam. Similar to the other locally deteriorated beams, the mid-span cross-section started to yield at a load of 230 kN which imposed a deflection equal to 7.30 mm and a measured strain of 1520 με. At a load equal to 260 kN, the beam started yielding with a maximum deflection of the bottom flange equal to 8.6 mm. As can be seen in Figure 4.15 (a), the failure mode was observed to be sudden failure by rupture in the wrapping sheets following by peeling-off of the CFRP strips. The failure applied load of 347 kN was 1.33times the applied load at yield and the mid-span deflection of 48.70 mm was 5.66 times the equivalent deflection at yield. The load-deflection and load-strains performances of the beam at different locations can be seen in Figure 4.15 (b and c).

4.4.3 THE EFFICIENCY OF THE WRAPPING SYSTEM

As discussed before, two deteriorated steel beams of Group 3 were strengthened by using one layer of CFRP strip with and without wrapping system. As shown in Figure 4.16(a), the using of wrapping system for bonded CFRP is not an efficient technique to increase the ultimate load capacity, while it has a minor effect on increasing the yielding load capacity from 250 to 260 kN. Therefore, using wrapping sheets in the end will not

decrease the required development length needed to reach the maximum strength of the CFRP strip. The corresponding load-strain and moment-rotation performance of the Group 3 beams can be seen in Figure 4.16 (b and c).

4.5 RESULTS OF GROUP 4 BEAMS

The proposed retrofitting scheme used in this group is an unbonded CFRP sheets with a ductile anchorage system. As discussed before in Chapter 3, the main objective of this proposed scheme is to strengthen the beam such that to reach the full capacity of the CFRP sheets by using a tensile stress transfer system to two ductile anchorages, located at the beam ends. The ductile anchorage system is designed to yield before the rupture of the CFRP sheets occurs. In this particular study, the failure mode for all beams in this group was controlled by CFRP sheets rupture. As shown before in Figure 3.18, the proposed scheme is composed of an unbonded CFRP sheet(s) which were wrapped around two steel plates at its ends (Part 1). In order to avoid stress concentration and rupture of the FRP sheets, part 1 of the system had rounded corners (see Fig. 3.18). Duct tape was used to cover the contact area between part 1 and the CFRP sheets such that any possible bond stress between them to be inexistent. Part 1 was then linked to the steel plate (part 3) which is anchored to the tension flange of the tested beam by using four high stress tensile steel bolts through two steel link members (part 2). The steel link members were designed as a conventional tensile test dog-bone specimen. Based on this setup, the forces in the steel link member are tensile axial forces only without any moments on them. Three beams were tested in group 4 such as: BF-H0.33-F1(1)-A1D1,

BF-H0.33-F1(1)-A2D1, and BF-H0.33-F1(1)-A2D2. All these tested beams had a locally deterioration simulated at beam mid-span cross-section as for beam BF-H0.33.

4.5.1 BEAM BF-H0.33-F1(1)-A1D1

One layer of Tyfo SCH-11UP was used to strengthen the deteriorated steel beam BF-H0.33-F1(1)-A1D1 by wrapping it around the anchorage system (part one) with an overlap of 350 mm. This overlap zone was used to avoid debonding between the CFRP sheets. The steel link member (A1) was designed to have rupture in the CFRP sheet before yielding. Beam BF-H0.33-F1(1)-A1D1 started to yield at a load of 240 kN, while the deflection was recorded as 7.30 mm. At a load of 323 kN with a corresponding deflection at the mid-span of the tension flange equal to 43.90 mm which means 6.00 times the maximum deflection at yield, the failure mode was characterized by rupture in the CFRP sheet and is shown in Figure 4.17 (a). The average strain in the CFRP sheet and the coupons at failure was reported as 10600 με and 350 με, respectively. The applied load versus the deformations and strains at different locations are shown in Figure 4.17 (b and c).

4.5.2 BEAM BF-H0.33-F1 (1)-A2D1

Similar to beam BF-H0.33-F(1)-A1D1, one layer of unbonded anchorage Tyfo SCH-11UP was used to strengthen the beam BF-H0.33-F(1)-A2D1. The steel link member (A2), used in this beam was designed to have a lower yield stress than the ultimate strength of the CFRP sheet. At a load of 246 kN and a mid-span deflection of 7.80 mm, this beam started to yield, while the average strain in the steel link member was

measured as being 370 με. The steel link member started to yield at a load of 310 kN. The failure mode was observed to be rupture in the CFRP sheet, as can be seen in Figure 4.18 (a). The failure load was recorded as 320 kN, 1.3 times the applied load at yield, and the corresponding deflection at failure was measured as 43.95 mm, 5.58 times the measured deflection at yield. The average strain in the coupons at failure was reported as 1900 με. The corresponding Load-deflections and Load-strains diagrams at different locations are shown in Figure 4.18 (b and c).

4.5.3 BEAM BF-H0.33-F1 (5)-A1D2

Five layer of Tyfo SCH-11UP were used to strengthen the deteriorated steel beam BF-H0.33-F(5)-A2D2 by wrapping them around the anchorage system (part one).Among the three rounds of CFRP sheets, the first two round were wet while the last one was dry. The steel link member (A1) was designed to yield before the rupture in the CFRP sheets occurs. At a deflection of 7.70 mm the beam started to yield, while the applied load was recorded to be 250 kN. At the mustered yielding load, the average strain in the coupons was measured as 270 με which means that the steel link member was in the elastic zone. When the applied load was 304 kN which means 1.22 times the applied load at yield, rupture in the CFRP sheets at the anchorage was observed (see Figure 4.19 (a)). The average strain in the steel link members at failure was recorded as 1150 με, while the measured deflection 32.00 mm was 4.19 times the measured deflection at yield. The load-deflection and load-strains performances of the beam at different locations can be seen in Figure 4.19 (b and c).

4.5.4 THE EFFICIENCY OF THE PROPOSED DUCTILE ANCHORAGE SYSTEM

Based on the results of Group 4 beams, the proposed ductile anchorage system shows a high ability to transfer the load from the unbonded CFRP sheets to the tension flange at their zero moment zones using ductile steel link members. The failure mode of all the tested beams was observed to be rupture of the CFRP sheets since this ductile anchorage system prevents early peel off of the CFRP sheet. The failure mode of beam BF-H0.33-F1(1)-A2D2 shows that the end anchorage detail has a great effect on the failure mode, and as a result, on the ultimate capacity. If well detailed, the ductile guarantees a ductile behaviour of the composite steel beams until failure occurs. Figure 4.20 shows the performance of this proposed retrofitting scheme.

4.6 GENERAL DISCUSSION

An experimental investigation was carried out on the behaviour of corroded steel beams before and after retrofitting. Based on the experimental results, the local corrosion showes a slight effect on the load-deformation behaviour of deteriorated steel beam, whereas this effect increases with the increase of length of corroded area along the beam, as can be seen in Figure 4.21. In addition, by using the high performance adhesive MB-3 which is a viscous epoxy adhesive with saturated CFRP sheets, it was observed a better efficiency in the behaviour than by using the common adhesive Tyfo S. This Figure also shows that the type of the adhesive doesn't have any influence on the beam stiffness and this last parameter depends only on the type of CFRP composite material. Figure 4.22 shows the behaviour of beams BF-H0.33 and BF-N0.50 before and after strengthening with bonded CFRP sheets. By analysing the results given in the aforementioned Figure

4.22, it can be conducted that bonded CFRP has a minor effect on the elastic behaviour of the strengthened beam, while it has a major effect on the inelastic behaviour. In addition, by using bonded CFRP as a retrofiting scheme doesn't means that we have an effective system, since the effeciancy of this technique is based on the type of the CFRP material and the type of the adhesive used in this scheme.

Table 4.1 Summary of the test results

	Beam	Load Capacity at Yield						Load Capacity at Failure					Mode of Failure
		Yield Strain			Yield Deflection			CFRP Failure			Steel Failure		
		Load	M.S.* Defl.	M.S. tensile Strain	Load Py	M.S. Defl. Δy	M.S. tensile Strain	Load Pu	M.S. Defl. Δu	M.S. CFRP Strain	Load Pu	M.S. Defl. Δu	
		(kN)	(mm)	(με)	(kN)	(mm)	(με)	(kN)	(mm)	(με)	(kN)	(mm)	
G1	BFO	245	7.7	1568	245	7.7	1568	_	_	_	331	73.6	Steel-buckling
	BF-H0.33	180	5.8	1530	242	8.0	7000	_	_	_	330	69.8	Steel-buckling
	BF-N0.33	175	5.9	1550	190	6.4	1640	_	_	_	311	74.3	Steel-buckling
	BF-N0.50	140	5.5	1540	155	5.8	1660	-	-	-	290	95.4	Steel-buckling
G2	BF-H0.33-F1(5)-B1	_	_	_	245	7.9	_	307	18.1	4882	_	_	CFRP Peeling
	BF-N0.50-F1(5)-B1	181	5.7	1548	181	5.7	1548	262	12.1	4363	_	_	CFRP Peeling
	BF-H0.33-F1(5)-B2	200	6.5	1450	253	8.2	3000	375	51.0	10032	_	_	CFRP rupture
	BF-N0.50-F1(5)-B2	195	6.5	1630	195	6.5	1630	307	24.0	10514	-	-	CFRP rupture
G3	BF-H0.33-F2(1)-B2	190	6.2	1430	250	8.4	2671	344	46.1	10032	_	_	CFRP Peeling
	BF-H0.33-F2(1)-B2w	230	7.3	1520	260	8.6	3227	347	48.7	—	—	—	CFRP peeling
G4	BF-H0.33-F1(1)-A1D1	_	_	_	240	7.3	4100	323	43.9	10600	_	_	CFRP rupture
	BF-H0.33-F1(1)-A2D1	_	_	_	246	7.8	1710	320	44	11800	_	_	CFRP rupture
	BF-H0.33-F1(5)-A2D2	—	—	—	250	7.7	2450	304	32	4150	—	—	CFRP rupture

*) M.S. the mid-span of the beam

Table 4.2 Summary of the comparison results

	Beam	$\frac{P_u}{P_y}$	$\frac{\Delta_u}{\Delta_y}$	$K_e = \frac{P_y}{\Delta_y}$ (kN/mm)	$\frac{P_p}{P_u}$	$K_i = \frac{P_u - P_y}{\Delta_u - \Delta_y}$ (kN/mm)	$\frac{M_y}{M_{y(BFO)}}$ %	$\frac{M_u}{M_{u(BFO)}}$ %	$\frac{\Delta_y}{\Delta_{y(BFO)}}$ %
G 1	**BFO**	1.35	9.6	31.8	0.95	1.3	100	100	100
	BF-H0.33	1.36	8.7	30.3	0.95	1.4	99	100	100
	BF-N0.33	1.64	11.6	29.7	0.92	1.8	78	94	83
	BF-N0.50	1.87	16.5	26.7	0.93	1.5	63	88	75
G 2	**BF-H0.33-F1(5)-B1**	1.25	2.3	31.0	——	6.1	100	93	103
	BF-N0.50-F1(5)-B1	1.45	2.1	31.8	——	12.7	74	79	74
	BF-H0.33-F1(5)-B2	1.48	6.2	30.9	——	2.85	103	113	106
	BF-N0.50-F1(5)-B2	1.57	3.7	30.0	——	6.4	80	93	84
G3	**BF-H0.33-F2(1)-B2**	1.38	5.5	29.8	——	2.5	102	104	109
	BF-H0.33-F2(1)-B2w	1.33	5.7	30.2	——	2.2	106	105	112
G4	**BF-H0.33-F1(1)-A1D1**	1.35	6.0	32.9	——	2.3	98	98	95
	BF-H0.33-F1(1)-A2D1	1.3	5.6	31.5	——	2.0	100	97	101
	BF-H0.33-F1(5)-A2D2	1.2	4.2	32.5	——	2.2	102	92	100

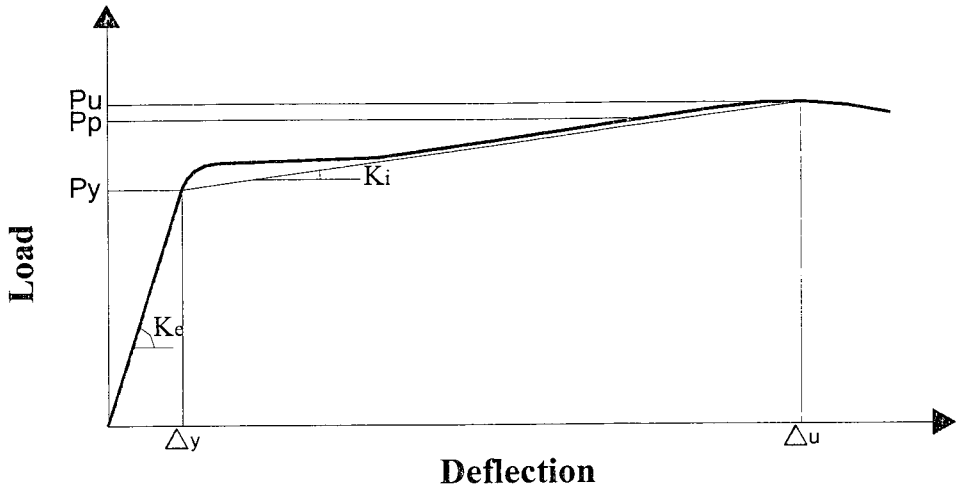

(a) Non strengthened steel beam

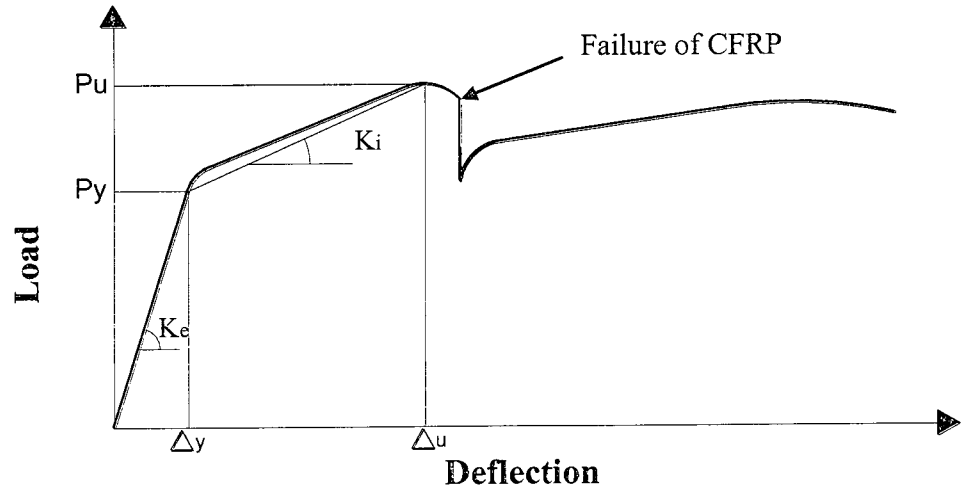

(b) Strengthened steel beam

Figure 4.1 Definitions of the yield and ultimate loads with their corresponding deflections; (a) Non-strengthened steel beam, and b) Strengthened steel beam.

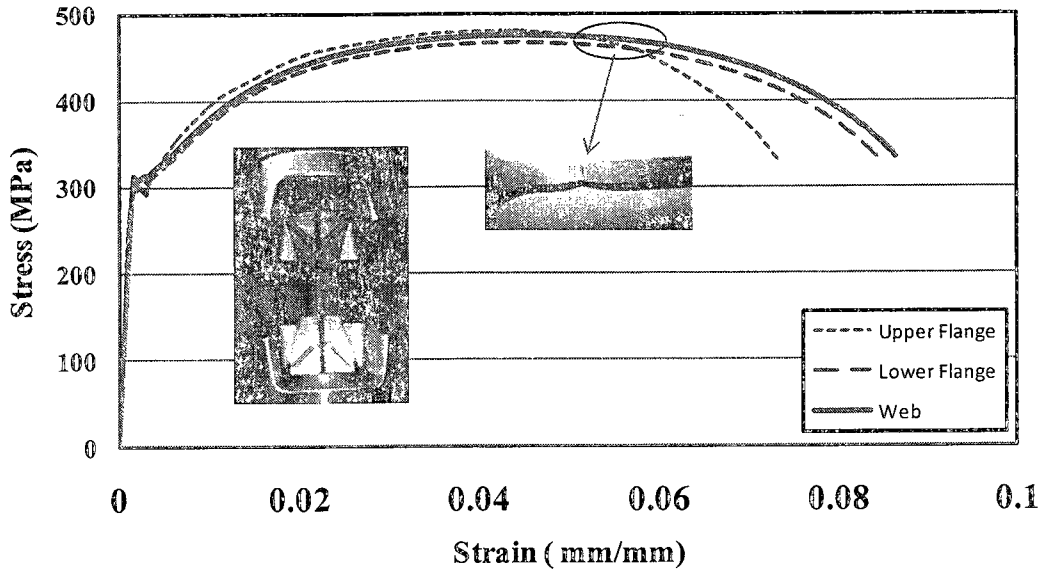

Figure 4.2 Stress-Strain curves for beam coupons

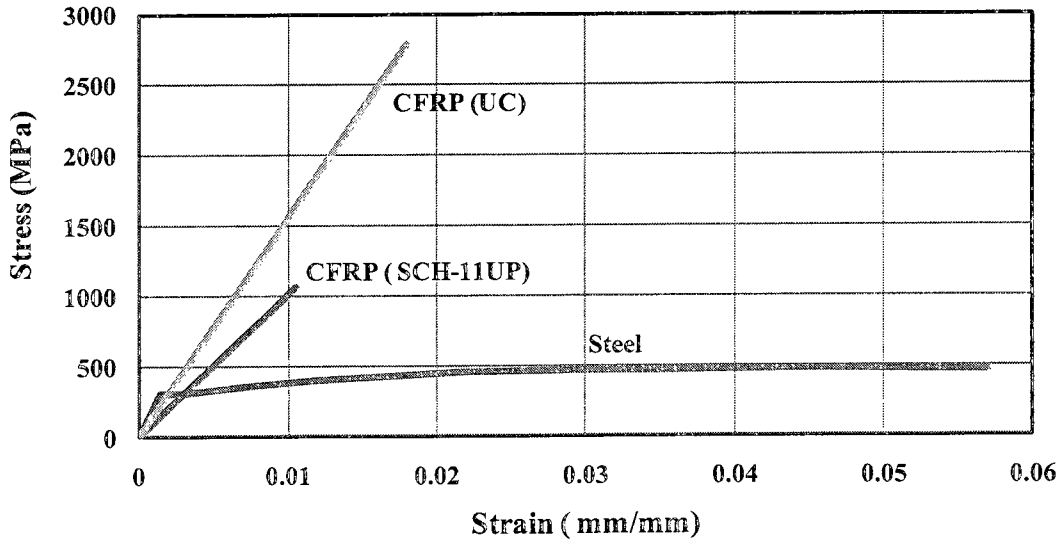

Figure 4.3 Stress-Strain curves for the steel coupons, Tyfo® SCH-11UP sheets and Tyfo® UC strips

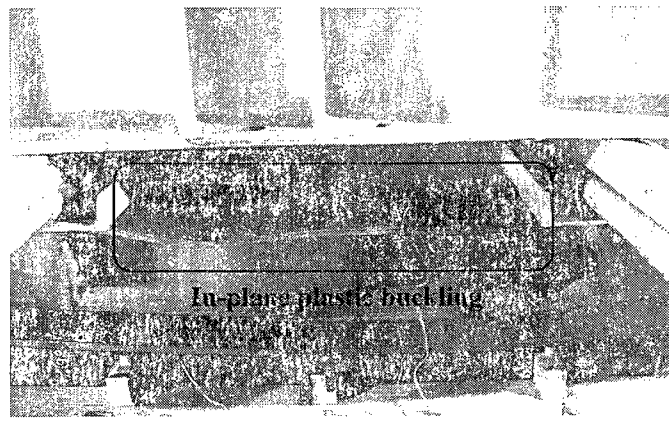

(a)

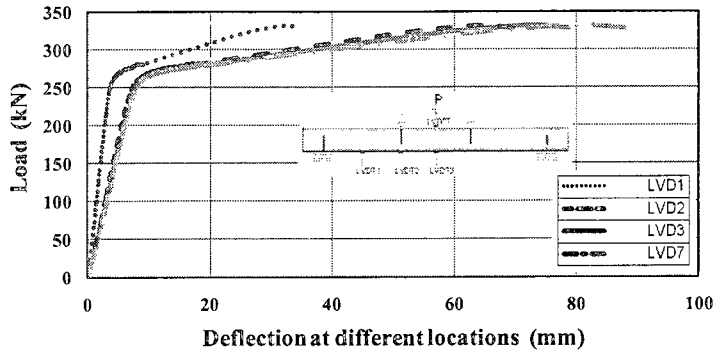

(b)

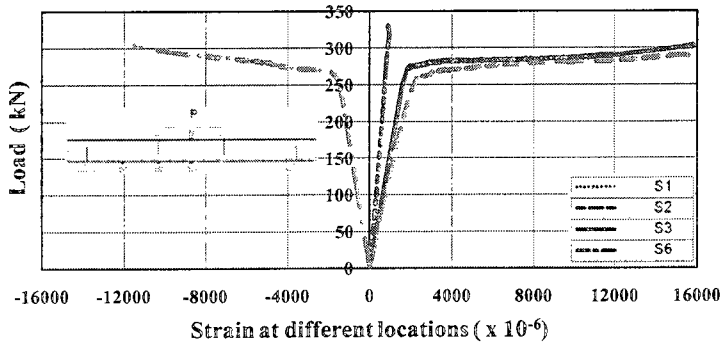

(c)

Figure 4.4 Test results of beam BFO; (a) Mode of failure, (b) Load-deflection, (c) Load-strain

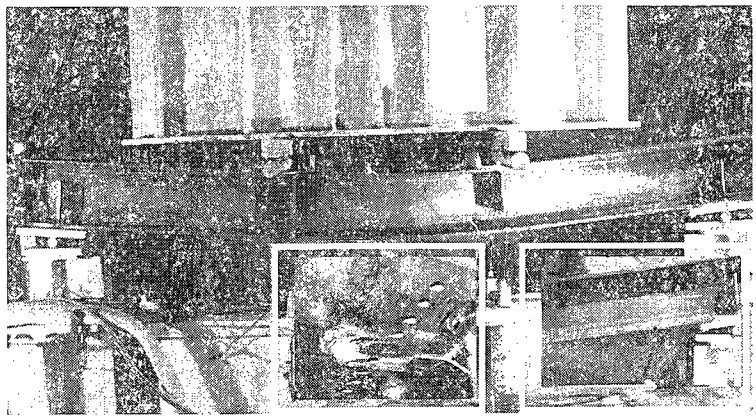

(a)

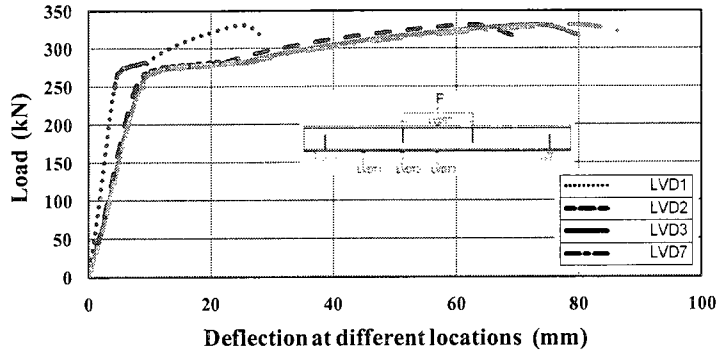

(b)

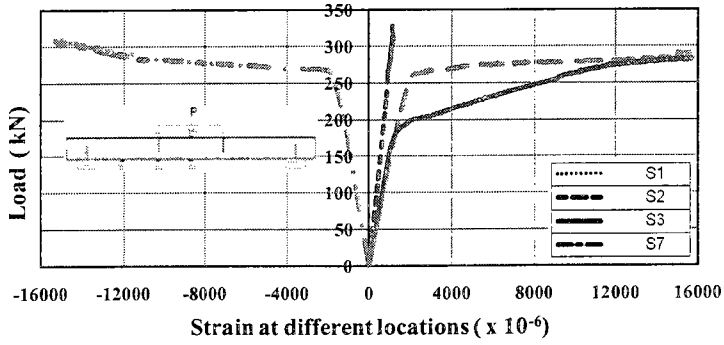

(c)

Figure 4.5 Test results of beam BF-H0.33; (a) Mode of failure, (b) Load-deflection, (c) Load-strain

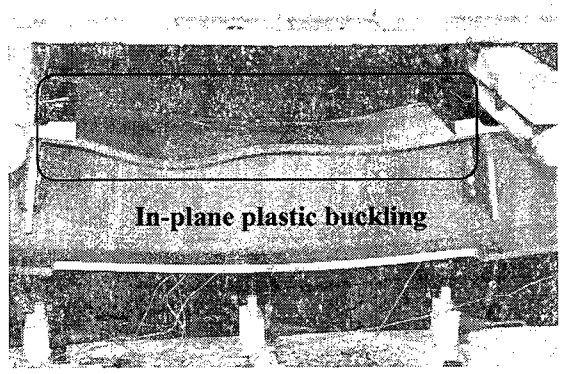

(a)

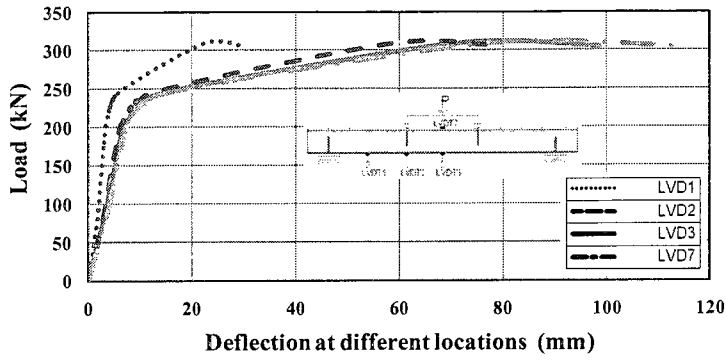

(b)

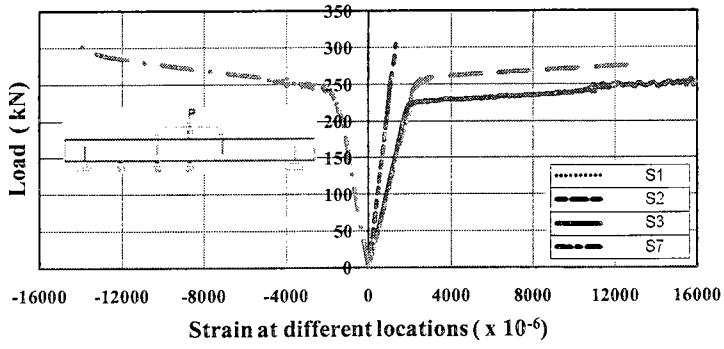

(c)

Figure 4.6 Test results of beam BF-N0.33; (a) Mode of failure, (b) Load-deflection, (c) Load-strain

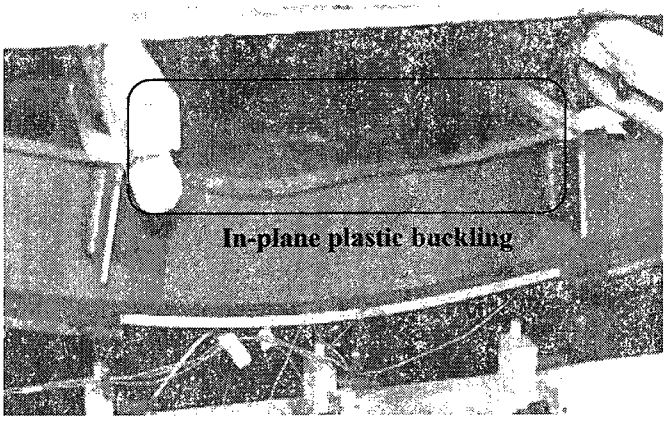

(a)

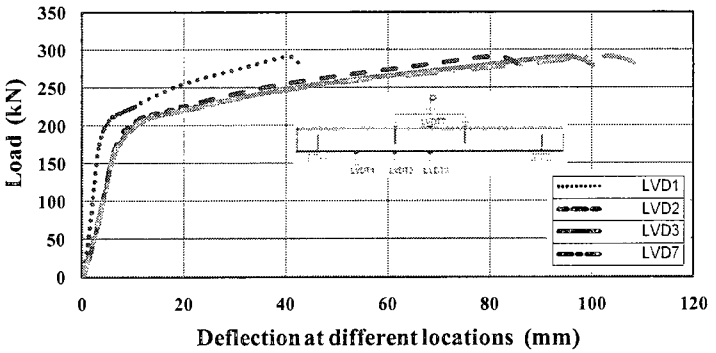

(b)

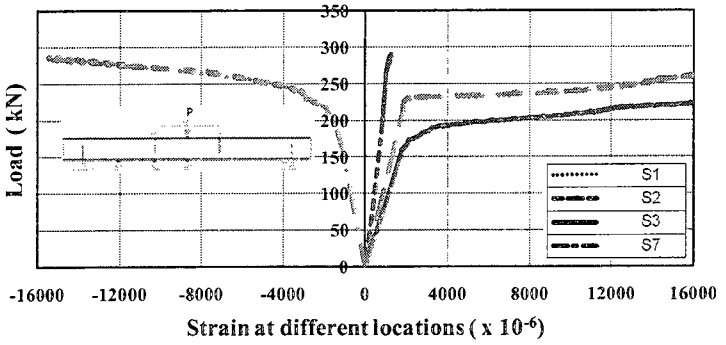

(c)

Figure 4.7 Test results of beam BF-N0.50; (a) Mode of failure, (b) Load-deflection, (c) Load-strain

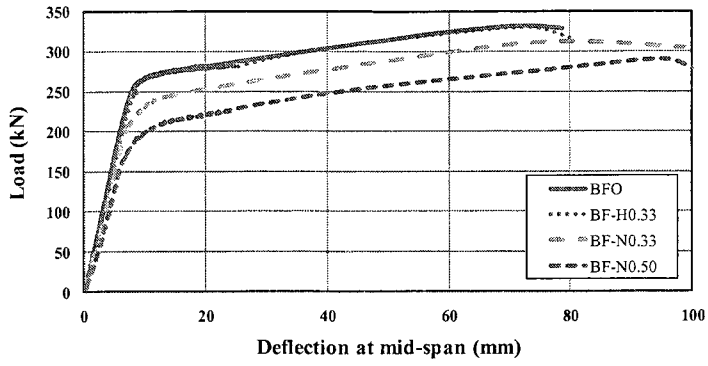

(a)

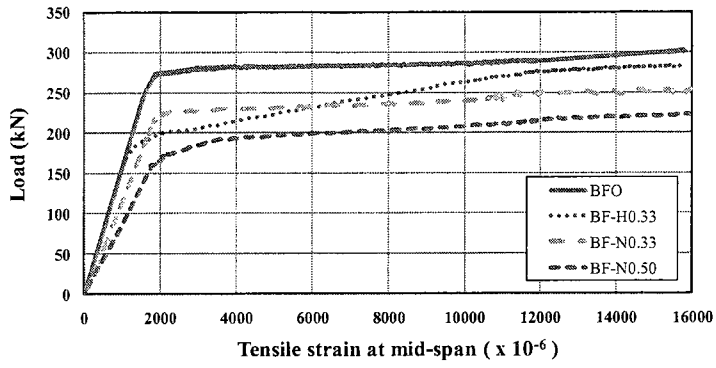

(b)

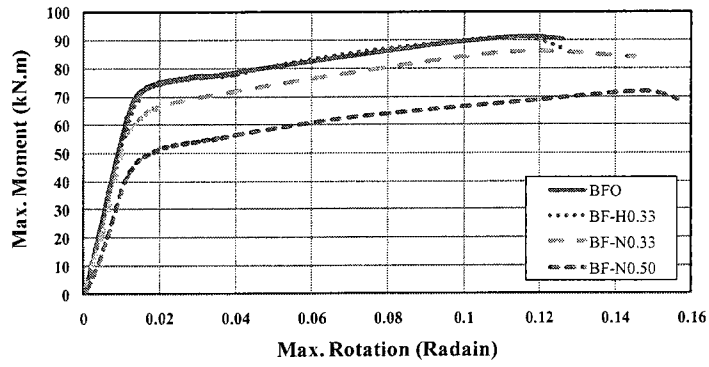

(c)

Figure 4.8 Performance of group 1 beams; (a) Load-deflection, (b) Load-strain, (c) Moment-rotation

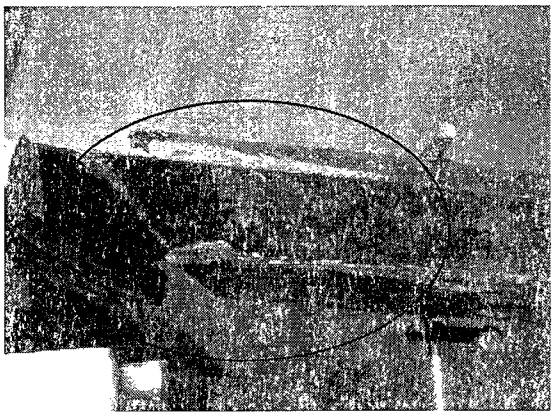

(a)

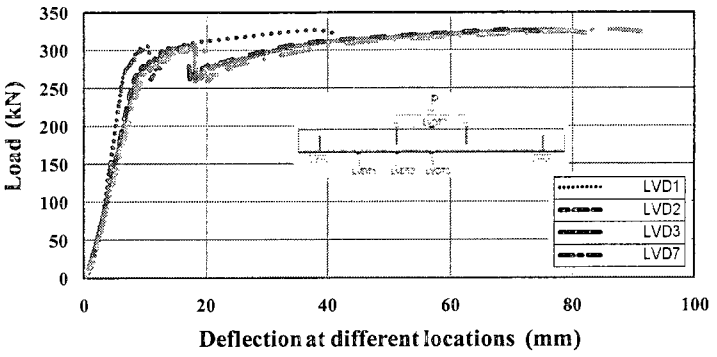

(b)

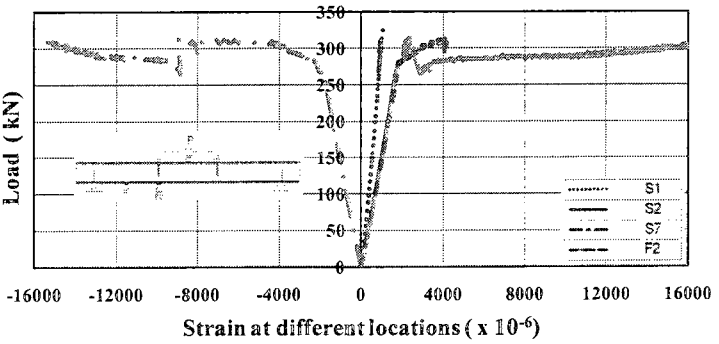

(c)

Figure 4.9 Test results of beam BF-H0.33-F1(5)-B1; (a) Mode of failure, (b) Load-deflection, (c) Load-strain

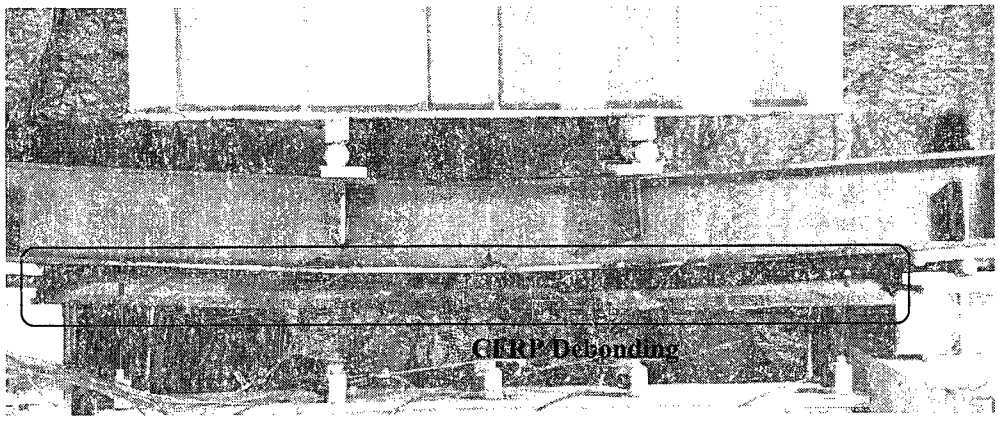

(a)

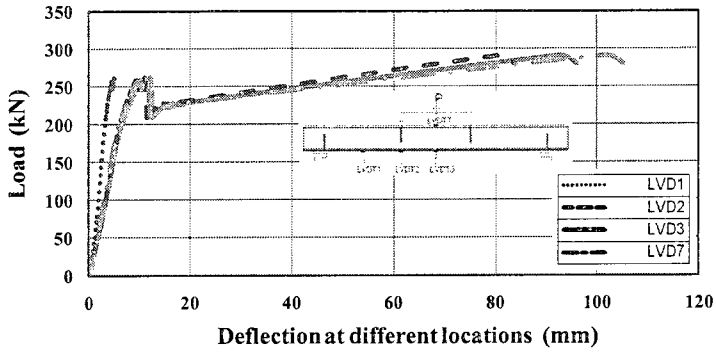

(b)

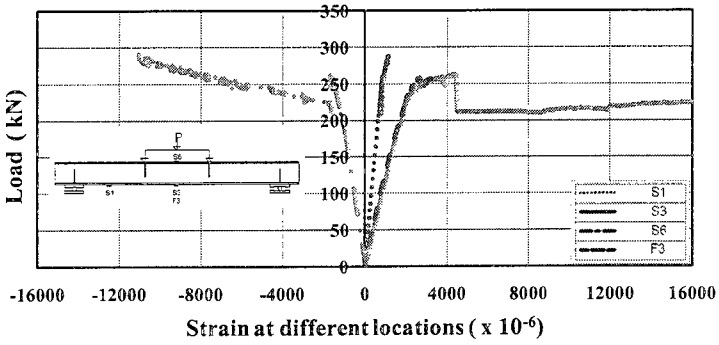

(c)

Figure 4.10 Test results of beam BF-N0.50-F1(5)-B1; (a) Mode of failure, (b) Load-deflection, (c) Load-strain

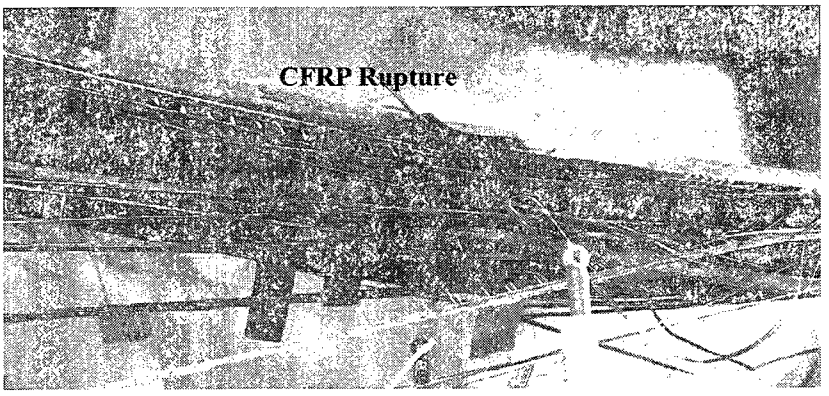

(a)

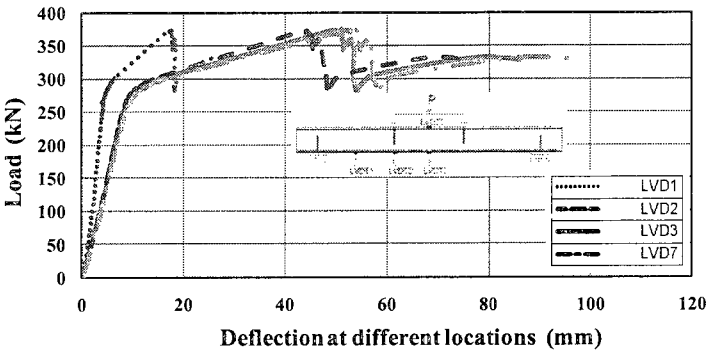

(b)

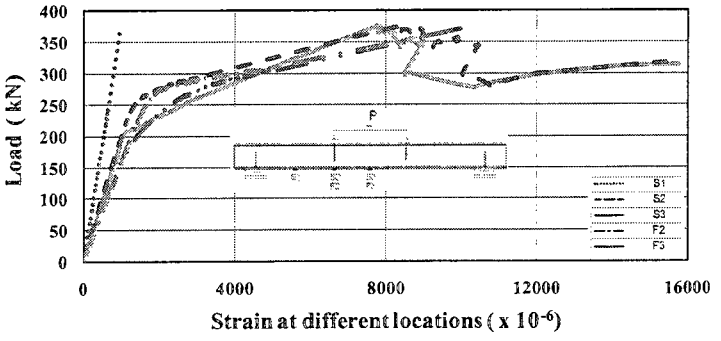

(c)

Figure 4.11 Test results of beam BF-H0.33-F1(5)-B2; (a) Mode of failure, (b) Load-deflection, (c) Load-strain

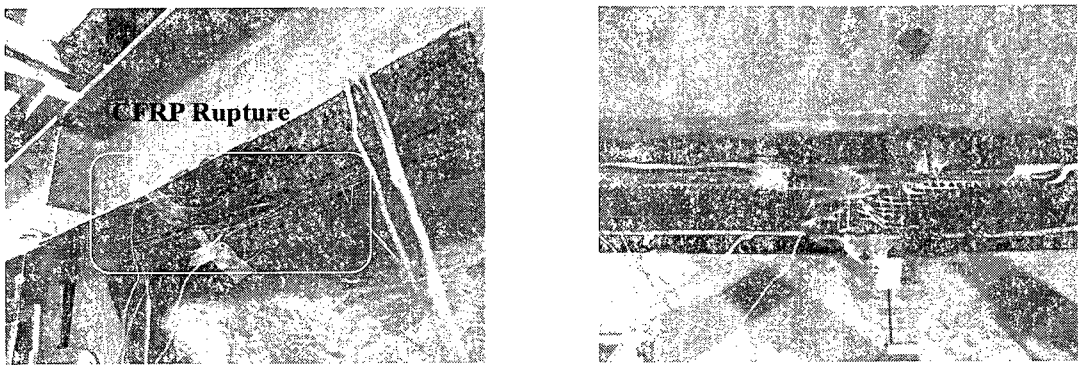

(a)

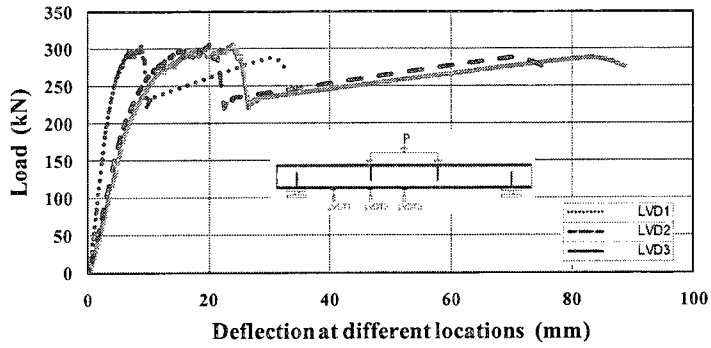

(b)

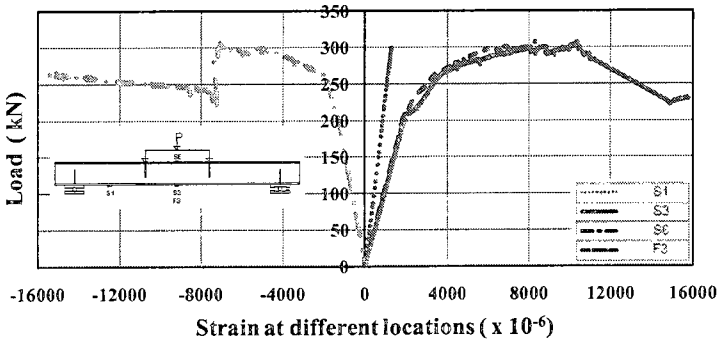

(c)

Figure 4.12 Test results of beam BF-N0.50-F1(5)-B2; (a) Mode of failure, (b) Load-deflection, (c) Load-strain

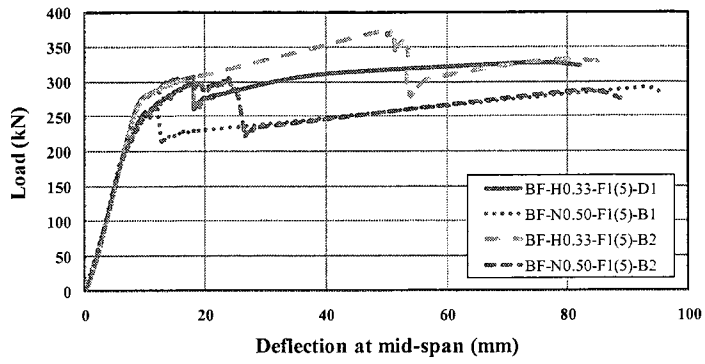

(a)

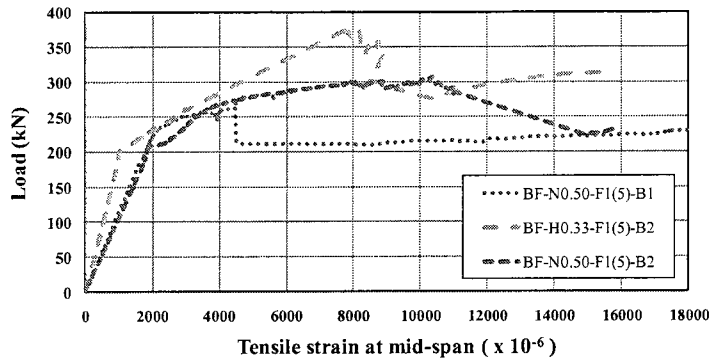

(b)

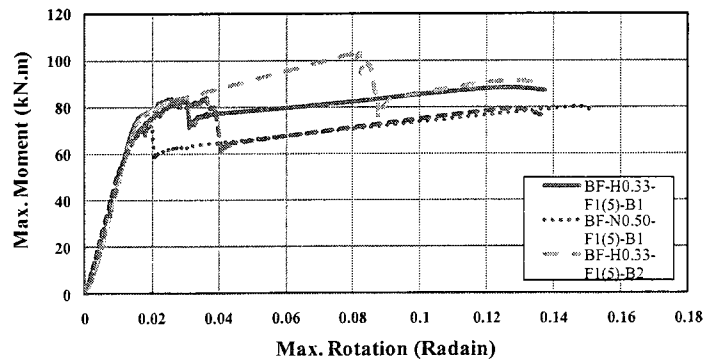

(c)

Figure 4.13 Performance of group two beams; (a) Load-deflection, (b) Load-strain, (d) Moment-rotation

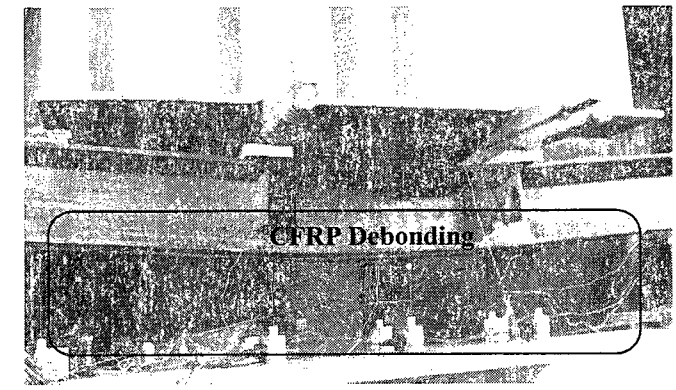

(a)

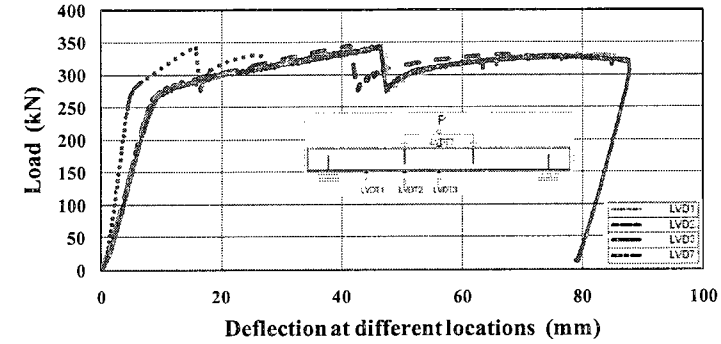

(b)

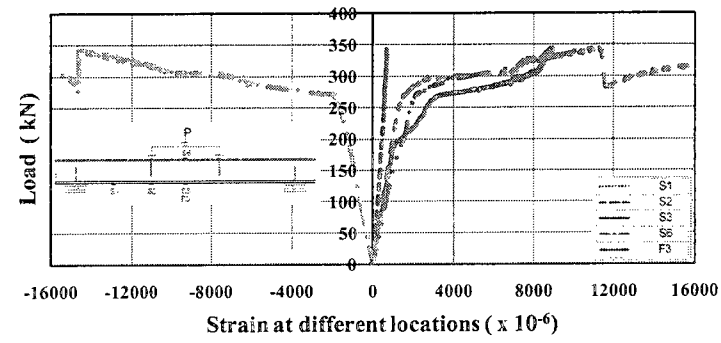

(c)

Figure 4.14 Test results of beam BF-H0.33-F2(1)-B2; (a) Mode of failure, (b) Load-deflection, (c) Load-strain

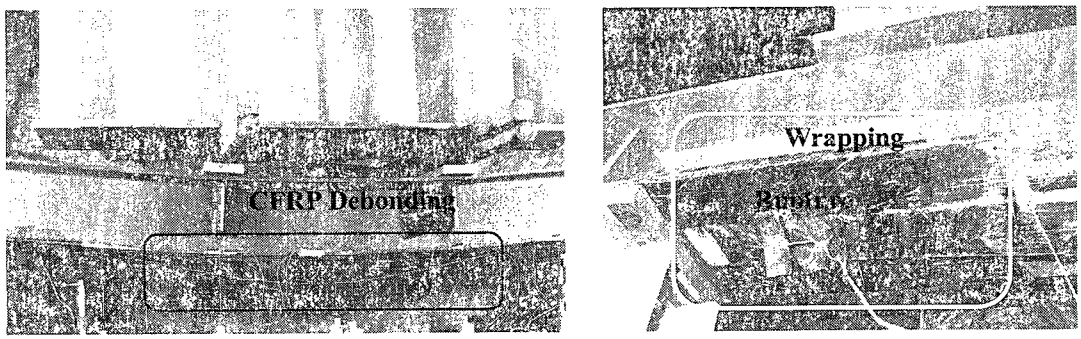

(a)

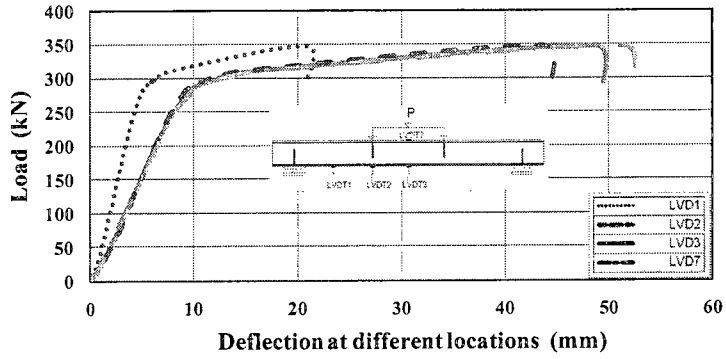

(b)

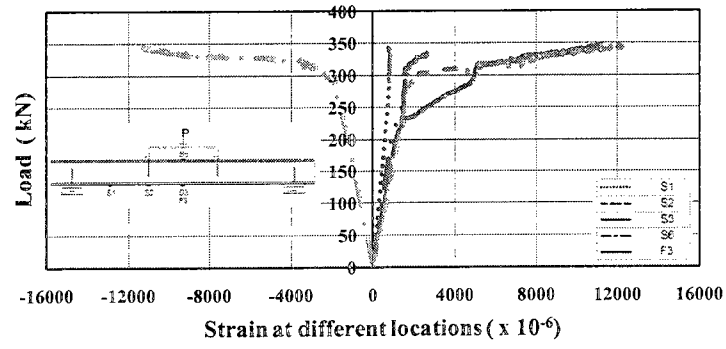

(c)

Figure 4.15 Test results of beam BF-H0.33-F2(1)-B2w; (a) Mode of failure, (b) Load-deflection, (c) Load-strain

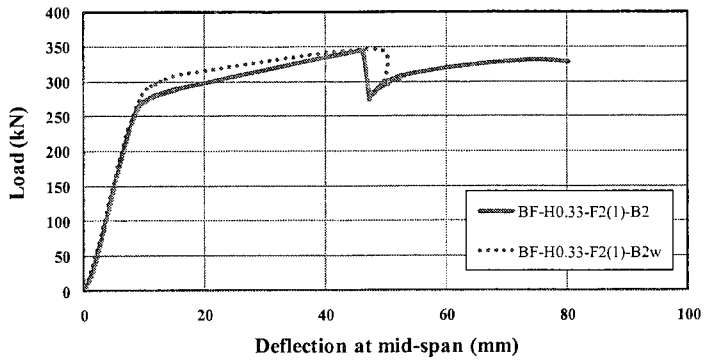

(a)

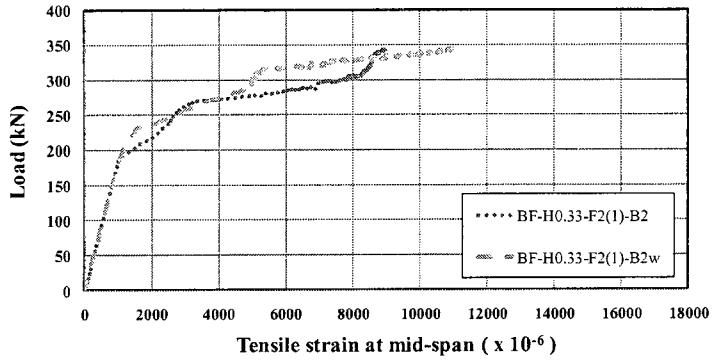

(b)

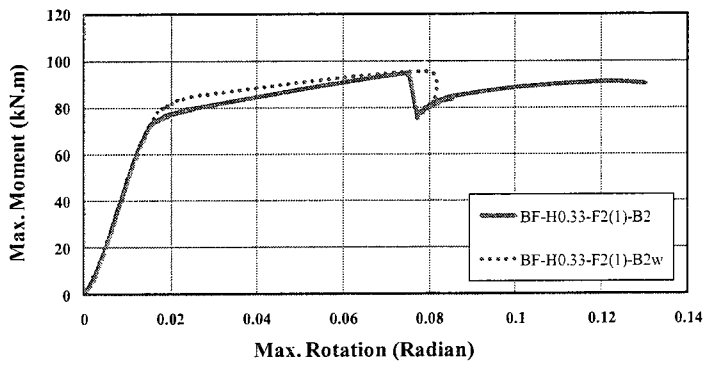

(c)

Figure 4.16 Performance of group 3 beams; (a) Load-deflection, (b) Load-strain, (d) Moment-rotation

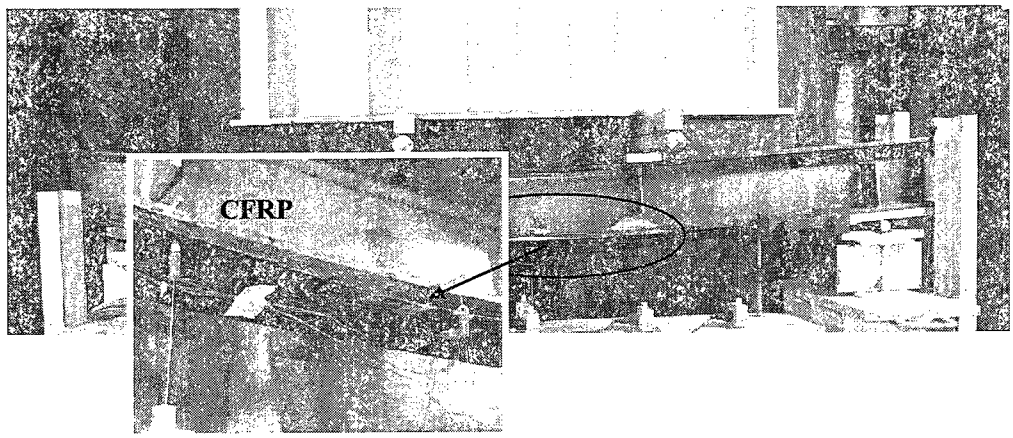

(a)

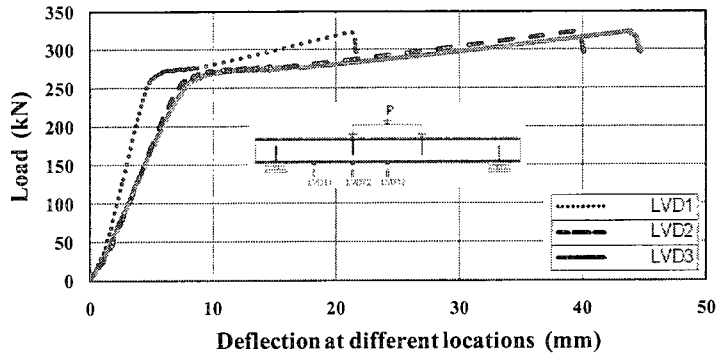

(b)

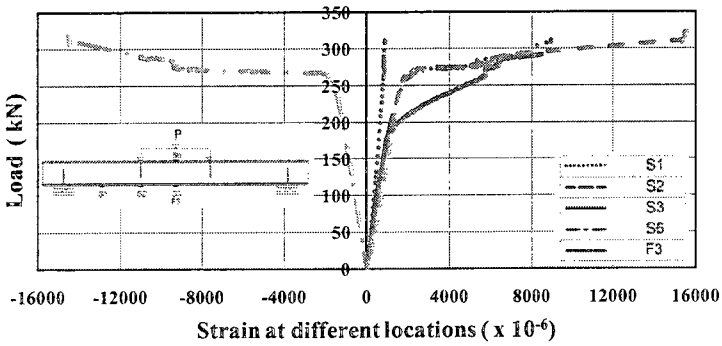

(c)

Figure 4.17 Test results of beam BF-H0.33-F1(1)-A1D1; (a) Mode of failure, (b) Load-deflection, (c) Load-strain

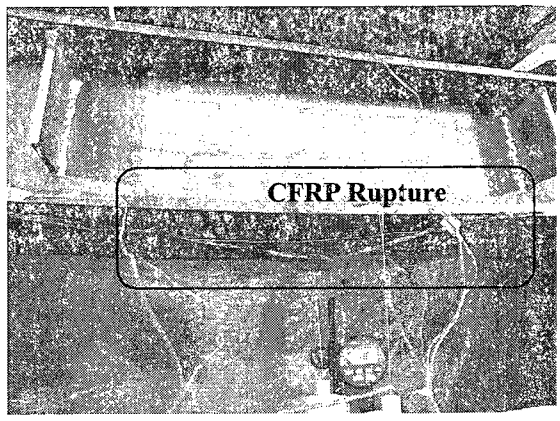

(a)

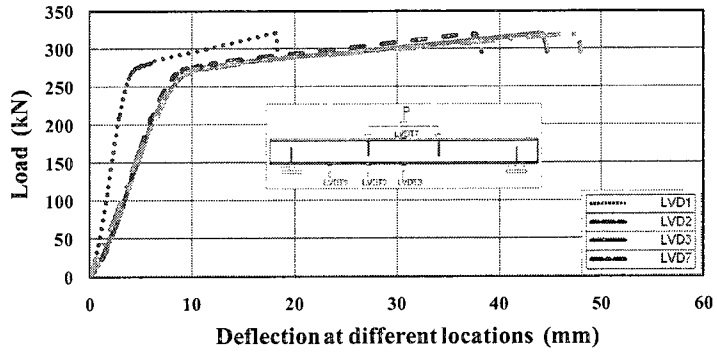

(b)

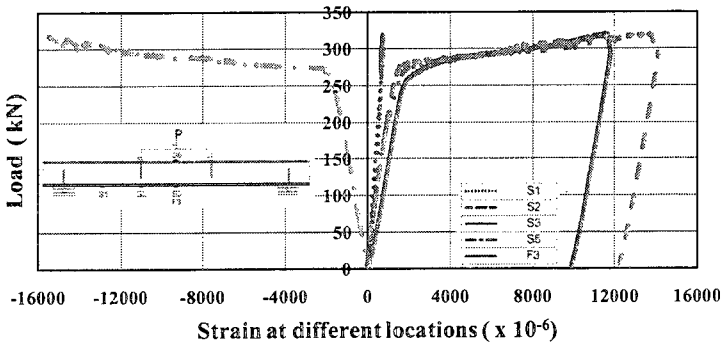

(c)

Figure 4.18 Test results of beam BF-H0.33-F1(1)-A2D1; (a) Mode of failure, (b) Load-deflection, (c) Load-strain

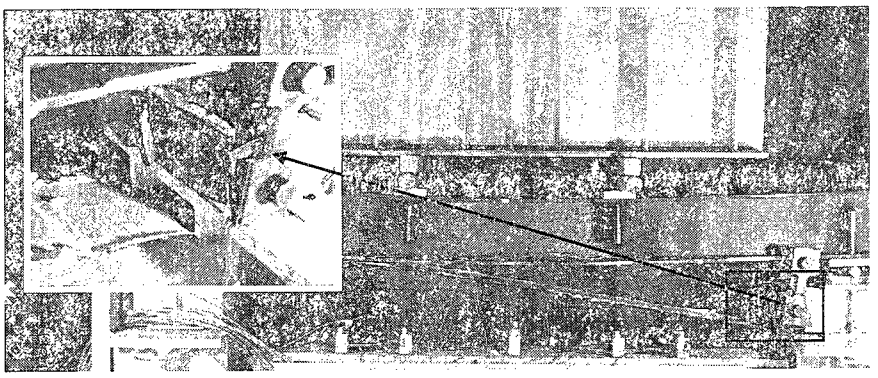

(a)

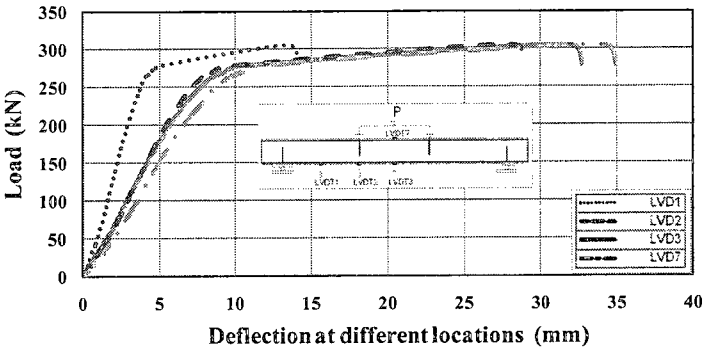

(b)

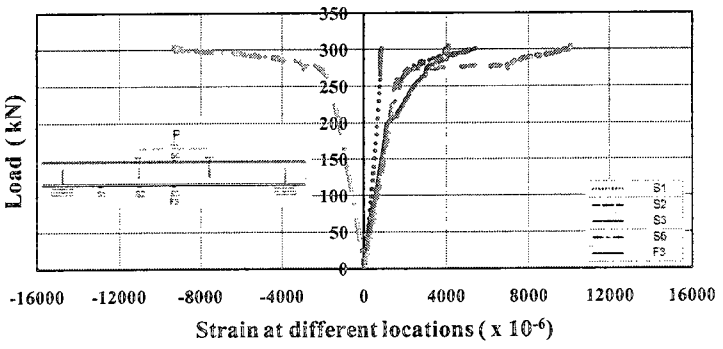

(c)

Figure 4.19 Test results of beam BF-H0.33-F1(5)-A2D2; (a) Mode of failure, (b) Load-deflection, (c) Load-strain

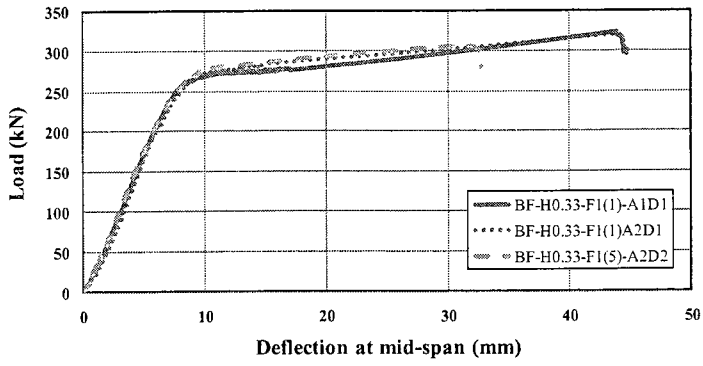

(a)

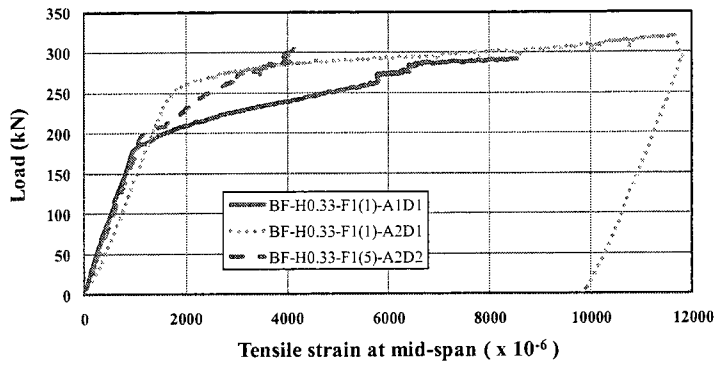

(b)

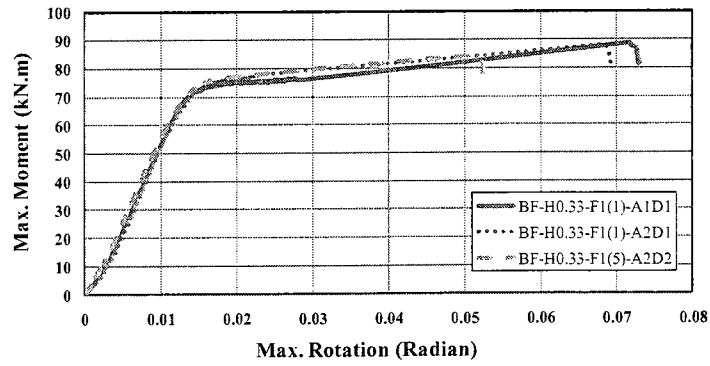

(c)

Figure 4.20 performance of group four beams; (a) Load-deflection, (b) Load-strain, (d) Moment-rotation

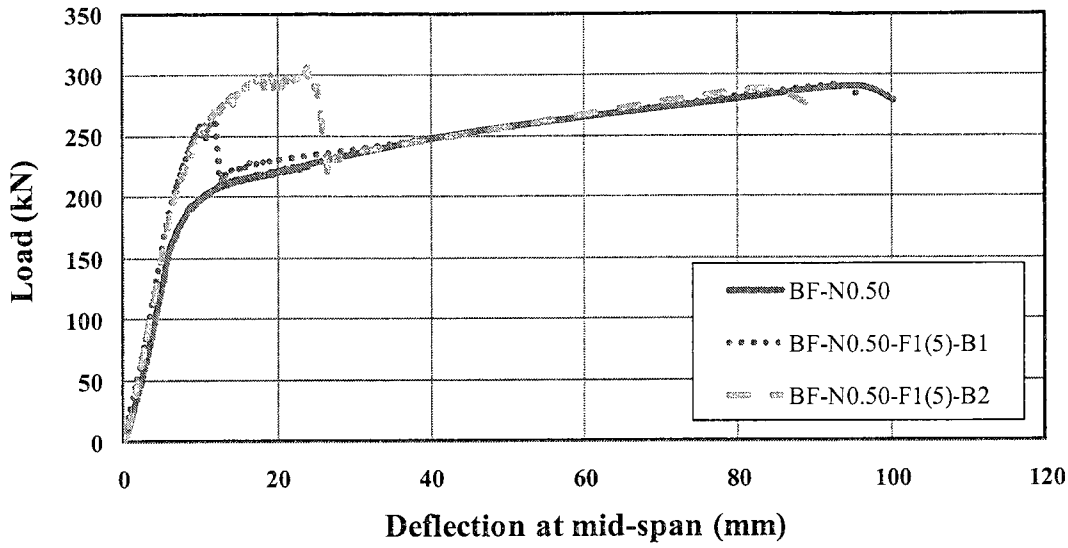

Figure 4.21 Load-deflection relative performance of beams: BF-N0.50, BF-N0.50-F1(5)-B1 and BF-N0.50-F1(5)-B2

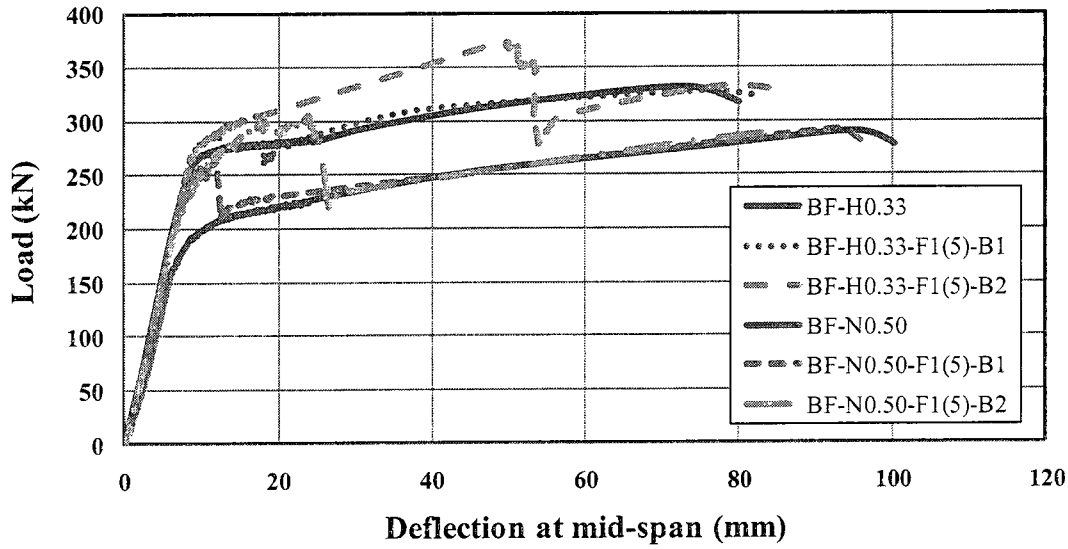

Figure 4.22 Load-deflection relative performance of beams: BF-H0.33, BF-H0.33-F1(5)-B1, BF-H0.33-F1(5)-B2, BF-N0.50, BF-N0.50-F1(5)-B1 and BF-N0.50-F1(5)-B2

CHAPTER 5

NUMERICAL MODEL

5.1 INTRODUCTION

The main objective of this chapter is to set up a numerical method that is capable of predicting the elastic and the post-yield behaviour of unstrengthened and strengthened deteriorated steel girders. This proposed method can be used by designers to calculate the reduction in the moment capacity of the deteriorated steel girders within a reasonable level of accuracy. The analysis approach is based on a moment-curvature analysis which satisfies equilibrium and compatibility. The following assumptions were considered in this analysis: i) plane sections remain plane after deformation; ii) deformations are small; iii) a simplified material characteristic was used for the steel wide flange beam; iv) linear elastic behaviour of CFRP; v) bilinear relation between the bond length and the ultimate tensile strength in the bonded CFRP; vi) linear relation between the total number of CFRP layers and the minimum bonded development length; and vii) the stress in all CFRP layers is the same for the same tensile strain in the steel flanges (i.e. perfect bond until peel off of FRP). The results of the tested beams which presented in Chapter 4 were used to validate this numerical method.

It is noted that the discussion in this chapter is limited to the flexural analysis of unstrengthened and strengthened corroded steel girders using bonded CFRP. A bilinear relation between the bond length and the ultimate tensile strength for Tyfo SCH-11UP and Tyfo UC was assumed in this numerical model. Based on the experimental results and modes of failure, only three modes of failure were considered in this analysis such as:

in-plane plastic buckling for deteriorated steel beams; unbonded and rupture of CFRP for the rehabilitated/strengthened steel beams.

5.2 SECTION ANALYSIS IN FLEXURE

The mechanical properties for the steel material of the W-shape beams were determined by testing three dog-bone coupon specimens which were cut from the web and the flanges as described in Chapter 3. The measured stress-strain curves for the coupons were used to generate a best fit stress-strain curve which was used as input for the analytical model as shown in Figure 5.1. A bilinear relation between the bond length per layer and the ultimate tensile strength in this layer is shown in Figure 5.2. The bond length per layer was defined as:

$$L_{b/layer} = \frac{L_b}{n} \tag{5.1}$$

where L_b is the total bond length and n the total number of layers

Based on this bilinear relation, unbonded failure mode can be expected when bonding Tyfo SCH-11UP sheets to steel using Tyfo S and the bond length per layer is less than 205 mm. When MB-3 is used instead of Tyfo S, the minimum bonded length per layer which is required to have rupture in the CFRP sheets as a failure mode is only 90 mm. while, for Tyfo UC bonded by MB-3 the minimum bond length per layer required to have rapture failure mode.

In this chapter, efforts are made to develop a numerical model that is capable of predicting the remaining flexural capacity of deteriorated steel girders as well as the magnitude of the yielding moment. The full moment-curvature relationship of any steel cross-section is established by increase incrementally the strain at the extreme

compression fiber (see Figure 5.3). In the first step it is assumed that for a given strain, ε_c, the neutral axis depth is Y`. The corresponding curvature of this section can be calculated as:

$$\phi = \frac{\varepsilon_c}{(h - Y')} \tag{5.2}$$

Based on the assumed linear strain through the depth of the section as shown in Figure 5.3, the strain at any level in the section, ϵ_x, can be defined as:

$$\varepsilon_x = \text{ø} \qquad y$$

(5.3)

The strain is calculated at the inner and outer surfaces of the flanges of the steel beam, at which the geometric properties have changed. Once the strain at the different layers is known the stress distribution, $f_s(x)$, can be determined from the appropriate stress-strain relationship of the steel material as:

$$f_s(x) = \begin{cases} \epsilon_x E & \epsilon_x \leq 0.00155 \\ 310 & 0.00155 < \epsilon_x \leq 0.004 \\ 310 + (\epsilon_x - 0.004)(E_1) & 0.004 < \epsilon_x \leq 0.014 \\ 400 + (\epsilon_x - 0.014)(E_2) & 0.014 < \epsilon_x \leq 0.045 \end{cases} \tag{5.4}$$

where E is the elastic modulus of the steel, E_1 and E_2 are the second and third slope stiffness, respectively.

Once the force contribution of the steel cross-section is calculated, the total force on the cross-section can be calculated as:

$$F = F_1 + F_2 + F_3 + F_4 \tag{5.5}$$

where F_1 is the force in the compression flange, F2 is the force in the compression part of the web, F_3 is the force in the tension part of the web tension flange, and F4 is the force in the tension flange.

The depth of the neutral axis is iterated until the total force on the cross-section which was calculated using Equation 5.5, is equal to zero. Once the force equilibrium is satisfied, the flexural capacity associated to the considered mode of failure can be easily computed with the following Equation:

$$M = \Sigma F_i d_i \tag{5.6}$$

As discussed before in Chapter 4, the failure mode for the control beam was observed to be in-plane plastic buckling. A sectional analysis was conducted for the control beam to calculate the corresponding strain at the extreme compression fiber at failure. The failure was defined when the moment capacity of the section reaches the experimentally measured maximum moment capacity of the control beam, i.e. 91 kN.m. The maximum compression strain was calculated as 0.014. Based on all 4 tested beams of Group 1, the failure mode was defined when the strain in compression reached 0.014 or the strain in the tension flange was 0.045.

On the other hand, for all strengthened deteriorated tested beams the failure modes were observed to be unbonding or rupture of the CFRP as discussed before. Based on the observed failure modes and the bilinear relation between the bond length and the ultimate tensile strength, the failure mode for steel section strengthened using 5 layers of bonded Tyfo SCH-11UP sheets with Tyfo S epoxy was defined when the strain in tension has reached 0.0046. In the case of using MB-3 epoxy instead of Tyfo S, the failure mode occurred when the strain in tension has reached 0.0105. For a steel cross-section

strengthened with 1 strip of Tyfo UC with MB-3 epoxy, the failure was defined when the strain in the tension has reached 0.01. Once the moment-curvature relationship of the section is known, the load-deflection of the deteriorated steel beams with a given loading configuration and support conditions can be determined by integration of the curvature. Any commonly accepted method such as Conjugate Beam method or Moment Area method can be applied.

5.3 VALIDATION OF THE ASSUMPTIONS USED IN THIS NUMERICAL MODEL

Eighteen sections were used in this numerical model. Out of the eighteen sections, fifteen sections were used to simulate the behaviour of the tested steel beams and to validate this numerical model, while the other six sections were used to predict the remaining yielding moment of full scale deteriorated steel girders. Table 5.1 shows a summary of the numerical yielding and the ultimate moments of all sections used in this numerical model.

First, three sections were used to simulate the behaviour of unstrengthened deteriorated steel sections. Section S1 simulates the same section of the control beam BFO, section $S1_{33\%}$ simulates the mid-span section of beams BF-H0.33 and BF-N0.33 while section $S1_{50\%}$ presents the mid-span section of beam BF-N0.50. Experimental results of Group 1 beams were used to validate the moment curvature of sections S1, $S1_{33\%}$, and $S1_{50\%}$ as shown in Figure 5.4.

Nine sections were used to present the behaviour of strengthened deteriorated steel beams using bonded CFRP. Figure 5.5 shows the experimental and the analytical moment-curvature of non-deteriorated and deteriorated steel section strengthened with

CFRP sheets bonded using Tyfo S. Sections S1F1B1, $S1_{33\%}$F1B1, and $S1_{50\%}$F1B1 were conducted to simulate the behaviour of beams BF-H0.33-F1(5)-B1 and BF-N0.50-F1(5)-B1. Sections S1F1B2, $S1_{33\%}$F1B2, $S1_{50\%}$F1B2, and sections S1F2B2, $S1_{33\%}$F2B2, $S1_{50\%}$F2B2 were used to simulate the behaviour of beams BF-H0.33-F1(5)-B2, BF-N0.33-F1(5)-B2 and beams BF-H0.33-F2(1)-B2, respectively, as shown in Figures 5.6 and 5.7.

As shown in Figure 5.8 for a 33% and 50% loss of the tension flange area, the yielding moments decreased by 27% and 40%, respectively. While the ultimate moment capacities reduced by 10% and 18.5 %, respectively. The ultimate moment capacity of the strengthened cross-section increased by 12.7% in case of using bonded CFRP sheets with MB-3 while the ultimate moment capacity decreased by 9% when using Tyfo S instead of MB-3, as shown in Figure 5.9. In addition, from Figure 5.9 it is conducted that there was no increasing in the yielding moment due to the very small strain in the tension flange at yield. The ultimate moment capacity of the deteriorated sections with 33% and 50% loss improved by 8.3% and 8% when using MB-3 with Tyfo SCH-11UP while when using Tyfo S instead of MB-3 it was decreased by 13.6 and 15%, respectively, (see Figures 5.10, 5.11).

As a conclusion of the previous discussion, the difference between the analytical and the experimental moment-curvature shows that the previous assumptions which were considered in this analysis satisfy an acceptable level of accuracy. The effect of strengthening steel beams by using CFRP is almost negligible for the yielding moment. In addition to the CFRP and epoxy type, bond length is the main parameter which controls the mode of failure and as a result the ultimate capacity.

5.4 YIELDING LOAD FOR CORRODED STEEL GIRDERS

The yield load of the corroded steel girders can be defined as the load at which the girder begins to deform plastically. Before reaching its yield load, the girder will deform elastically and will return to the original shape when the applied load is removed. Beyond the yield load some plastic deformation will be permanent and non-reversible after releasing the load (residual deformations). It is often difficult to exactly define the yielding load of the steel girder from the load-deflection behaviour. As a result, most of the common definitions of the yielding are based on the stress-strain curve of the material which defines the yield at a certain level of stress. There is more than one definition for the yielding from the stress-strain curve for the material. The yielding can be defined as the first point where the curve starts to deviate from a straight line, the proportional elastic limit (PEL). The slope of the straight line is Young's modulus. The elastic limit is defined as a point on the curve beyond which plastic deformation will occur after release the load. Figure 5.12 shows the definitions of proportional elastic limit and the elastic limit for a ductile material. In the case of other ductile materials for which the onset of yield is not characterized by a horizontal portion in the stress-strain curve, the offset method is applied. In this case, a straight line is drawn parallel to the initial elastic line but displaced from it by an arbitrary value of permanent strain. This value depends on many factors such as; the material and the application and commonly is 0.2% as shown in Figure 5.13. As shown in this Figure, the stress corresponding to the intersection point between the 0.2% offset straight line and the stress-strain curve is the yield proof stress. Based on this short discussion about the yield strength, in the current analytical study the yield strength is considered to be the yield proof stress. The same concept will be used to

calculate the yielding load capacity of corroded steel girders as shown in Figure 5.14. As shown in this Figure, the proof yield load P_{yp} was calculated by drawing a straight line with the same slope of the elastic stiffness but from a deflection that is equal to $0.05\Delta_y$, where Δ_y is the elastic deflection of the control beam. The intersection of this straight line and the load-deflection curve gives the proof yielding load capacity P_{yp}. The proportional yielding load or the first yielding point is the load corresponding to the first yielding section. The arbitrary displacement value of 0.05 of the displacement at yield (i.e. 1/20 of Δ_y) is seen to be an acceptable value for the plastic residual displacement of a deteriorated girder that is intended to be strengthened. As shown in Figure 5.14, it seems that the proportional yielding load for corroded steel girder is not affected by the simulated length of corroded tension flange area while, the proof yielding load considers this influence

Using the section analysis which was conducted in section 5.2, the load-deflection curve for all the tested unstrengthened and strengthened beams using bonded CFRP was carried out. Figure 5.15 shows the experimental, the proof, and the proportional yielding load capacity for the tested beams. Table 5.2 presents a comparison of the experimental, proportional, and proof yielding moment for the tested beams. As shown in this table, three deteriorated steel beams, as defined in the first group were used to validate this proposed method.. The comparison between the numerical values and the experimental values shows that the percentage of error (between measured experimental values and analytical predictions) when using the proof capacity is within 0.6% while in case of the proportional limit it can reach up to 26.4% for steel beams with locally deterioration. The

same comparison was conducted for the strengthened deteriorated beams of Groups 2 and 3.

5.5 DETERIORATION FACTOR (Ψ_d)

In order to provide structural analysts with a simplified method for calculating the yielding and ultimate moment capacity of deteriorated steel girders, the reduced yielding moment of the beam (My_{det}) due to deterioration is calculated by multiplying the original yielding moment (My_o) of the undamaged beam by the deterioration factor (Ψ_d). Deterioration factor, Ψ_d, was defined as the ratio of the reduced yielding moment to the undamaged yielding moment using the following formula:

$$\psi_d = \frac{My_{det}}{My_o} \tag{5.7}$$

There are several parameters which affect the behaviour of the unstrengthened and strengthened deteriorated steel beams such as: the cross-sectional area and the clear span of the original beam; the simulation of corrosion and its location through defining a reduced tension flange area along a specific beam length; and the load pattern. In this section a parametric study is conducted to investigate the influence of these parameters on the deterioration factor (Ψ_d).

Three load patterns are considered in this parametric study: LC1, LC2, and LC3. The first load pattern LC1 simulates the load of one concentrated force in the beam mid-span. The pattern LC2 considers two concentrated loads in the ends point of the third beam span, and LC3 is the distributed load along the entire beam span. Since corrosion affects mainly the bottom flange of the steel beam, two levels of area reduction of the

bottom flange 33% and 50% were considered. Figure 5.16 shows that the deterioration factor (Ψ_d) of the unstrengthened deteriorated steel beam decreases by increasing the length of the corroded area L_C. As is shown in this Figure 5.16, for the same percentage of area reduction, there is no significant change in the relation between the reduction factor Ψ_d and the increasing in length of the corroded area L_c for the varied load patterns. On the other hand, this Figure shows that the common method for calculating the yielding capacity does not consider the length of the corroded area as well as the load pattern. However, this Figure was validated by using the experimental results of beams, BF-H0.33, BF-N0.33, and BF-N0.50.

To investigate the influence of the original cross-sectional area and the clear span length (L_o), two different undamaged steel cross-sections of the control beam (initial beam belonging to group 1) were considered in this investigation. The first section S1 has the same depth (h) of 157 mm as the tested beams in the experimental program, while the second section S2 has a depth equal to 457mm. Both sections have the same ratio of the beam depth to the clear span (h/Lo) equal to 0.1 as shown in Figure 5.18. Sections $S1_{33\%}$ and $S1_{50\%}$ simulate the deteriorated cross-sections of the original section S1. Sections $S2_{33\%}$ and $S2_{50\%}$ simulate the deteriorated cross-section of the section S2. The deterioration factor and the yielding capacity of each section are shown in Table 5.1. As shown in Figure 5.17, for the same beam depth to the clear span (h/Lo) ratio and the same percentage of area reduction at the level of the bottom flange, the reduction in the yielding moment capacity is not the same. As can be observed in this Figure, the reduction in the yielding moment capacity of the smaller beam is higher than the reduction in moment capacity of the beam with a 457 mm depth for the same percentage

of corroded tension flange area. Herein, an explanation is that the reduction in the moment of inertia of S1 cross-section is higher than that in S2 cross-section for the same level of area reduction. On the other hand, when the same reduction in the moment of inertia is considered for both cross-sections, the reduction of the yielding capacity is the same (see Figure 5.18).

To study the influence of strengthening with CFRP, two types of CFRP composite materials were used to rehabilitate deteriorated steel beams in order to increase their remaining yielding capacity. Tyfo SCH-11UP sheets were bonded to the bottom flange of the steel girders once by using Tyfo S epoxy and for another beam by using MB-3 epoxy, while Tyfo UC strip was bonded using MB-3. Figures 5.19-A and B show the increasing in the reduction factor (Ψ_d) for three different rehabilitation methods when a reduction of the bottom flange area equal to 33% and 50% was considered. The experimental results of the tested beams: BF-H0.33-F1(5)-B1; BF-H0.33-F1(5)-B2 and; BF-H0.33-F2(1)-B2 were used to validate the proposed method and are illustrated in Figure 5.19-A, while the experimental results of the tested beams BF-N0.50-F1(5)-B1 and BF-N0.50-F1(5)-B2 were used to validate the proposed method are depicted in Figure 5.19-B.

Based on this parametric study, the following conclusions are drawn for the unstrengthened and strengthened deteriorated beams:

- The location and the area of corrosion (deterioration) have a significant effect on the remaining yielding moment capacity of the deteriorated steel girder especially when the corrosion is within the middle one-third of the clear span. However, these parameters (location and area of corrosion) have an insignificant effect when they are outside the middle one-third of the span.

- The load pattern does not have a significant effect over the reduction factor as long as the maximum moment will occur in the middle one-third of the clear span.
- The clear span of the deteriorated steel girder has a minor effect on the remaining yielding moment capacity while it has a major effect on the failure mode and in consequence on the remaining ultimate capacity.
- Describing the level of damage of the tension flange by the reduction ratio of the moment of inertia is more accurate than describing it by the reduction ratio of the tension flange area.
- Using CFRP to reinforce steel girders has a significant effect on the yielding moment capacity in case of rehabilitated deteriorated steel girders while it has an insignificant effect in case of strengthening of non-deteriorated steel girders.

Table 5.1 Numerical Yielding and Ultimate Moment for different sections

	Section	Losses % in tension flange	CFRP	Epoxy	My (kN.m)	Mr (kN.m)
Group 1	**S1**	_	_	_	67.1	91.6
	$S1_{33\%}$	33%	_	_	48.8	81.8
	$S1_{50\%}$	50%	_	_	39.8	74.6
Group 2	**S1F1B1**	_	SCH-11UP	Tyfo S	67.7	83.4
	$S1_{33\%}$F1B1	33%	SCH-11UP	Tyfo S	53.2	70.7
	$S1_{50\%}$F1B1	50%	SCH-11UP	Tyfo S	44.0	63.3
	S1F1B2	_	SCH-11UP	MB-3	67.7	103.3
	$S1_{33\%}$F1B2	33%	SCH-11UP	MB-3	53.1	88.6
	$S1_{50\%}$F1B2	50%	SCH-11UP	MB-3	44.0	80.6
Group 3	**S1F2B2**	_	Tyfo UC	MB-3	67.5	92.7
	$S1_{33\%}$F2B2	33%	Tyfo UC	MB-3	51.0	77.1
	$S1_{50\%}$F2B2	50%	Tyfo UC	MB-3	41.6	68.6
	S2	_	_	_	445.8	_
	$S2_{33\%}$	33%	_	_	342.0	_
	$S2_{50\%}$	50%	_	_	290.0	_
	S3	_	_	_	1812.5	_
	$S3_{33\%}$	33%	_	_	1317.2	_
	$S3_{50\%}$	50%	_	_	1067.4	_

F1 Tyfo SCH-11UP
F2 Tyfo UC
B1 Tyfo S
B2 MB-3

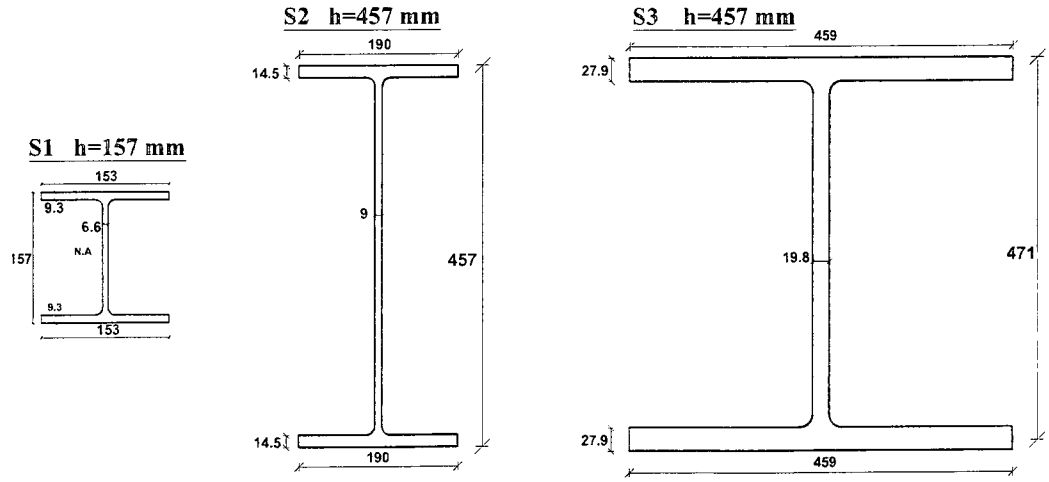

Table 5.2 Experimental, Proportional, and Proof yielding moment for tested beams

	Beam	My (kN.m)				
		Exp.	Prop.	Pro.	My_{prop} / My_{exp}	My_{Pro}/My_{exp}
Group 1	BFO	245	244	244	99.6%	**99.6%**
	BF-H0.33	242	178	241	73.6%	**99.6%**
	BF-N0.33	190	178	191	93.7%	**100.5%**
	BF-N0.50	155	145	156	93.6%	**100.6%**
Group 2	BF-H0.33-F1(5)-B1	245	194	245	79.2%	**100%**
	BF-N0.50-F1(5)-B1	181	160	186	88.4%	**102.7%**
	BF-H0.33-F1(5)-B2	253	194	245	76.7%	**96.8%**
	BF-N0.50-F1(5)-B2	195	160	185	81.6%	**95%**
Group 3	BF-H0.33-F2(1)-B2	250	185	246	74%	**98.4%**

Exp. Experimental yielding load
Prop. Proportional yielding load
Pro. Proof yielding load

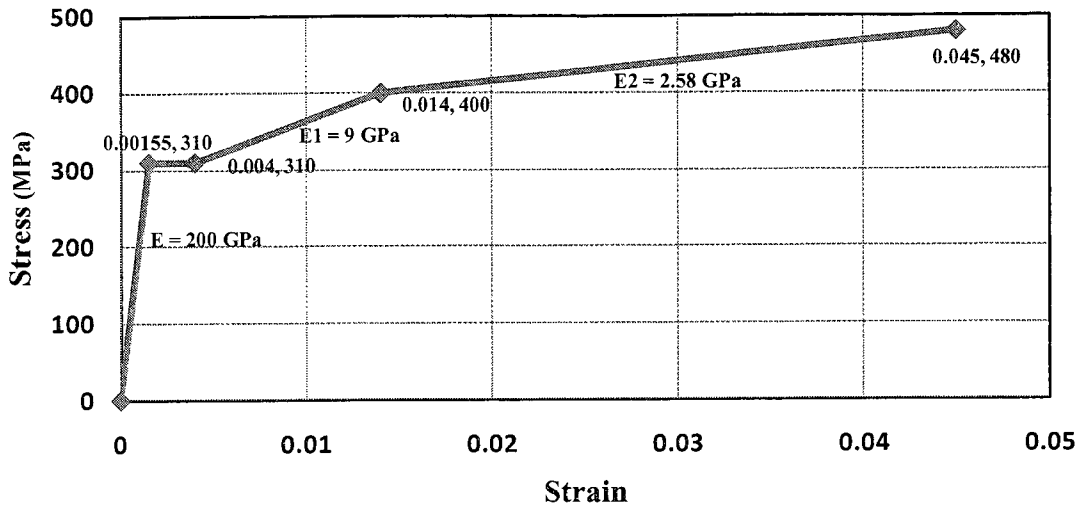

Figure 5.1 Design Stress-Strain curve for steel section

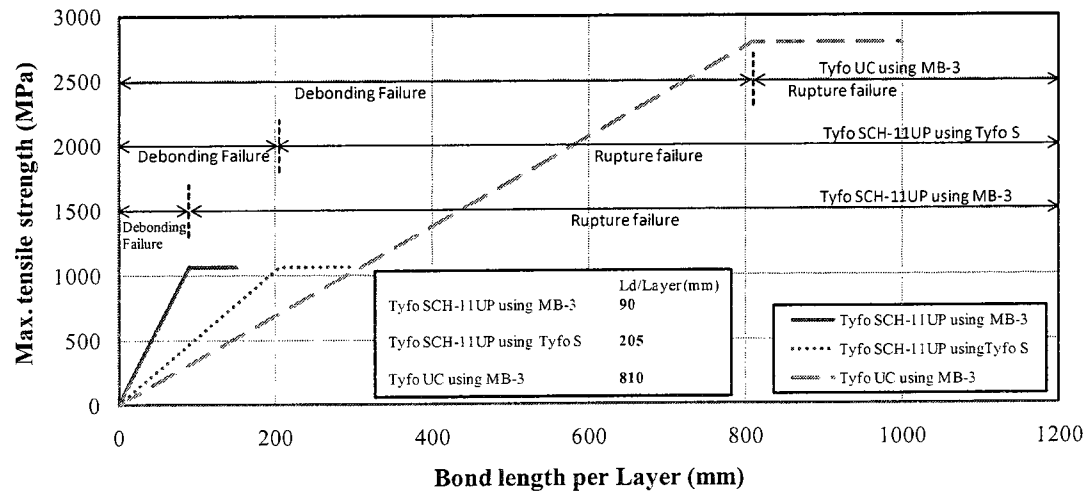

Figure 5.2 Development length per layer for Tyfo SCH-11UP and Tyfo UC

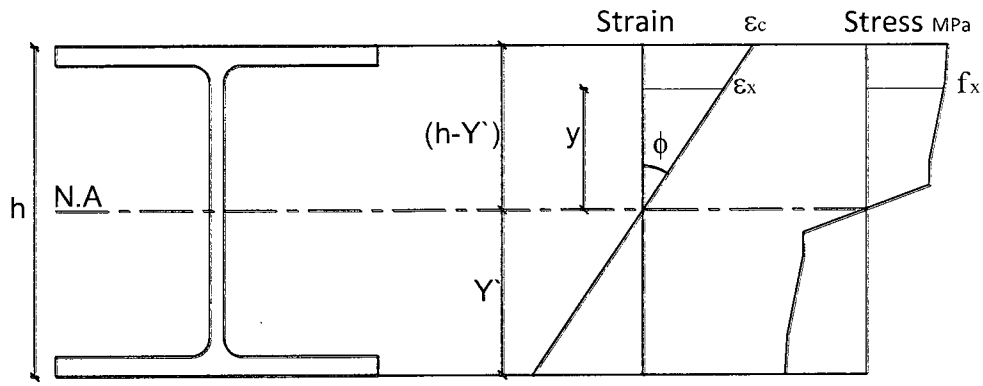

Figure 5.3 Assumed linear strain profile and corresponding stress profile applicable for elastic and post-yield range

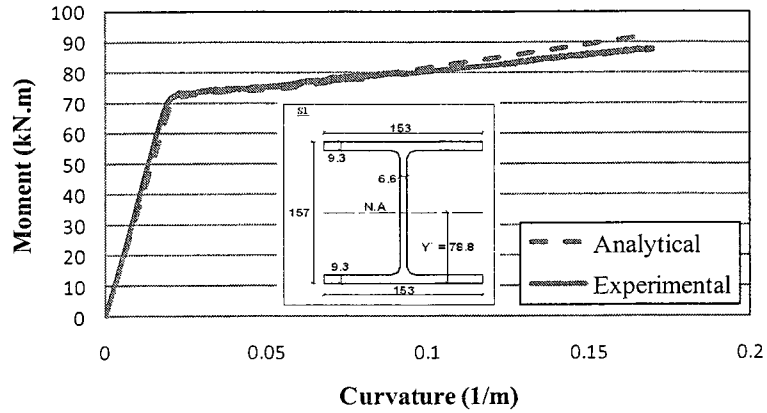

(a) Section S1

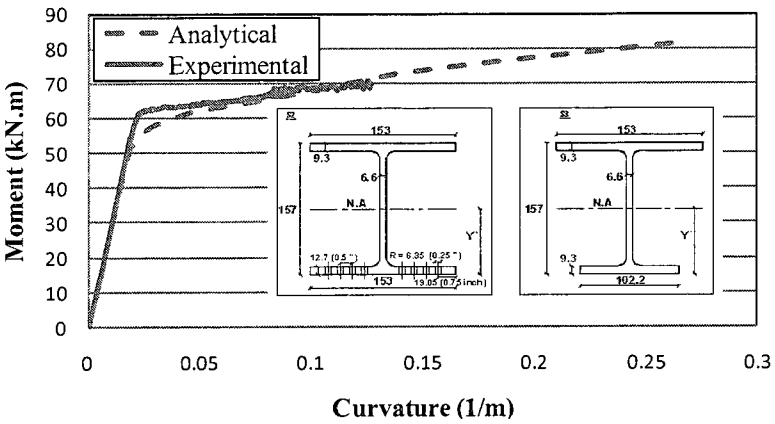

(b) Section $S1_{33\%}$

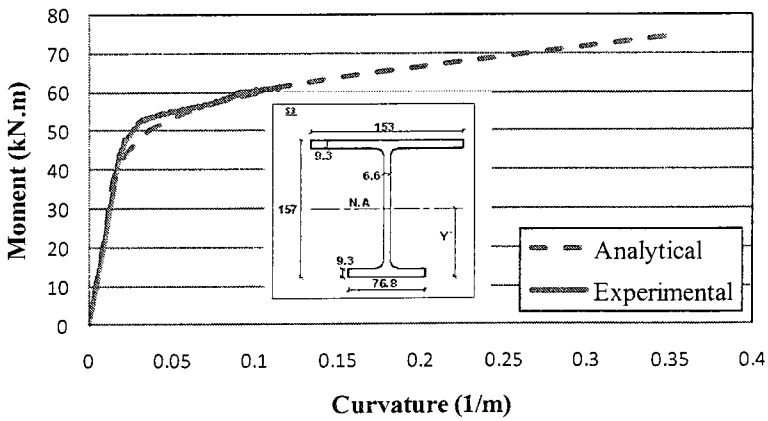

(c) Section $S1_{50\%}$

Figure 5.4 Analytical and experimental Moment-Curvature for sections: (a) S1; (b) $S1_{33\%}$; (c) $S1_{50\%}$

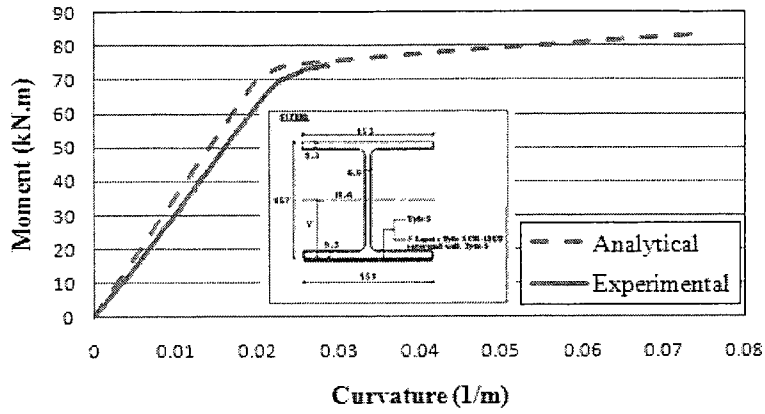

(a) Section S1F1B1

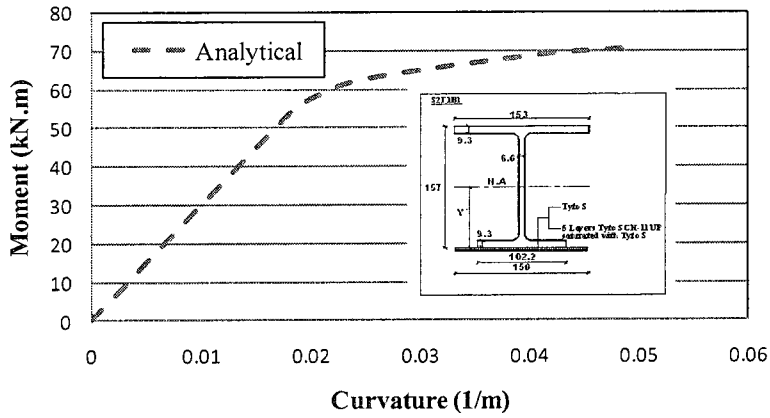

(b) Section $S1_{33\%}F1B1$

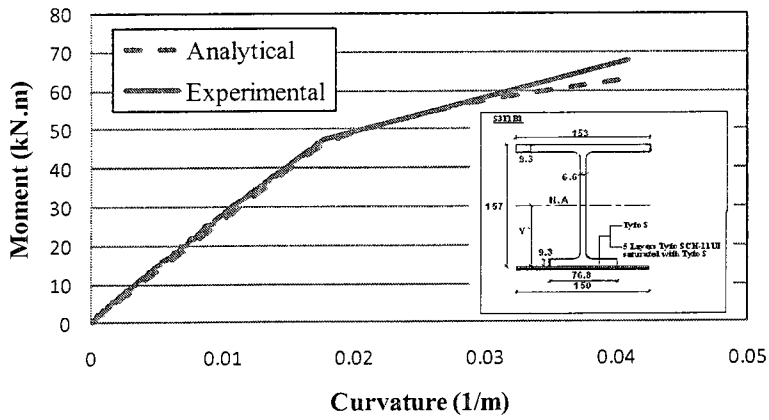

(c) Section $S1_{50\%}F1B1$

Figure 5.5 Analytical and experimental Moment-Curvature for sections: (a) S1F1B1; (b) $S1_{33\%}F1B1$; (c) $S1_{50\%}$

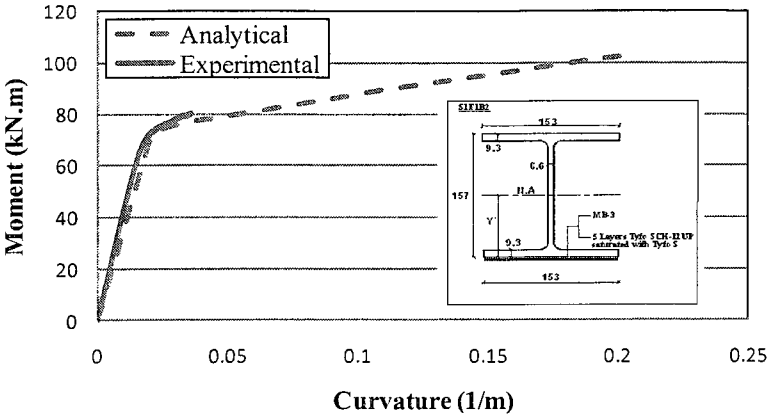

(a) Section S1F1B2

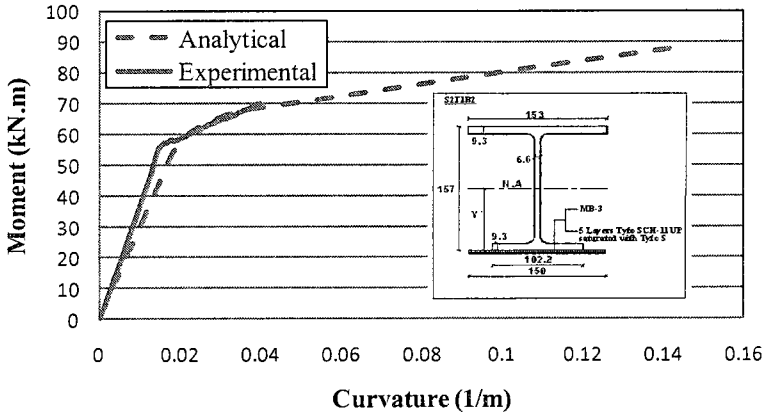

(b) Section $S1_{33\%}F1B2$

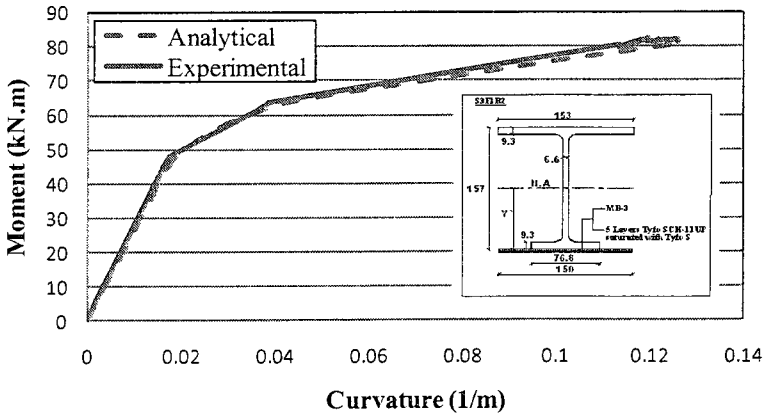

(c) Section $S1_{50\%}F1B2$

Figure 5.6 Analytical and experimental Moment-Curvature for sections: (a) S1F1B2; (b) $S1_{33\%}F1B2$; (c) $S1_{50\%}F1B2$

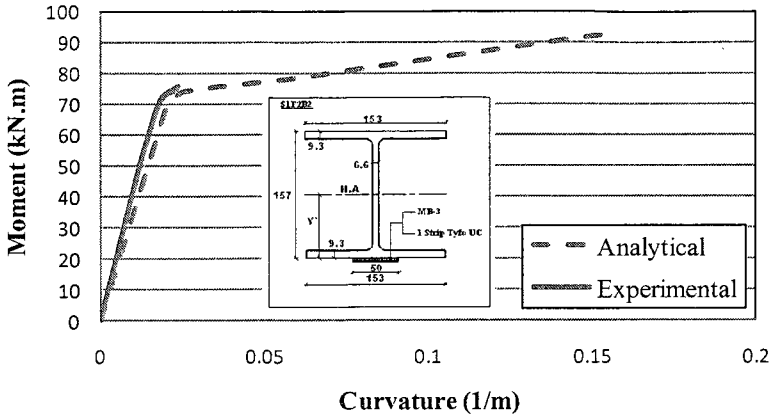

(a) Section S1F2B2

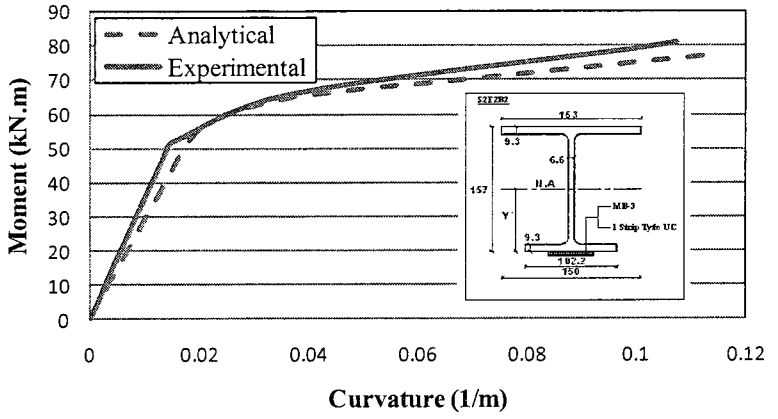

(b) Section $S1_{33\%}F2B2$

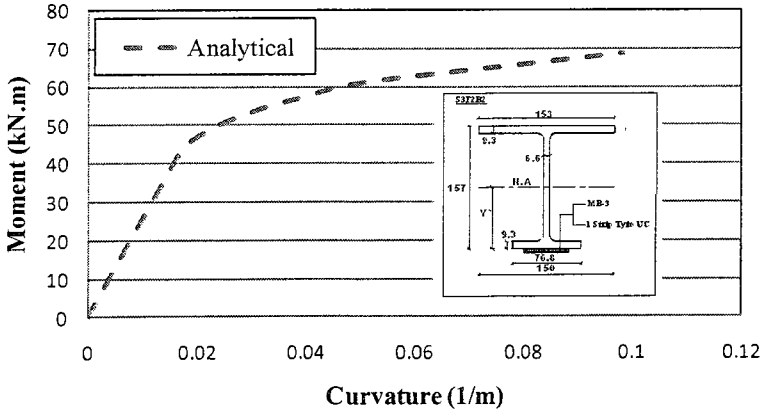

(c) Section $S1_{50\%}F2B2$

Figure 5.7 Analytical and experimental Moment-Curvature for sections: (a) S1F2B2; (b) $S1_{33\%}F2B2$; (c) $S1_{50\%}F2B2$

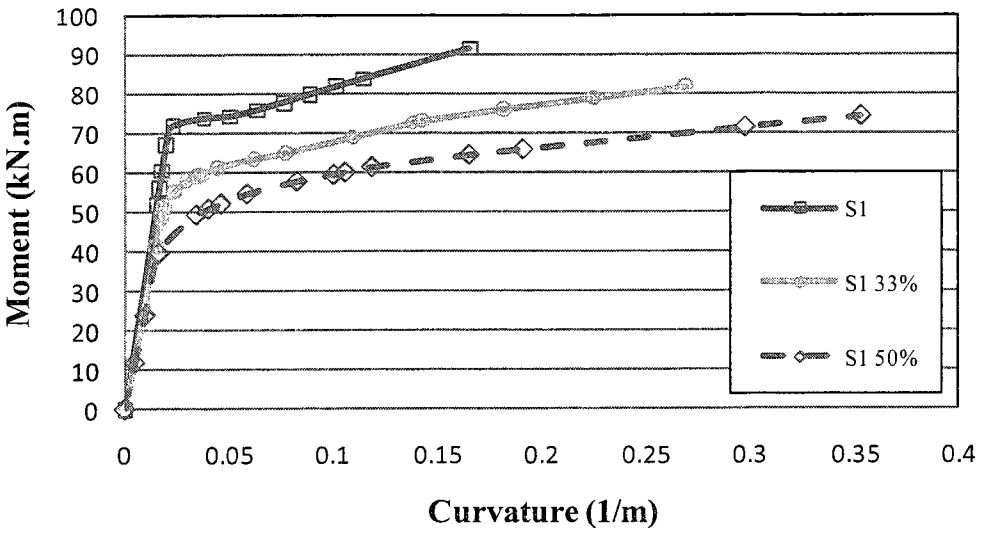

Figure 5.8 Analytical Moment-Curvature for sections S1, $S1_{33\%}$, and $S1_{50\%}$

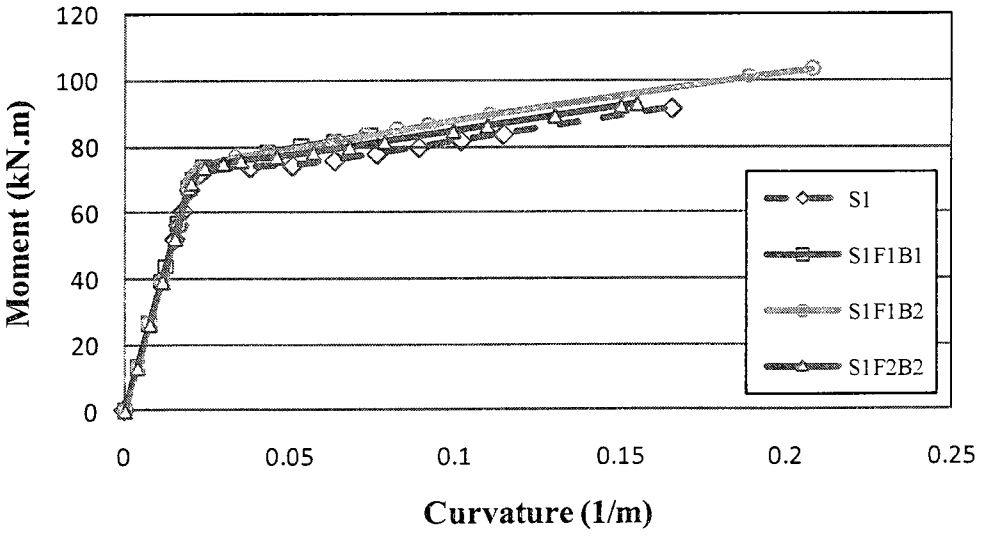

Figure 5.9 Analytical Moment-Curvature for sections S1 with CFRP (F1B1) 5 layers of Tyfo SCH-11UP with Tyfo S, (F1B2) 5 layers of Tyfo SCH-11UP with MB-3, (F2B2) 1 strip of Tyfo UC with MB-3

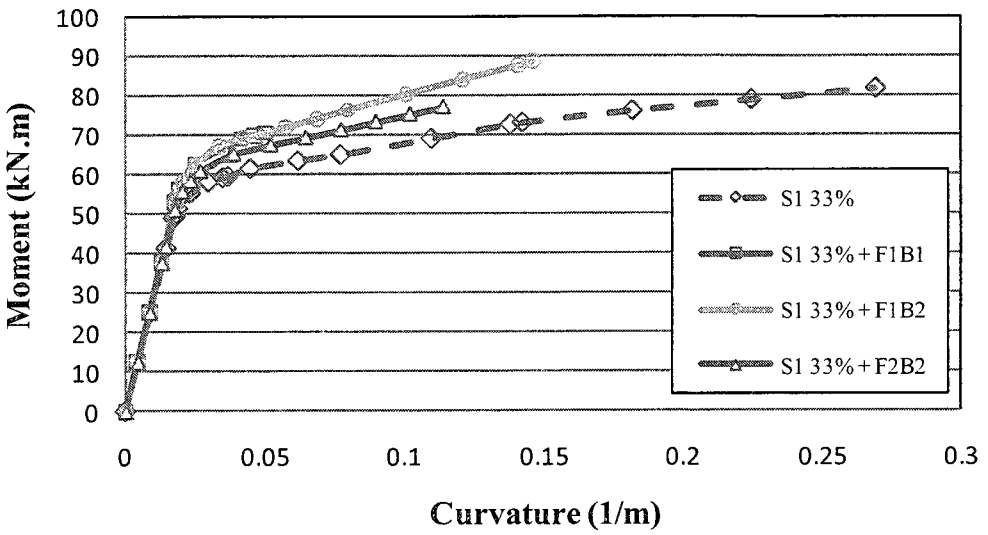

Figure 5.10 Analytical Moment-Curvature for sections $S1_{33\%}$ with CFRP (F1B1) 5 layers of Tyfo SCH-11UP with Tyfo S, (F1B2) 5 layers of Tyfo SCH-11UP with MB-3, (F2B2) 1 strip of Tyfo UC with MB-3

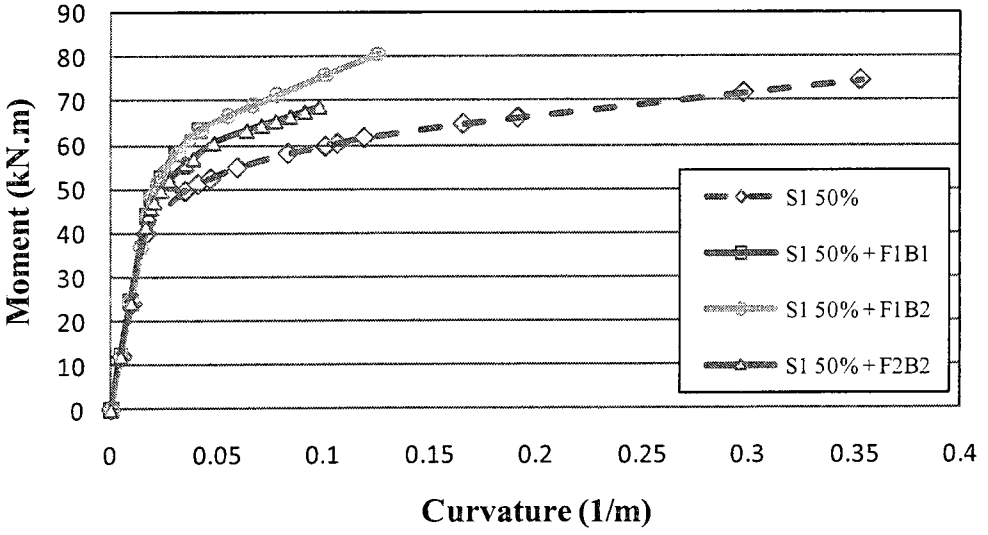

Figure 5.11 Analytical Moment-Curvature for sections $S1_{50\%}$ with CFRP (F1B1) 5 layers of Tyfo SCH-11UP with Tyfo S, (F1B2) 5 layers of Tyfo SCH-11UP with MB-3, (F2B2) 1 strip of Tyfo UC with MB-3

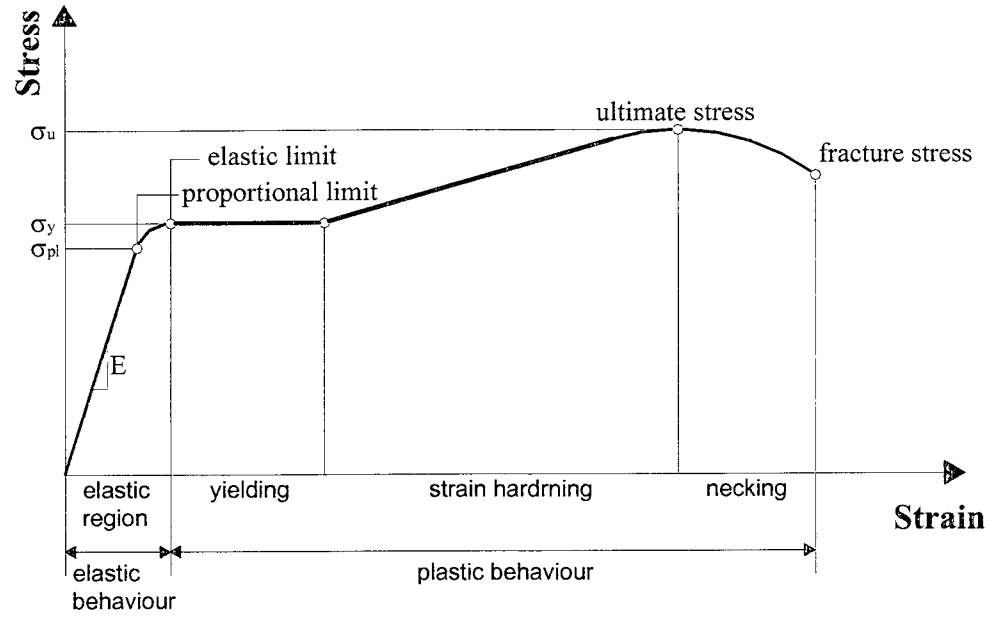

Figure 5.12 Stress-Strain curve for ductile material

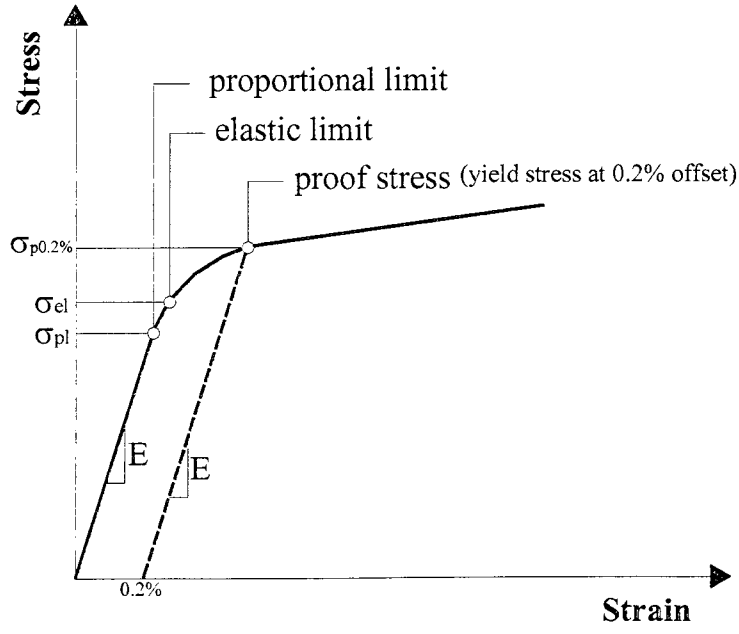

Figure 5.13 Determination of yield stress by using the offset method

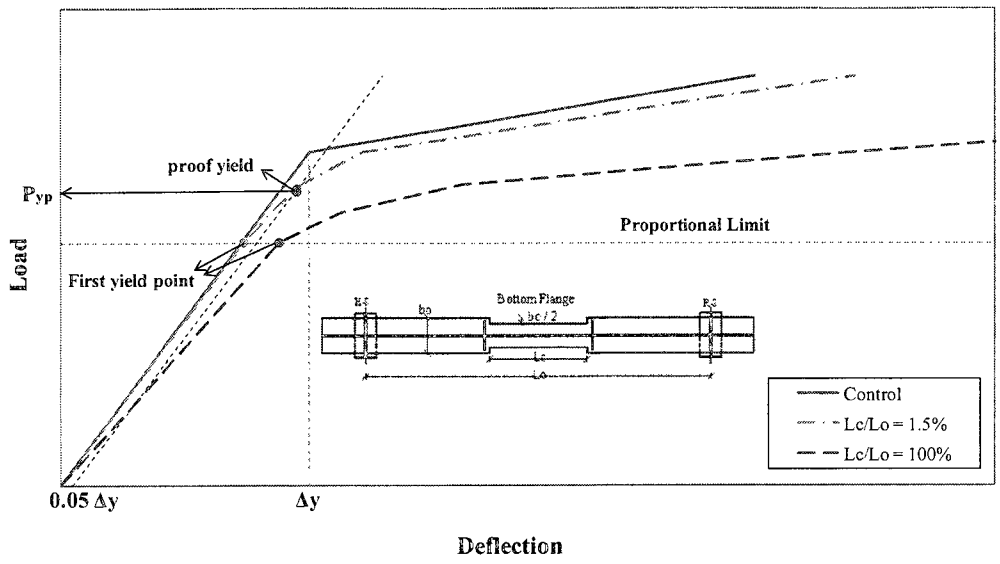

Figure 5.14 Numerical Load-Deflection for corroded steel girder

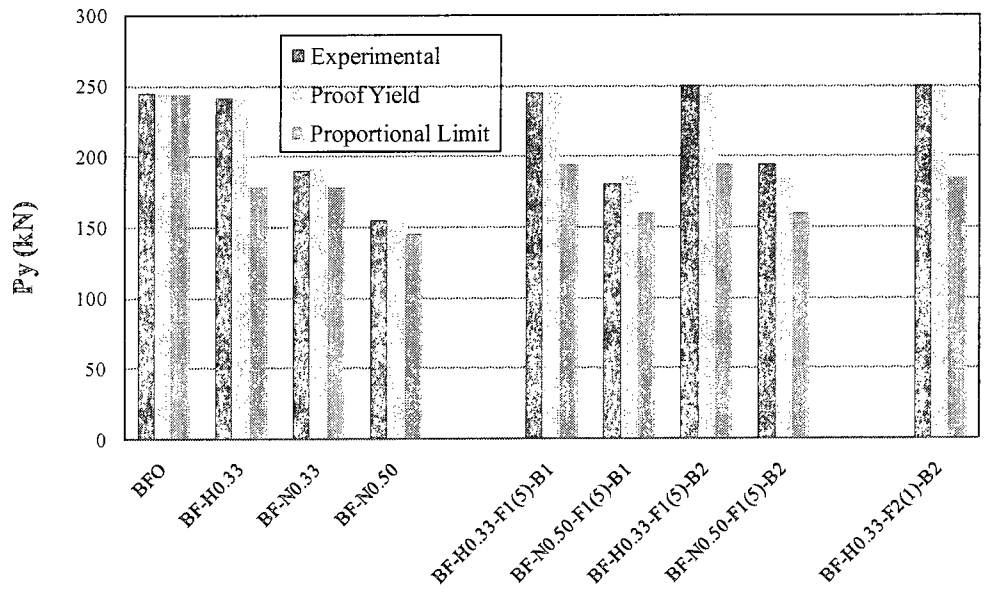

Figure 5.15 Experimental, proof yield, and proportional Limit of the tested beams

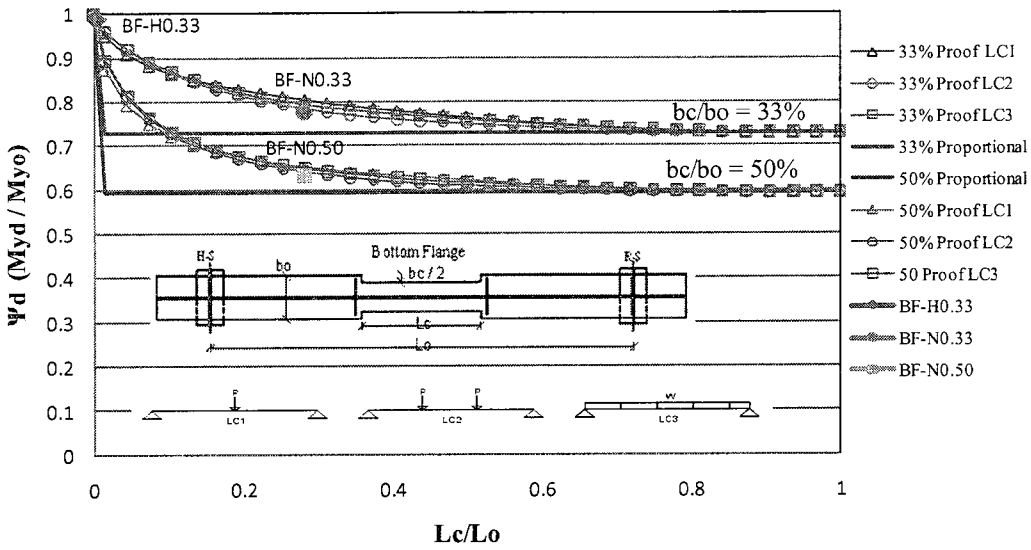

Figure 5.16 Deterioration factor vs. corroded length ratio for unstrengthened deteriorated beam

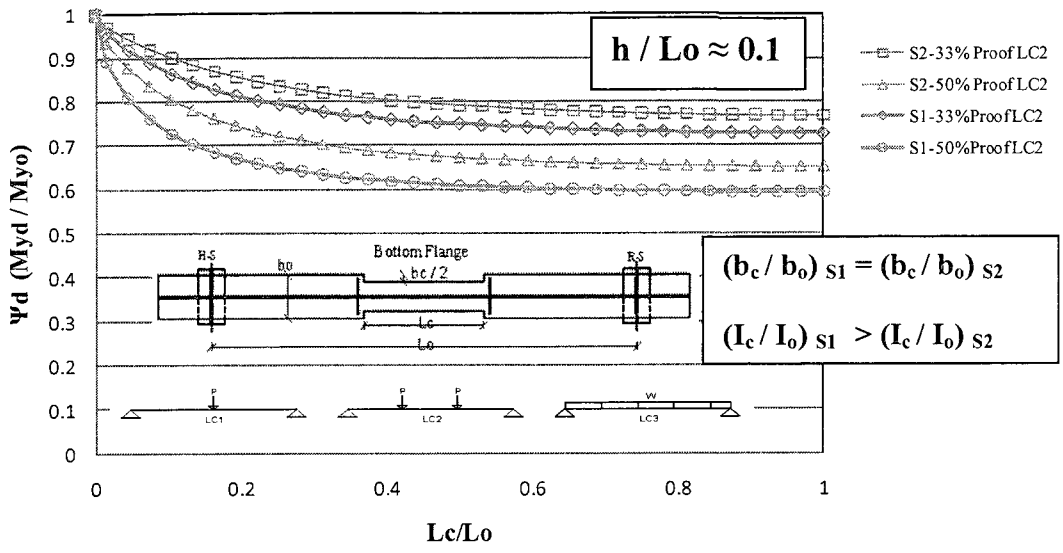

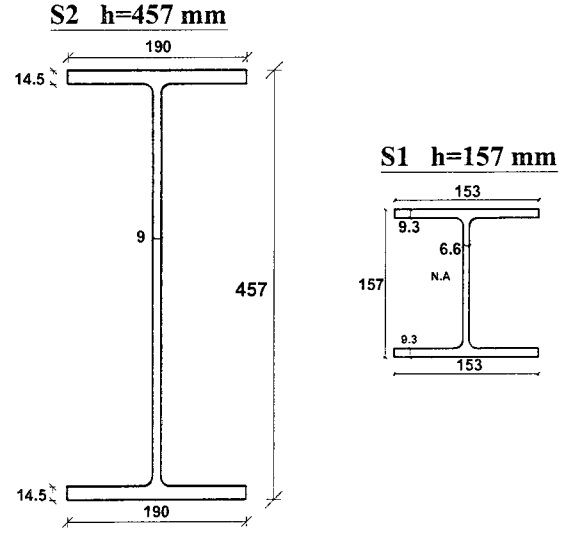

Figure 5.17 Deterioration factor vs. corroded length ratio for two unstrengthened deteriorated beams with different inertia losses

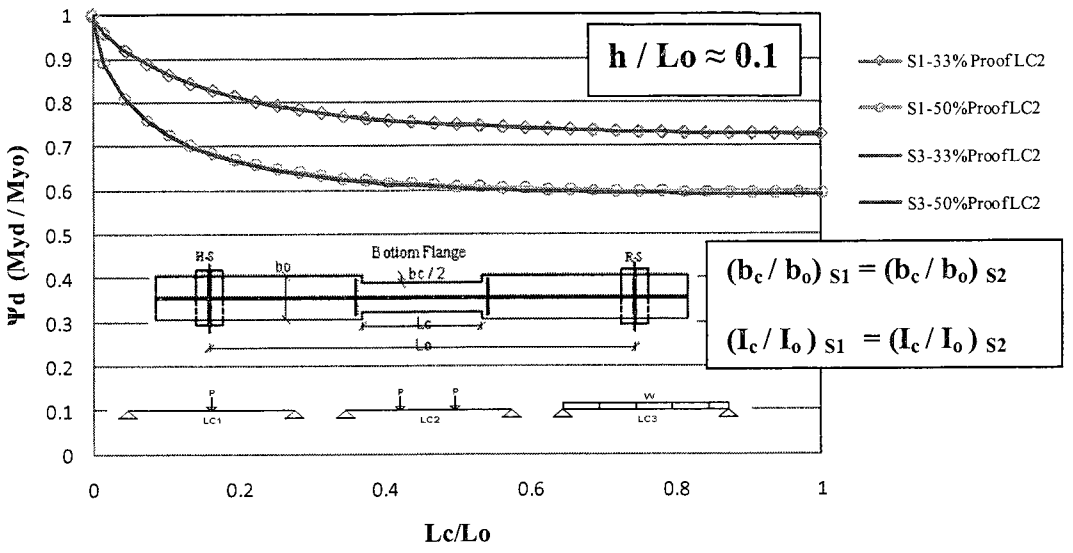

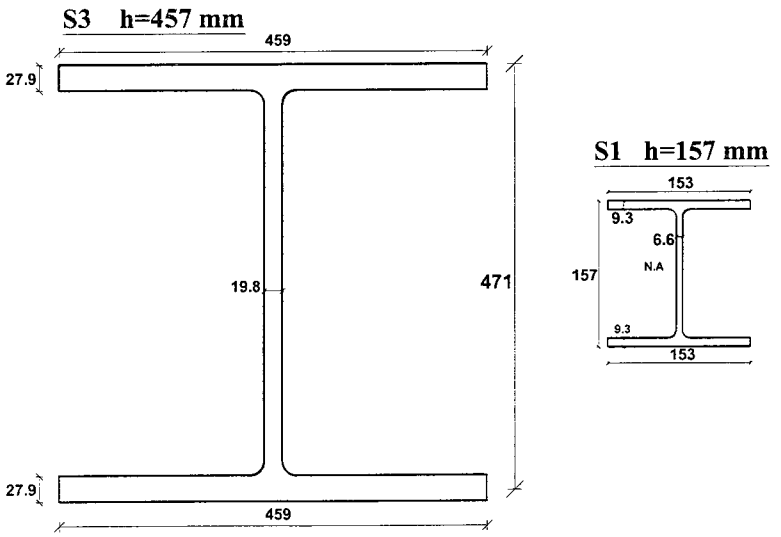

Figure 5.18 Deterioration factor vs. corroded length ratio for two unstrengthened deteriorated beams with the same inertia losses

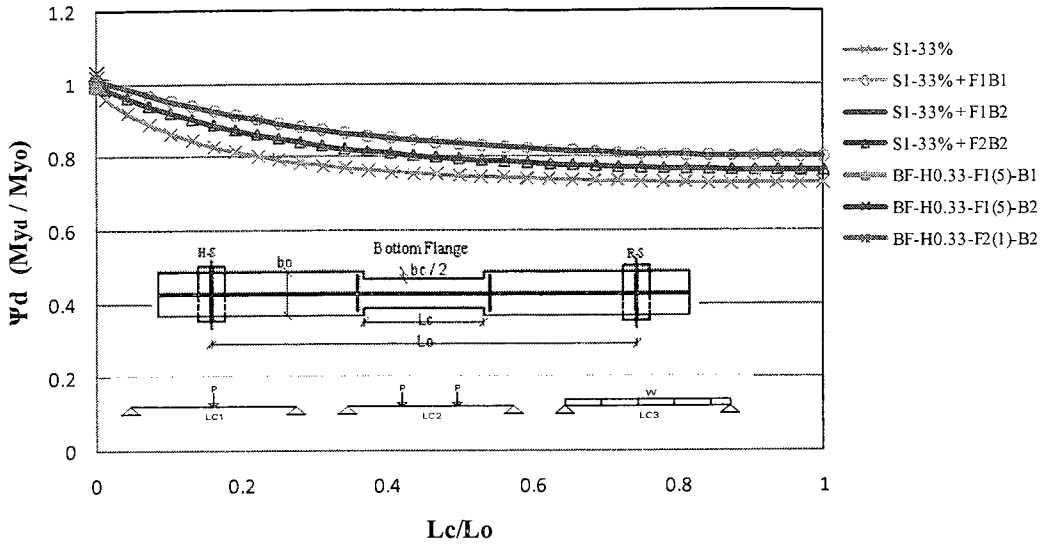

(a) 33% area reduction of the bottom flange

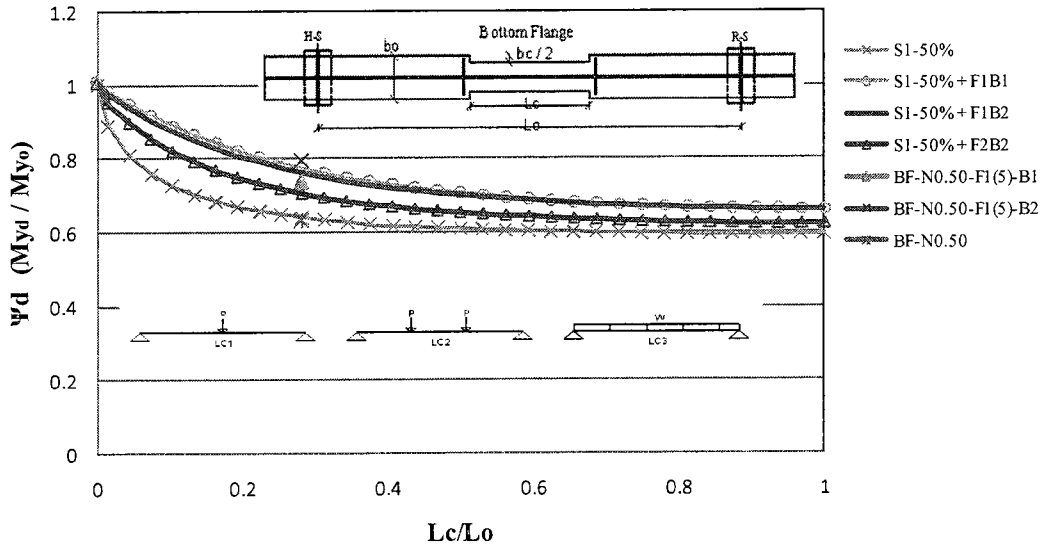

(b) 50% area reduction of the bottom flange

Figure 5.19 Deterioration factor vs. corroded length ratio for strengthened deteriorated beam using 5 layers of Tyfo SCH-11UP with Tyfo S (F1B1), 5 layers of Tyfo SCH-11UP with MB-3 (F1B2), 1 strip of Tyfo UC with MB-3 (F2B2)

CHAPTER 6

CONCLUSIONS, RECOMMENDATIONS AND FUTURE WORK

6.1 SUMMARY

Large number of existing highway bridges in North America were designed and built in the mid-1900s for a design life of 75 years. As a result, a high percentage of the existing steel bridge infrastructures are in need to develop either a cost-effective upgrading or rehabilitation in coming decades. This research discusses experimental and analytical investigations that were conducted under monotonically increasing loading to predict the reduction in the flexural capacity of existing deteriorated steel girders and to develop retrofitting schemes capable of increasing its flexural capacity. In this experimental program, a series of thirteen medium-scale deteriorated steel beams were tested to examine the behaviour of the girder before and after the strengthening procedure was completed. The tested beams were divided into four groups such that: the first group (G1) is related to analyse the behaviour of the deteriorated steel girders in order to determine the remaining capacity and consists of four beams with different percentage of deterioration; the other three groups (G2, G3, and G4) were designed to evaluate the effectiveness of the proposed retrofit schemes. Among them, the second group contains four beams, strengthened with CFRP sheets bonded to the tension flange in the aim to characterize the static behaviour of steel girders strengthened with CFRP sheets. The third group consists of two beams strengthened with high-modulus CFRP laminate strips which were externally bonded to the bottom flange of the tested beam. Furthermore, in

group four, unbonded CFRP sheets were used to strengthen three deteriorated steel beams using ductile anchorage system at both ends of the beam. Two types of adhesive were used in this investigation to examine the influence of the epoxy type on the bonding behaviour. In addition to the experimental program, an analytical model was developed to set up a numerical method that is capable of predicting the elastic and post-yield behaviour of the unstrengthened and strengthened deteriorated steel girders.

6.2 CONCLUSIONS

Based on the results of the experimental and analytical investigations that were carried out on the behavior of corroded steel beams before and after strengthening, the following conclusions were drawn:

FOR UNSTRENGTHENED CORRODED STEEL BEAMS

1. The performance of beam BF-H0.33 shows that local corrosion is formed in only one section (at the tension flange and mid-span of the beam). It has a local effect on the strains magnitude of the corroded section and a slight effect on its load-deformation relationship. However, this effect increases with any increase of the corrosion length along the beam.
2. The load pattern does not have a major effect on the remaining flexural capacity of the deteriorated steel beam. However, by increasing the area of corrosion, the elastic stiffness is subjected to a significant reduction.

3. It is more accurate to describe the level of damage of the tension flange area by the reduction ratio of the moment of inertia than by the reduction ratio of the cross-section area.

FOR BONDED CFRP STRENGTHENED STEEL BEAMS

4. Bonded CFRP has a minor effect on the elastic behaviour of the strengthened beam, while it has a major effect on the inelastic behaviour.
5. Using bonded CFRP as a retrofiting scheme is not always an effective system for increasing the flexural capacity of the corroded steel girders, since the efficiency of this technique is based on the type of the CFRP material and the type of adhesive used in this scheme.
6. A better efficiency in the flexural capacity of CFRP-strengthened beams was obtained by using high performance adhesive (viscous epoxy adhesive) with saturated CFRP sheets than by using it with CFRP strips.
7. Using CFRP to reinforce steel girders has a significant effect on the yielding moment capacity in the case of rehabilitated deteriorated steel girders; however, it has an insignificant effect in the case of strengthening non-deteriorated steel girders.
8. Using end wrapping system around the bottom flange for steel beams strengthed with bonded CFRP sheets is not efficient in eliminating the debonding nor increasing the ultimate load capacity.

FOR STEEL BEAMS STRENGTHENED WITH UNBONDED CFRP SHEETS WITH END DUCTILE ANCHORS

9. The presence of the ductile anchorage system prevents the premature failure through peel off of the CFRP sheet and it increasses the flexural capacity of the steel beam. The effeciency of this system was sucessufly proved in this thesis.
10. Unbonded CFRP sheets with end ductile anchorage system guarantees a ductile failure while for a bonded CFRP system it experienced a brittle failure.
11. The end detail of the unbonded CFRP sheets has a significant influence on the efficiency of this proposed retrofitting scheme.

It should be noted that in all strengthening schemes that uses CFRP material, caution has to be taken to avoid galvanic corrosion as per recommendations of the design guidelines for use of FRP materials in strengthening.

6.3 RECOMMENDATIONS AND FUTURE WORK

It is important to emphasize that the aforementioned conclusions were built herein for the studied beams and the author believes that there are still many other issues that need to be investigated as follow:

- In order to validate the findings of this research and to confirm their applicability to full-scale steel bridge girders, further experimental investigation should be carried out on full-scale deteriorated steel girders before and after strengthening.
- Further experimental studies are needed to investigate the influence of the corrosion area, corrosion location, and corrosion type on the behaviour of the corroded steel girders in term of flexural capacity and stiffness losses.

- As the experimental and analytical program of this research was limited to rolled W-shape cross sections only, additional studies on the plate girders section should be pursued. Further studies focused on shear behavior of corroded steel girders strengthened with CFRP composite materials are required.
- Tests should be conducted to investigate the impact of the CFRP type, the adhesive type, chemical environment, and cyclic temperature changes on the long-term performance of the bond between the steel and the CFRP.
- In order to avoid the premature CFRP debonding and to improve the behaviour of the corroded steel girders in terms of flexural capacity, stiffness and ductile failure, research efforts need to be conducted in order to develop unbonded ductile strengthening techniques. This new retrofit method will maximize the benefits of the superior CFRP properties and increase the flexural capacity of the strengthened steel girder,
- Extensive research is required in the field of existing cast iron beams strengthened with CFRP composite materials. However, this retrofit technique is seen as being the most suitable for increasing the flexural capacity of these existing members.

REFERENCES

Albrecht, P., and Naeemi, A. H. (1984). Performance of weathering steel in bridges. NCHRP REP. 272, Transportation Research Board, National Research Council, Washington, D.C.

Albrecht, P., and Sahli, A.H. 1988. Static Strength of Bolted and Adhesively Bonded Joints for Steel Structures. ASTM STP 981. p. 229.

Al-Emrani, M., and Kliger, R. (2006). Analysis of interfacial shear stresses in beams strengthened with bonded prestressed laminates. Composites Part B: Engineering, 37(4-5), 265-272.

Al-Saidy, A. H., Klaiber, F. W., and Wipf, T. J. (2004). Repair of steel composite beams with carbon fibre-reinforced polymer plates. Journal of Composites for Construction, 8(2), 163-172.

Al-Saidy, A. H., Klaiber, F. W., and Wipf, T. J. (2007). Strengthening of steel–concrete composite girders using carbon fibre reinforced polymer plates. Construction and Building Materials, 21(2), 295-302.

Al-Saidy, A. H., Klaiber, F. W., Wipf, T. J., Al-Jabri, K. S., and Al-Nuaimi, A. S. (2008). Parametric study on the behavior of short span composite bridge girders strengthened with carbon fiber reinforced polymer plates. Construction and Building Materials, 22(5), 729-737.

Brockenbrough, R. L., and Merritt, F. S. (2006). Structural steel designer's handbook: AISC, AASHTO, AISI, ASTM, AREMA, and ASCE-07 design standards (4th ed.). New York: McGraw-Hill.

Buyukozturk, O., Gunes, O., and Karaca, E. (2004). Progress on understanding debonding problems in reinforced concrete and steel members strengthened using FRP composites. Construction and Building Materials, 18(1), 9-19.

CAN/CSA S16-09 Limit States Design of Steel Structures (2009), Canadian Standard Association, Rexdale. Ontario, Canada.

Canadian Institute of Steel Construction. (2007). Handbook of steel construction (9th, 3 revision ed.). Willowdale, Ont.: Canadian Institute of Steel Construction.

Chryssanthopoulos and S.S.J. Moy (eds), Proc. Int. Conf., Advanced Polymer Composites for structural applications in construction. ACIC 2004, 20-22 April 2004, Guilford UK. Cambridge, England: Woohead Publishing Limited.

Colombi, P., and Poggi, C. (2006). An experimental, analytical and numerical study of the static behavior of steel beams reinforced by pultruded CFRP strips. Composites Part B: Engineering, 37(1), 64-73.

Colombi, P., and Poggi, C. (2006). Strengthening of tensile steel members and bolted joints using adhesively bonded CFRP plates. Construction and Building Materials, 20(1-2), 22-33.

Dawood, M., Sumner, E., Rizkalla, S. H., and Schnerch, D. (2006). Strengthening steel bridges with new high modulus CFRP materials. 3rd International Conference on Bridge Maintenance, Safety and Management - Bridge Maintenance, Safety, Management, Life-Cycle Performance and Cost, July 16, 2006 - July 19, 1063-1064.

Deng, J., and Huang, P. (2007). Experimental study on debonding failure of steel beams strengthened with a CFRP plate. Jianzhu Jiegou Xuebao/Journal of Building Structures, 28(5), 124-129.

Deng, J., and Lee, M. M. K. (2007). Fatigue performance of metallic beam strengthened with a bonded CFRP plate. Composite Structures, 78(2), 222-231.

Deng, J., Lee, M. M. K., and Moy, S. S. J. (2004). Stress analysis of steel beams reinforced with a bonded CFRP plate. Composite Structures, 65(2), 205-215.

El Damatty, A. A., and Abushagur, M. (2003). Testing and modeling of shear and peel behaviour for bonded steel/FRP connections. Thin-Walled Structures, 41(11), 987-1003.

Fawzia, S., Al-Mahaidi, R., and Zhao, X. (2006). Experimental and finite element analysis of a double strap joint between steel plates and normal modulus CFRP. Composite Structures, 75(1-4), 156-162.

Frauenberger, A., Liu, X., Meyyappan, L., Mata, J., Gupta, T., Silva, P.F., Dagli, C.H., Pottinger, H.J., Nanni, A. and Marianos, W.N. Jr. (2003). FRP repair and health monitoring of railroad steel bridges No. 03-44. University of Missouri, Rolla.: CIES Report.

Gillespie Jr., J. W., Mertz, D. R., Kasai, K., Edberg, W. M., Demitz, J. R., and Hodgson, I. (1996). Rehabilitation of steel bridge girders: Large scale testing. Proceedings of the 11th Technical Conference of the American Society for Composites, October 7, 1996 - October 9, 231-240.

Gioncu, V., and Petcu, D. (1997). Available rotation capacity of wide-flange beams and beam-columns part 1. Theoretical approaches. Journal of Constructional Steel Research, 43(1-3), 161-217.

Gioncu, V., and Petcu, D. (1997). Available rotation capacity of wide-flange beams and beam-columns part 2. Experimental and numerical tests. Journal of Constructional Steel Research, 43(1-3), 219-244.

Hollaway, L. C., Zhang, L., Photiou, N. K., Teng, J. G., and Zhang, S. S. (2006). Advances in adhesive joining of carbon fibre/polymer composites to steel members for repair and rehabilitation of bridge structures. Advances in Structural Engineering, 9(6), 791-803.

Hollaway, L.C., and Cadei, J. Progress in the technique of upgrading metallic structures with advanced polymer composites, Prog Struct Engng Mater 4 (2002), pp. 131–148.

Jones, S. C., and Civjan, S. A. (2003). Application of fiber reinforced polymer overlays to extend steel fatigue life. Journal of Composites for Construction, 7(4), 331-338.

Kayser, J. R., and Nowak, A. S. (1987). EVALUATION OF CORRODED STEEL BRIDGES. Bridges and Transmission Line Structures, 35-46.

Kayser, J. R., and Nowak, A. S. (1989). Reliability of corroded steel girder bridges. Structural Safety, 6(1), 53-63.

Kulicki, J. M., Z. Prucz, D. F. Sorgenfrei, D. R. Mertz, and W. T. Young. NCHRP Report 333: Guidelines for Evaluating Corrosion Effects in Existing Steel Bridges. TRB, National Research Council, Washington, D.C., December 1990.

Lane, I.R., and Waed, J.A. (2000). Restoring Britains Bridge Heritage. Institution of Civil Engineering (South Wales Association) Transport Engineering Group Award.

Lenwari, A., Thepchatri, T., and Albrecht, P. (2005). Flexural response of steel beams strengthened with partial-length CFRP plates. Journal of Composites for Construction, 9(4), 296-303.

Lenwari, A., Thepchatri, T., and Albrecht, P. (2006). Debonding strength of steel beams strengthened with CFRP plates. Journal of Composites for Construction, 10(1), 69-78.

Lenwari, A., Thepchatri, T., and Albrecht, P. (2006). Debonding strength of steel beams strengthened with CFRP plates. Journal of Composites for Construction, 10(1), 69-78.

Lindt, V. D., Ahlborn, T. M., and Kethu, S. (2005). Alternate approach to approximating deteriorated steel beam end capacity. Transportation Research Record, (1928), 92-100.

Liu, X., Silva, P. R., and Nanni, A. (2001). Rehabilitation of steel bridge members with FRP composite materials. Proc., CCC 2001, Composites in Construction, Porto, Portugal, J. Figueiras, L. Juvandes, and R. Furia, eds., 613–617. 26.

Luke, S. (2001). The Use of Carbon Fibre Plates for the Strengthening of Two Metallic Bridges of a Historic Nature. Proceedings of the UK. FRP Composites in Civil Engineering, Vol. II, edited by J. G. Teng, pp. 975-983.

Miller, T. C., Chajes, M. J., Mertz, D. R., and Hastings, J. N. (2001). Strengthening of a steel bridge girder using CFRP plates. Journal of Bridge Engineering, 6(6), 514-522.

Miller, T.C. (2000). The rehabilitation of steel bridge members using advanced composite materials. Master's Thesis, University of Delaware, Newark, Delaware.

Moy, S.S.J., Barnes, F., Moriarty, J., Dier, A.F., Kenchington, A. and Iverson, B. (2000), "Structural Upgrade and Life Extension of Cast Iron Struts Using Carbon Fibre Reinforced Composites", Proceedings of the 8th International Conference on Fibre Reinforced Composites, Newcastle upon Tyne, UK, September 13-15, 2000, pp 3-10.

Nozaka, K., Shield, C. K., and Hajjar, J. F. (2005). Design of a Test Specimen to Assess the Effective Bond Length of Carbon Fiber Reinforced Polymer Strips Bonded to Fatigued Steel Bridge Girders. Journal of Composites for Construction, American Society of Civil Engineers, 9(4): 304-312.

Nozaka, K., Shield, C.K. and Hajjar, J.F. (2005). Effective bond length of carbon-fibre-reinforced polymer strips bonded to fatigued steel bridge I-girders. Journal of bridge Engineering, 10 (2), 195-205.

Nozaka, K., Shield, C.K., and Hajjar, J.F. (2001). Rehabilitation of Fatigued Steel Girders with Carbon Fiber Strips. No. 2004-02. University of Minnesota. MN/RC report.

Patnaik, A., Bauer, C., and Srivatsan, T. (2008). The extrinsic influence of carbon fibre reinforced plastic laminates to strengthen steel structures. Sadhana, 33(3), 261-272.

Photiou, N. K., Hollaway, L. C., and Chryssanthopoulos, M. K. (2006). Strengthening of an artificially degraded steel beam utilising a carbon/glass composite system. Construction and Building Materials, 20(1-2), 11-21.

Rahgozar, R. (2009). Remaining capacity assessment of corrosion damaged beams using minimum curves. Journal of Constructional Steel Research, 65(2), 299-307.

Sayed-Ahmed, E. (2006). Numerical investigation into strengthening steel I-section beams using CFRP strips. Structures Congress 2006, may 18, 2006 - may 21, , 2006 68.

Schnerch, D., Dawood, M., Rizkalla, S., and Sumner, E. (2007). Proposed design guidelines for strengthening of steel bridges with FRP materials. Construction and Building Materials, 21(5), 1001-1010.

Sen, R. and Libby, L. (1994). Repair of steel composite bridge sections using CFRP laminates. Final report submitted to Florida and US Department of Transportation. Virginia: NTIS.

Sen, R., Liby, L., and Mullins, G. (2001). Strengthening steel bridge sections using CFRP laminates. Composites Part B: Engineering, 32(4), 309-322.

Shaat A, Schnerch D, Fam A, and Rizkalla S. Retrofit of steel structures using Fiber-Reinforced Polymers (FRP): State-of-the-art. In: Transportation research board (TRB) annual meeting. 2004.

Shaat, A., and Fam, A. (2008). Repair of cracked steel girders connected to concrete slabs using carbon-fiber-reinforced polymer sheets. Journal of Composites for Construction, 12(6), 650-659.

Stratford, T., and Cadei, J. (2006). Elastic analysis of adhesion stresses for the design of a strengthening plate bonded to a beam. Construction and Building Materials, 20(1-2), 34-45.

Tavakkolizadeh, M., and Saadatmanesh, H. (2001). Galvanic corrosion of carbon and steel in aggressive environments. Journal of Composites for Construction, 5(3), 200-210.

Tavakkolizadeh, M., and Saadatmanesh, H. (2003). Fatigue strength of steel girders strengthened with carbon fiber reinforced polymer patch. Journal of Structural Engineering, 129(2), 186-196.

Tavakkolizadeh, M., and Saadatmanesh, H. (2003). Repair of damaged steel-concrete composite girders using carbon fiber-reinforced polymer sheets. Journal of Composites for Construction, 7(4), 311-322.

Tavakkolizadeh, M., and Saadatmanesh, H. (2003). Strengthening of steel-concrete composite girders using carbon fiber reinforced polymers sheets. Journal of Structural Engineering, 129(1), 30-40.

Varvani-Farahani, A., Haftchenari, H., and Panbechi, M. (2007). An energy-based fatigue damage parameter for off-axis unidirectional FRP composites. Composite Structures, 79(3), 381-389.

West, T.D. (2001). Enhancements to the bond between advanced composite materials and steel for bridge rehabilitation. Master's Thesis, University of Delaware, Newark, Delaware.

Wipf, T. J., Phares, B. M., Klaiber, F. W., Al-Saidy, A., and Lee, Y. (2005). Strengthening steel girder bridges with carbon fiber-reinforced polymer plates. Transportation Research Board - 6th International Bridge Engineering Conference: Reliability, Security, and Sustainability in Bridge Engineering, July 17, 2005 - July 20, 435-447.

Zhao, X., and Zhang, L. (2007). State-of-the-art review on FRP strengthened steel structures. Engineering Structures, 29(8), 1808-1823.

APPENDIX A

DESIGN EXAMPLE OF THE DUCTILE ANCHORAGE SYSTEM

In this appendix, design example of the ductile anchorage system was done using latest version of CAN/CSA S16-09 Limit States Design of Steel Structures (2009) to guaranty transferring the load from the CFRP composite materials to the tension flange of the tested beams without having failure in the ductile system.

Part one

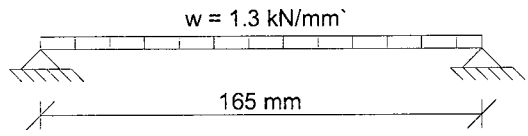

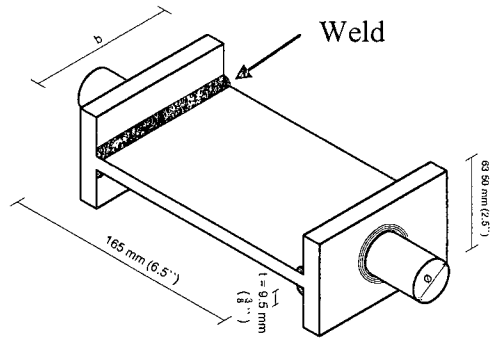

$(T_{CFRP})_{5\ layers}$ = $5 \times 150 \times 0.27 \times 1062 / 1000$ = 215 KN

$W = \frac{T_{CFRP}}{165} = \frac{215}{165} =$ 1.30 kN/mm

$Ma = \frac{w\,l^2}{8} = \frac{1.3 \times 150^2}{8} =$ 3656.25 kN.mm

F.O.S = 1.25

$M_y = \frac{M_a}{1.25} = \frac{3656.25}{1.25} =$ 2925 kN.mm

$M_y = F_y S_x$

F_y = 300 MPa ; t = 9.5 mm

Therefore,

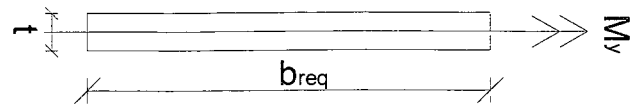

$b_{req} \cong$ 80mm

b = 100mm > b_{req} Ok

For the rode

Vr = 0.6 φ_b n m A_p F_u

Vr	Factored shear resistance	=	$\frac{T_{CFRP}}{2} \times 1.25$	=	135 KN
φ_b	Resistance factor			=	0.8
n	Number of rods			=	1
m	Number of shear planes			=	1
Fu	Specified minimum tensile strength			=	450 MPa

Therefore,

$A_{p\,req}$ = 625 mm^2

For diameter = 28.575 mm

A_p = 641.3 mm^2 > $A_{p\,req}$ Ok

Part three

Part three was designed to transfer the load to the tension flange using four high tensile bolts A325 with 0.75" diameter as shown in Figure 3.2.

$$V_{b\,req} = \frac{T_{CFRP}}{4} \times 1.25 = \frac{215}{4} \times 1.25 = 67 \text{ KN}$$

where $V_{b\,req}$ is the required factored shear resistance for one bolt.

For A325, 0.75" diameter

V_b = 100 KN > $V_{b\,req}$ Ok

where V_b is the factored shear resistance for one bolt.

All the distances from the center of the bolts holes to any edge were considered as the minimum distance according to table 6 in the CAN/CSA S16-09 Limit States Design of Steel Structures (2009).

Part two

Two types of ductile coupons were used in the anchorage system as shown below:

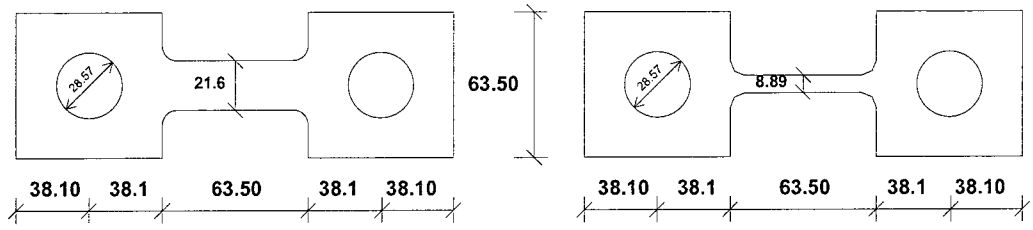

t_s = 12.7 mm

Fy = 300 MPa

F_u = 450 MPa

$T_y = A_C \times Fy$ = 82 KN

$T_u = A_C \times F_u$ = 123 KN

(a) A1

t_s = 6.35 mm

Fy = 300 MPa

F_u = 450 MPa

$T_y = A_C \times Fy$ = 17 KN

$T_y = A_C \times Fy$ = 25.5 KN

(b) A2

APPENDIX B

MAX. MOMENT-ROTATION AND LONGITUDINAL DEFLECTION PROFILE OF ALL TESTED BEAMS

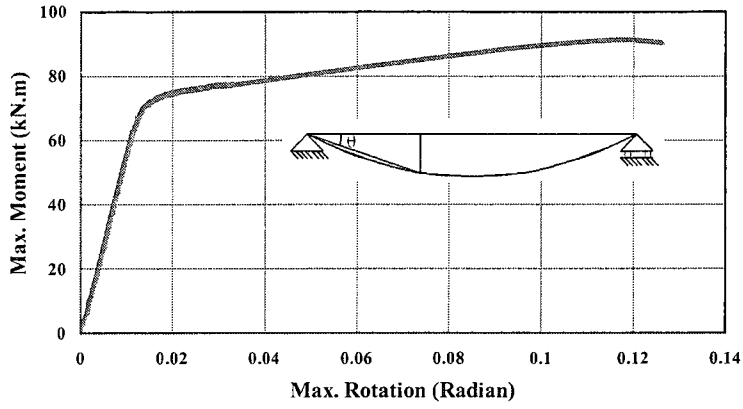

(a)

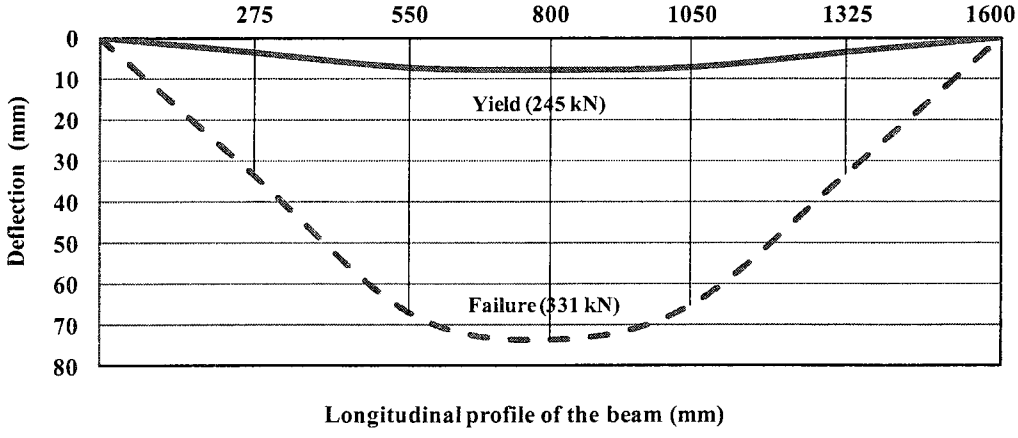

(b)

Figure B.1 Test results of beam BFO (a) Moment-Rotation; (b) Deformed shape

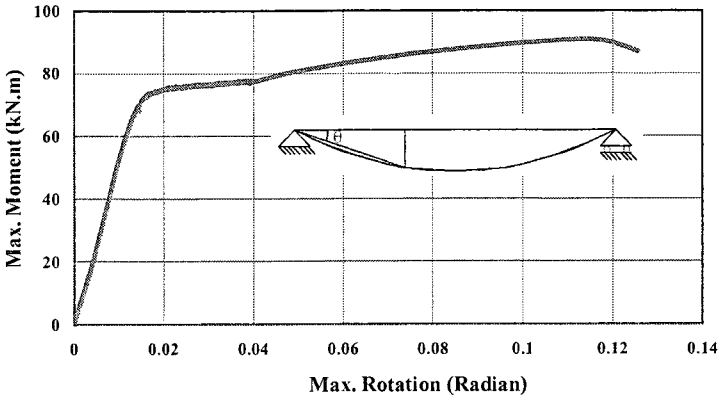

(a)

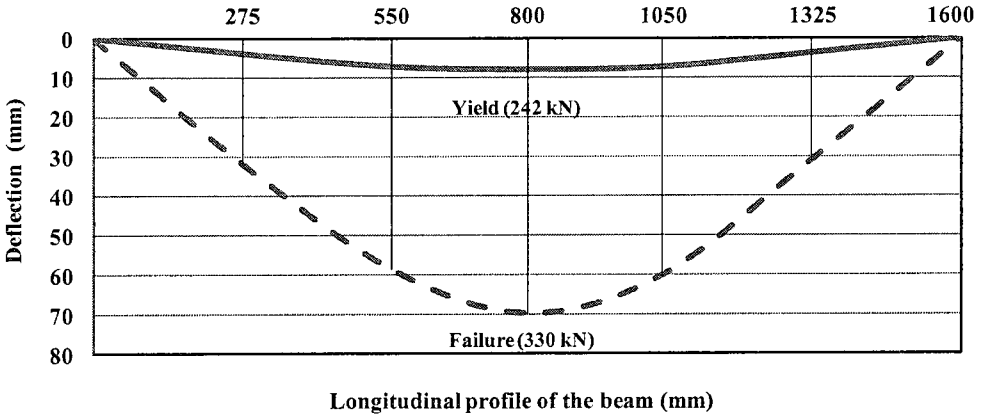

(b)

Figure B.2 Test results of beam BF-H0.33 (a) Moment-Rotation; (b) Deformed shape

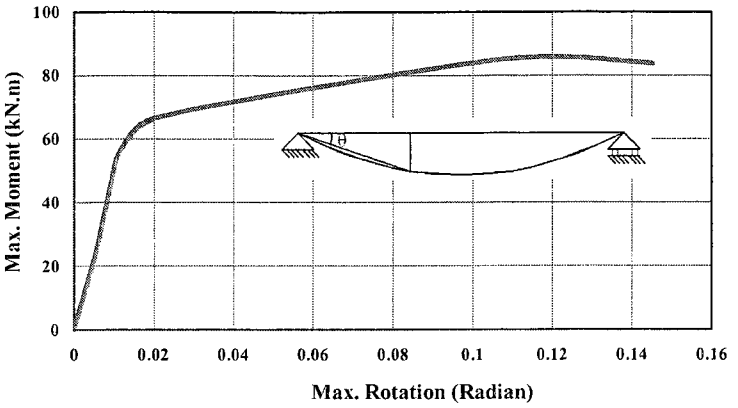

(a)

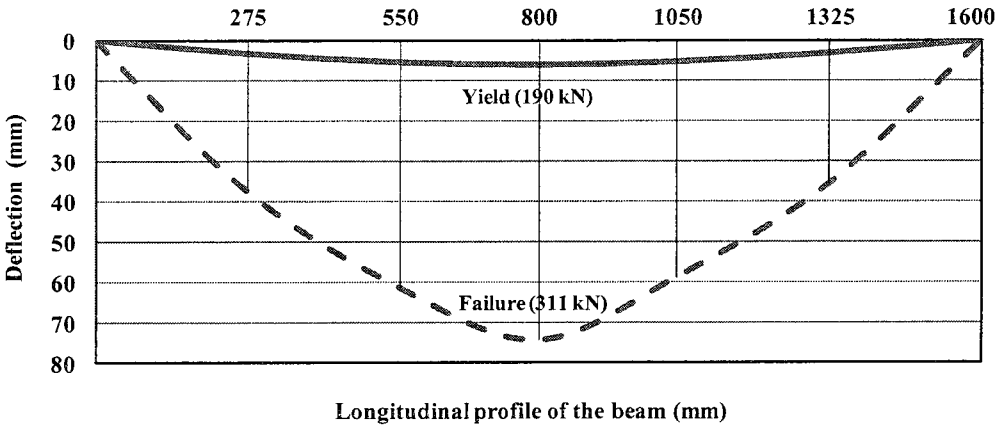

(b)

Figure B.3 Test results of beam BF-N0.33 (a) Moment-Rotation; (b) Deformed shape

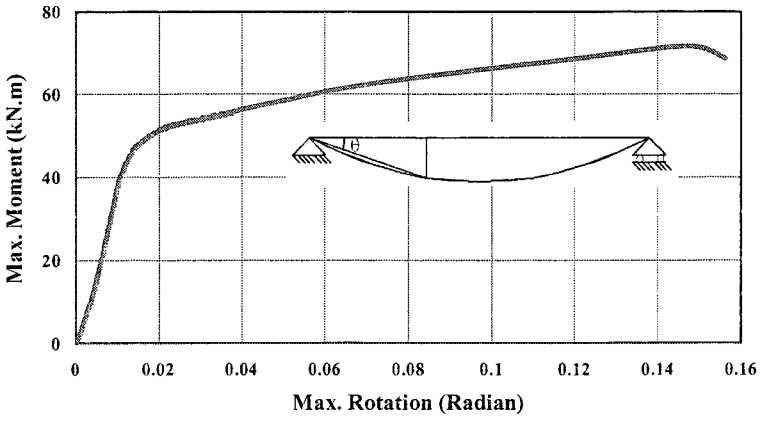

(a)

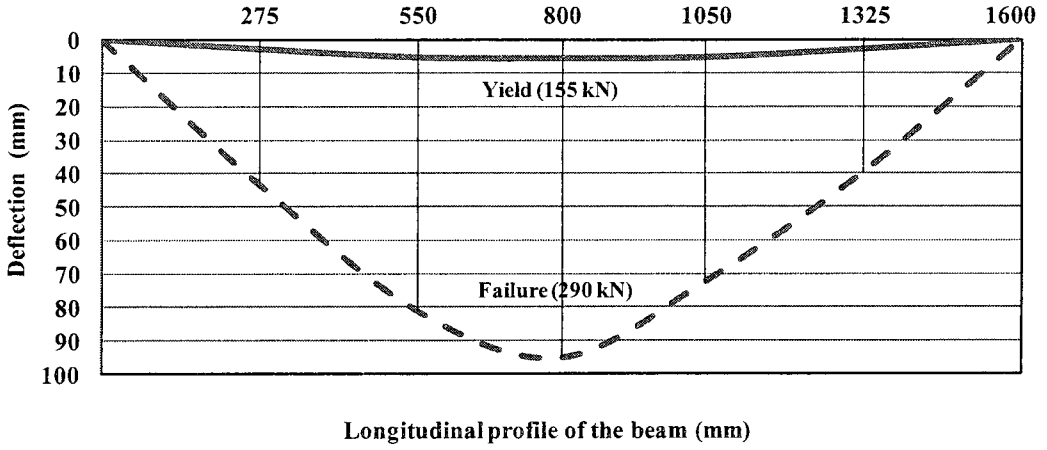

(b)

Figure B.4 Test results of beam BF-N0.50 (a) Moment-Rotation; (b) Deformed shape

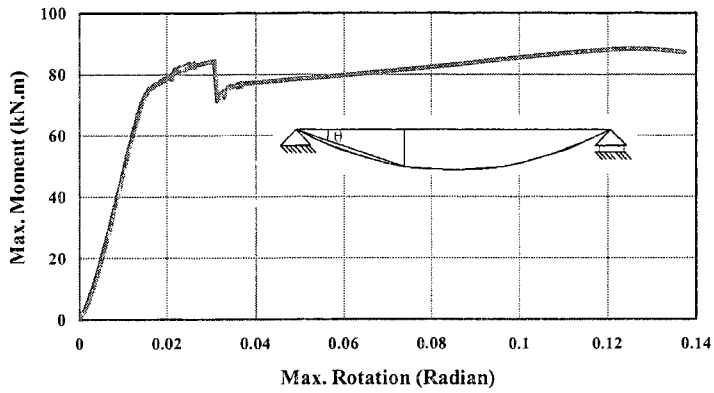

(a)

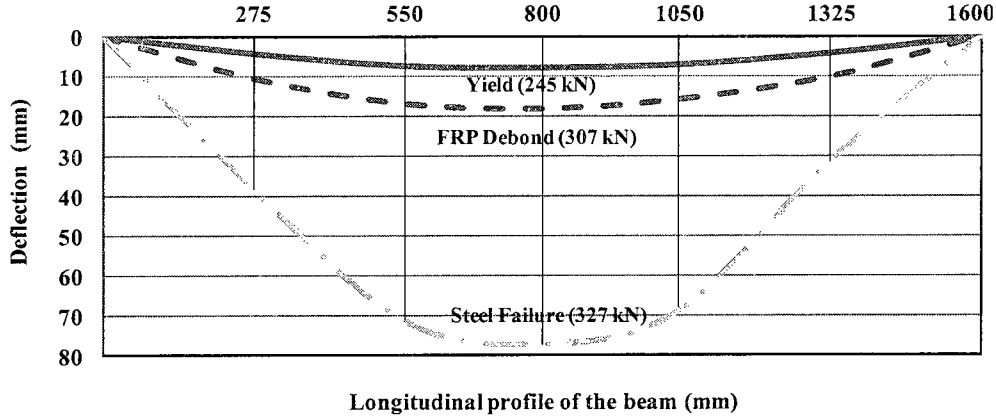

(b)

Figure B.5 Test results of beam BF-H0.33-F1(5)-B1 (a) Moment-Rotation; (b) Deformed shape

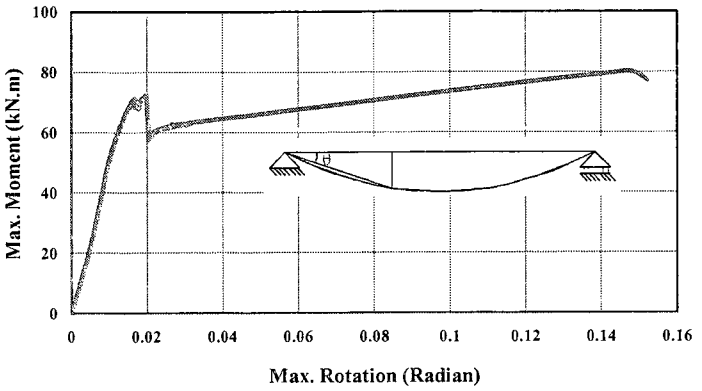

(a)

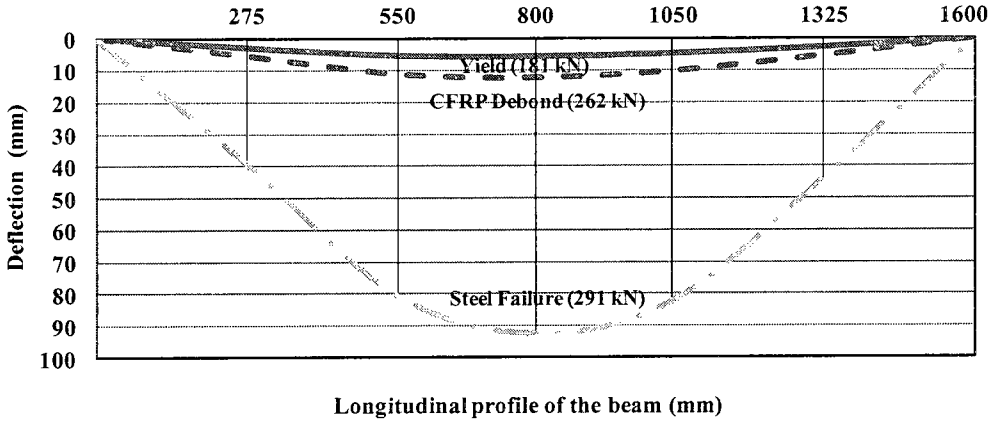

(b)

Figure B.6 Test results of beam BF-N0.50-F1(5)-B1 (a) Moment-Rotation; (b) Deformed shape

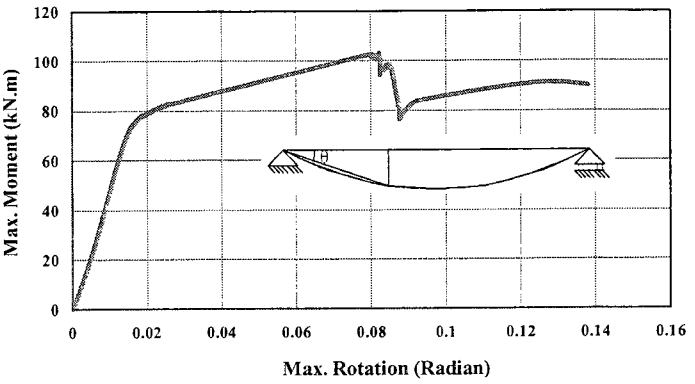

(a)

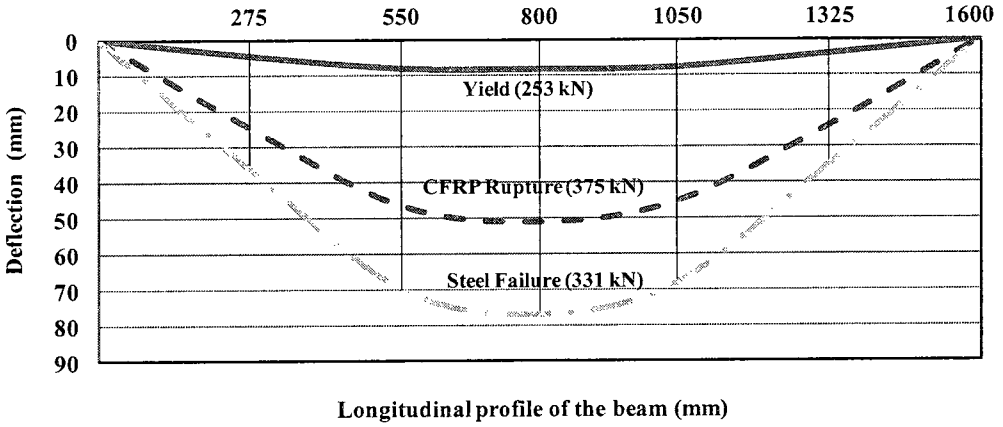

(b)

Figure B.7 Test results of beam BF-H0.33-F1(5)-B2 (a) Moment-Rotation; (b) Deformed shape

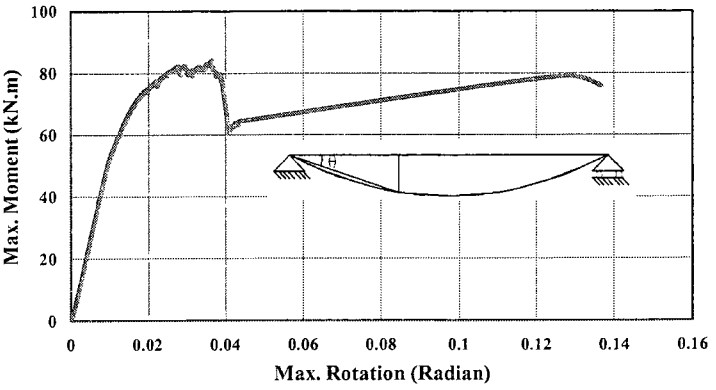

(a)

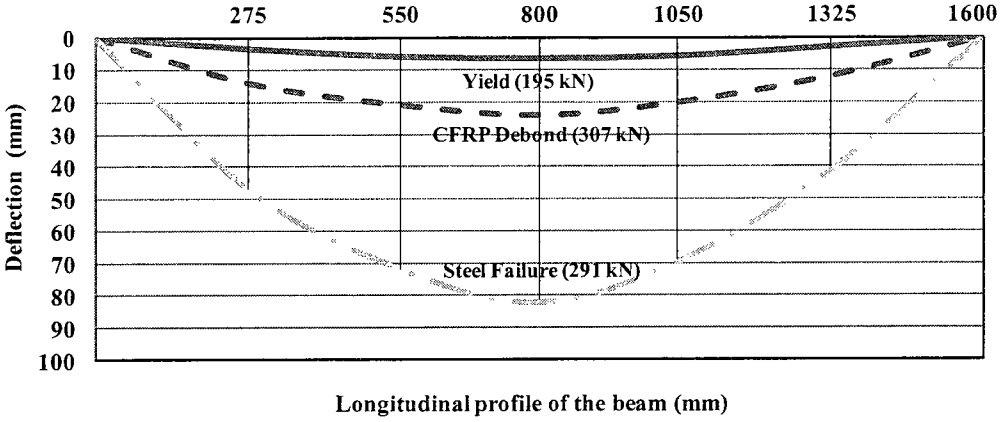

(b)

Figure B.8 Test results of beam BF-N0.50-F1(5)-B2 (a) Moment-Rotation; (b) Deformed shape

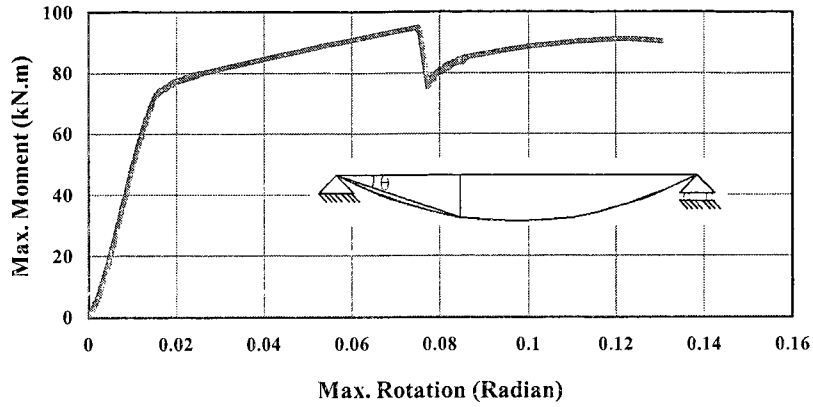

(a)

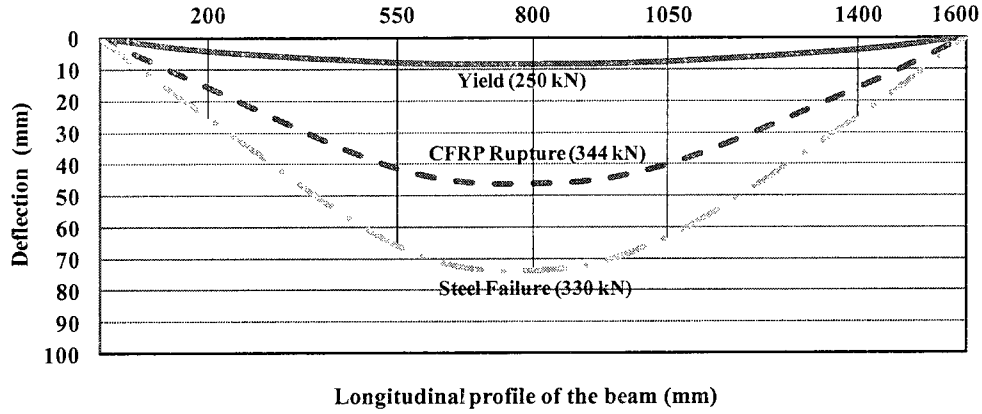

(b)

Figure B.9 Test results of beam BF-H0.33-F2(1)-B2 (a) Moment-Rotation; (b) Deformed shape

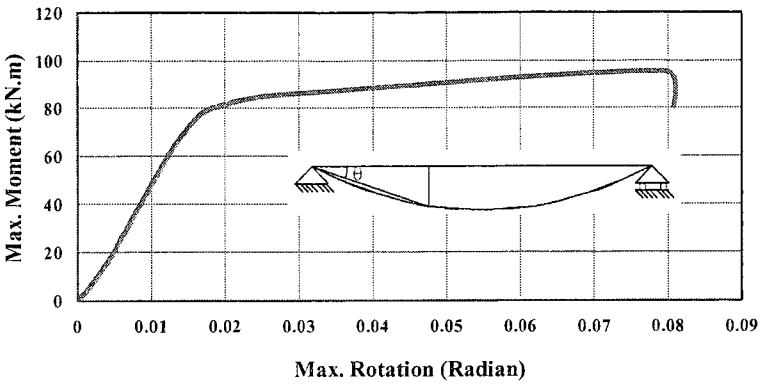

(a)

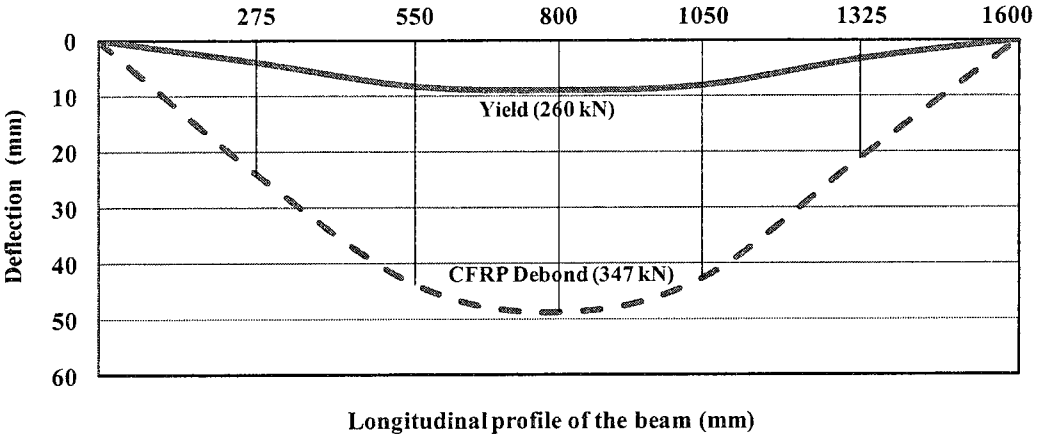

(b)

Figure B.10 Test results of beam BF-H0.33-F2(1)-B2w (a) Moment-Rotation; (b) Deformed shape

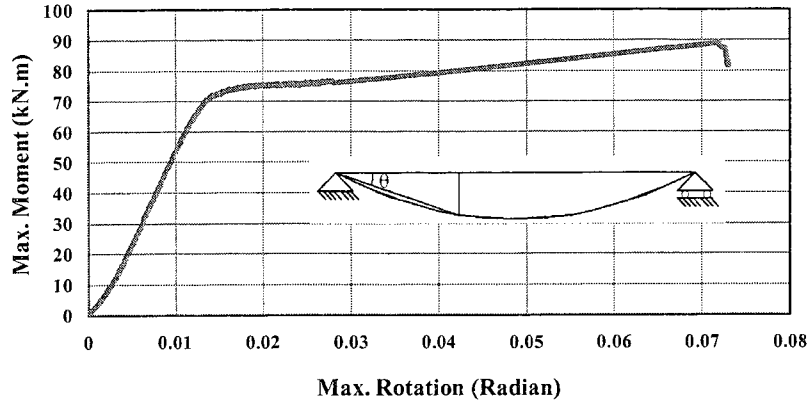

(a)

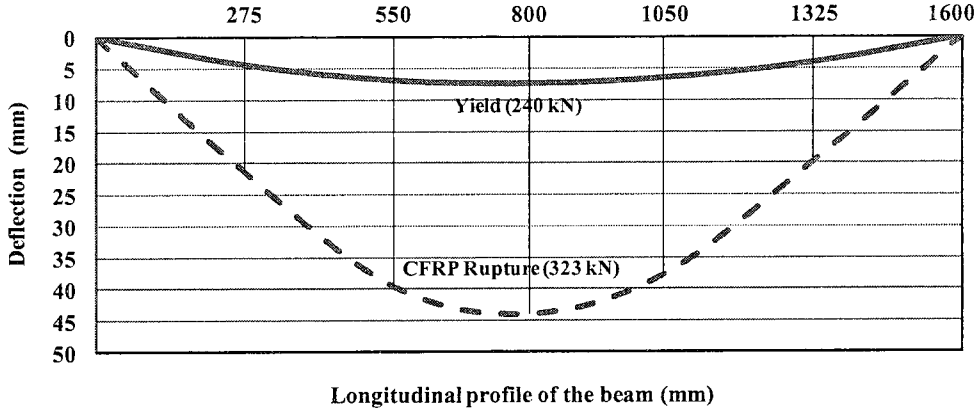

(b)

Figure B.11 Test results of beam BF-H0.33-F1(1)-A1D1 (a) Moment-Rotation; (b) Deformed shape

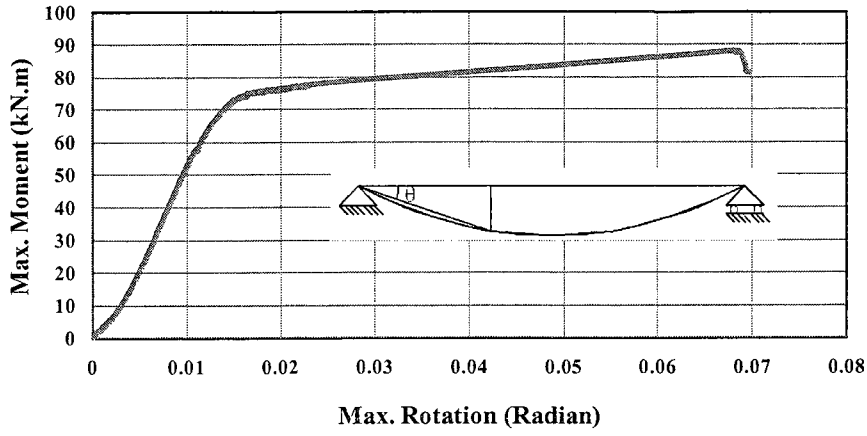

(a)

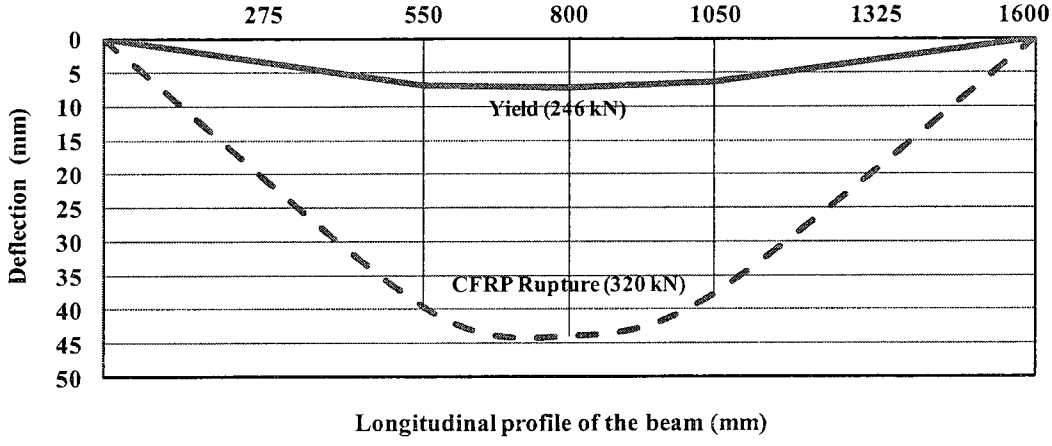

(b)

Figure B.12 Test results of beam BF-H0.33-F1(1)-A2D1 (a) Moment-Rotation; (b) Deformed shape

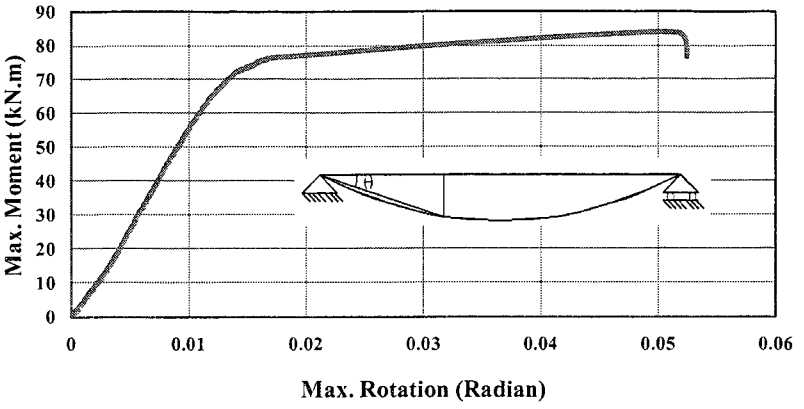

(a)

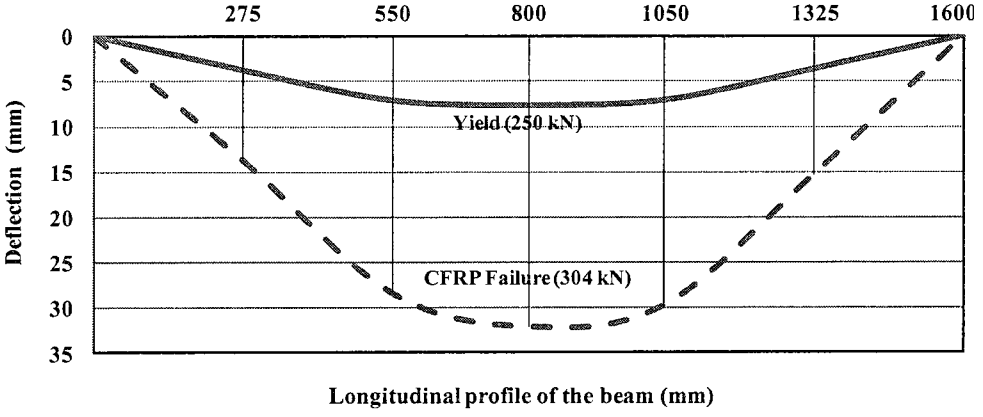

(b)

Figure B.13 Test results of beam BF-H0.33-F1(5)-A2D2 (a) Moment-Rotation; (b) Deformed shape